WORLD METEOROLOGICAL ORGANIZATION

GLOBAL ATMOSPHERE WATCH

WORLD DATA CENTRE FOR GREENHOUSE GASES

WMO WDCGG DATA SUMMARY

WDCGG No. 33

GAW DATA

Volume IV-Greenhouse Gases and Other Atmospheric Gases

PUBLISHED BY
JAPAN METEOROLOGICAL AGENCY
IN CO-OPERATION WITH
WORLD METEOROLOGICAL ORGANIZATION

MARCH 2009

Acknowledgements

This issue of *Data Summary* reports the latest status of greenhouse gases and related gases in the global atmosphere. This *Data Summary* has been prepared by the World Meteorological Organization (WMO) World Data Centre for Greenhouse Gases (WDCGG), in cooperation with WMO using data from a global observation network consisting of many contributors (Appendix: LIST OF CONTRIBUTORS). These contributors include organizations and individuals involved in observations and research at stations and laboratories that measure greenhouse gases and other atmospheric gases within the framework of the WMO Global Atmosphere Watch (GAW) and other cooperative monitoring and research programmes. The WDCGG thanks all of these organizations and individuals, particularly those from the global air sampling network of the National Oceanic and Atmospheric Administration (NOAA), for their efforts in maintaining the observation programme and providing continuous observational data. Not all of the contributors may be explicitly acknowledged in this publication, owing to lack of space, but it should be noted that all the organizations and individuals that have submitted data to the WDCGG are equal contributors to this new issue of the *Data Summary*.

CONTENTS

Summary

This *Data Summary* reports the results of basic analyses of greenhouse gas data submitted to the WMO World Data Centre for Greenhouse Gases (WDCGG). This issue covers observations from 1968 to 2007, based on data reported to the WDCGG by October 2008. The *Data Summary* includes analyses of global, hemispheric and latitudinal monthly mean mole fractions of greenhouse and related gases, and provides useful information on the state of mole fractions of these gases.

Only monthly mean mole fractions are used for the analyses, but the WDCGG greatly appreciate those stations that submit daily and hourly mean mole fractions, which are important for analysing the variations on shorter time scales. All the data submitted to the WDCGG are available on its web site, http://gaw.kishou.go.jp/wdcgg.html.

To quantify mole fractions, this *Data Summary* uses the units ppm, ppb and ppt, which correspond to the SI units μmol/mol, nmol/mol and pmol/mol, respectively.

Variations in the mole fractions of some greenhouse gases in the atmosphere are presented as a combination of seasonal cycles and deseasonalized long-term trends. Growth rates are presented as time derivatives of the long-term trends. The analytical results are summarized below for each greenhouse and related gas.

Carbon Dioxide (CO_2)

The level of carbon dioxide (CO_2), which contributes most to global warming, has been increasing since the pre-industrial period. The global average mole fraction of CO_2 in 2007 reached a new high of 383.1 ppm, which is 137% of that in the pre-industrial period. The increase of 1.9 ppm from 2006 to 2007 was larger than the average for the 1990s (about 1.5 ppm/year).

The global growth rate of CO_2 has a significant interannual variation, with an average of 2.00 ppm/year for the period 1997-2007. Growth rates higher than 2 ppm/year in 1987/1988, 1997/1998, 2002/2003 and 2005 resulted from warmer conditions caused by El Niño-Southern Oscillation (ENSO) events. The anomalously strong El Niño event in 1997/1998 resulted in worldwide high increases in 1998. The large growth rates in 2006 may have been related to the global high temperature in 2006. The exceptionally low growth rates in 1992, including negative values in northern high latitudes, may have been due to low global temperatures following the eruption of Mt. Pinatubo in 1991. Variations in CO_2 mole fraction can be seen both on seasonal and long-term scales. The seasonal amplitudes are large in northern high and mid-latitudes and small in the Southern Hemisphere. Seasonal cycles in the Northern Hemisphere mainly reflect seasonal variations in the absorption/emission in the biosphere, while the seasonal cycle in the Southern Hemisphere reflects oceanic variations and biomass burning in addition to the influence of activities in the biosphere. In southern low latitudes, there is no clear annual cycle, but a semiannual cycle can be determined. This is probably due to two factors in opposing phase —direct influence of sources and sinks in the Southern Hemisphere and propagation of the seasonal variation from the Northern Hemisphere.

Methane (CH_4)

Methane (CH_4) is the second most significant greenhouse gas, whose level has been increasing since the beginning of the 19th century. The annual average mole fraction was 1789 ppb in 2007, an increase of 6 ppb since 2006 and of 2 ppb since 2003. The mole fraction is now 256% of that in the pre-industrial period.

The latitudinal gradient of CH_4 mole fraction is large from the northern mid-latitudes to the Tropics, suggesting that the major sources are located in northern high and mid-latitudes.

The growth rates decreased significantly in some years, including 1992, when negative values were recorded in northern high and mid-latitudes. However, both hemispheres experienced high growth rates in 1998, caused by an exceptionally high global mean temperature. The global growth rates decreased to almost zero in 2000–2001, suggesting that the global CH_4 budget seemed to be in a steady state. The growth rates increased temporally in 2002 and 2003 with the occurrence of an El Niño event. In 2007, the growth rates increased again globally.

The global growth rate averaged 11.5 ppb/year for the period 1984–1990, but decreased markedly in the 1990s. The average global growth rate for the period 1997–2007 was 2.7 ppb/year. Some possible causes of this changing growth rate have been proposed but the issue remains unresolved.

CH_4 mole fractions vary seasonally, with high values in winter and low values in summer. Unlike CO_2, the amplitudes of the seasonal cycle of CH_4 are large, not only in the Northern Hemisphere but also in southern high and mid-latitudes. In southern low latitudes, a distinct secondary maximum in boreal winter overlies the annual cycle. This is attributed to large-scale transportation of CH_4 from the Northern Hemisphere.

Nitrous Oxide (N_2O)

Nitrous oxide (N_2O) is an important greenhouse gas whose level is increasing on a global scale. N_2O data

submitted to the WDCGG show that mole fractions are increasing in both hemispheres. The global mean mole fraction reached a new high of 320.9 ppb in 2007, 0.8 ppb higher than the year before. The mean growth rate of the global mean mole fraction over the period 1997–2007 was 0.77 ppb/year. This increase in mole fraction corresponds to 119% of that in the pre-industrial period.

Halocarbons and Other Halogenated Species

Halocarbons, most of which are anthropogenic, are effective greenhouse gases and some also act as ozone-depleting compounds. Levels of some halocarbons (e.g. CFCs) increased in the 1970s and 1980s, but the increase has almost ceased by now as a result of the regulation of production and emission under the Montreal Protocol on Substances that Deplete the Ozone Layer and its Adjustments and Amendments.

The mole fractions of CFC-11 peaked around 1992 and then started decreasing. The growth rate of CFC-12 has declined since around 1990 and is now nearly zero. The mole fractions of CFC-113 stopped increasing in the 1990s, and have shown a slight decrease over the last decade. The mole fractions of HCFC-22, HCFC-141b and HCFC-142b, which are industrial replacements of CFCs, are increasing. The mole fractions of Halon-1211 and Halon-1301 are increasing, but their growth rates have decelerated. The mole fractions of CCl_4 were at a maximum around 1991 and have since decreased slowly. The mole fractions of CH_3CCl_3 peaked around 1992 and decreased thereafter. The mole fractions of HFC-134a, HFC-152a and SF_6 are increasing.

Surface Ozone (O_3)

Ozone (O_3) plays important roles in the atmospheric environment through radiative and chemical processes. It absorbs solar UV radiation in the stratosphere, influencing the vertical temperature profile, and circulates the atmosphere with absorbed energy. Ozone also absorbs terrestrial IR radiation, contributing to the greenhouse effect as a greenhouse gas.

The mole fraction of O_3 near the surface, so-called surface ozone, reflects various processes. While some of the O_3 in the troposphere comes from the stratosphere, the rest is chemically produced in the troposphere through oxidation of CO or hydrocarbons in the presence of rich NO_x.

The mole fraction of surface ozone is measured at many locations in various environments. Due to its uneven geographic distribution, however, it is difficult to identify a global long-term trend of surface O_3.

Carbon Monoxide (CO)

Carbon monoxide (CO) is not a greenhouse gas itself but influences the mole fractions of greenhouse gases by affecting hydroxyl radicals (OH). Its mole fractions in northern high latitudes have been increasing since the mid-19th century. In 2007, the global mean mole fraction of CO was about 96 ppb. The mole fraction is high in the Northern Hemisphere and low in the Southern Hemisphere, suggesting substantial anthropogenic emissions in the Northern Hemisphere.

Although the global mole fraction of CO increased until the mid-1980s, this growth ceased or was reversed thereafter (WMO, 1999a). There was a large fluctuation in growth rate, however, with high positive rates followed by high negative rates in northern latitudes and southern low latitudes from 1997 to 1999. The growth rates in the Northern Hemisphere increased again in 2002.

The monthly mean mole fractions show seasonal variations, with large amplitudes in the Northern Hemisphere and small amplitudes in the Southern Hemisphere. This seasonal cycle is driven by industrial emissions, biomass burning, large-scale transportation, and variations in the OH mole fraction, which acts as a sink.

Nitrogen Monoxide (NO) and Nitrogen Dioxide (NO_2)

Nitrogen oxides (NO_x, i.e., NO and NO_2) are not greenhouse gases, but influence the mole fractions of important greenhouse gases by affecting OH. In the presence of NO_x, CO and hydrocarbons are oxidized to produce ozone (O_3), which affects the Earth's radiative balance as a greenhouse gas and the oxidization capacity of the atmosphere by reproducing OH.

Most of the stations reporting NO_x data to the WDCGG are located in Europe. NO_x has a large temporal and geographic variability, and it is difficult to identify a long-term trend. In Europe, the NO_2 mole fractions are generally higher in southern regions than in northern regions.

Sulphur Dioxide (SO_2)

Sulphur dioxide (SO_2) is not a greenhouse gas but a precursor of atmospheric sulphate aerosols. Sulphate aerosols are produced by SO_2 oxidation through photochemical gas-to-particle conversion. SO_2 has also been a major source of acid rain and deposition throughout the industrial era.

Most of the stations reporting SO_2 data to the WDCGG are located in Europe. Generally, in Europe, the SO_2 mole fractions are higher in southern regions than in northern regions.

1. Introduction

Human activities have had major impacts on the global environment. Since the beginning of the industrial revolution, mankind has increasingly made use of land, water, minerals and other natural resources, and future growth of human populations and economies may further increase our impact on the environment. As the global climate, biogeochemical processes and natural ecosystems are closely interlinked, changes in any one of these systems may affect the others and be detrimental to humans and other organisms. Emissions of man-made gaseous and particulate matters alter the energy balance of the atmosphere, and consequently affect the interactions among the atmosphere, hydrosphere and biosphere. Nevertheless, we do not yet have sufficient understanding of chemical processes in the atmosphere or interactions among the atmosphere, hydrosphere and biosphere. The insufficiency of our understanding of the chemical processes occurring in the atmosphere and oceans is mainly due to our lack of observational data.

The World Meteorological Organization (WMO) launched Global Atmosphere Watch (GAW) in 1989 to promote systematic and reliable observations of the global environment, including greenhouse gases (CO_2, CH_4, CFCs, N_2O, *etc.*) and other related gases (*e.g.*, CO, NO_x, and SO_2) in the atmosphere. In October 1990, WMO designated the World Data Centre for Greenhouse Gases (WDCGG) at the Japan Meteorological Agency (JMA) in Tokyo as one of the GAW World Data Centres. These centres were designated to collect, archive and distribute data for greenhouse and related gases in the atmosphere and oceans from a number of observation sites throughout the world participating in GAW and other scientific monitoring programmes (Appendix: LIST OF OBSERVING STATIONS). In August 2002, the WDCGG took over the role of the Data Centre for Surface Ozone from the Norwegian Institute for Air Research (NILU) to collect surface ozone data.

With regard to the issue of global warming, the Kyoto Protocol to the United Nations Framework Convention on Climate Change came into force in February 2005. In March 2006, WMO commenced annual publication of the WMO Greenhouse Gas Bulletin . The fourth issue of the Bulletin was published in November 2008. The bulletin summarizes the state of greenhouse gases in the atmosphere. The WDCGG contributes to the bulletin through a swifter and smoother exchange of data.

Since its establishment, the WDCGG has provided its users with data and other information through its regular publications, including the *Data Summary* and *DVD* (Appendix: LIST OF WMO WDCGG PUBLICATIONS). All data and information are also available on the WDCGG web site to improve accessibility to data, information and products in line with the GAW Strategic Plan: (2008–2015) (WMO, 2007a). In 2007, the WDCGG published the Data Submission and Dissemination Guide (WMO, 2007b), which was designed to facilitate submission of observational data and access to archived data in the WDCGG.

The GAW Strategic Plan requests that World Data Centres assist data users of atmospheric chemistry observations. To this end, the WDCGG provides global and integrated diagnostics on the state of greenhouse gases as analytical information in the *Data Summary*. The methods of the WDCGG global analysis of major greenhouse gases are described in a GAW technical report (WMO, 2009). The contents of the *Data Summary* are designed to be revised and improved based on comments from data contributors and scientists. The WDCGG invites comments and suggestions regarding the *Data Summary* or any other publications. We hope the diagnostic information presented here will promote the use of data on greenhouse and other gases and will enhance appreciation of the value of the GAW programme.

All users are required to accept the following statement endorsed by the Commission for Atmospheric Sciences (CAS) at its thirteenth session: "For scientific purposes, access to these data is unlimited and provided without charge. By their use you accept that an offer of co-authorship will be made through personal contact with the data providers or owners whenever substantial use is made of their data. In all cases, an acknowledgement must be made to the data providers or owners and to the data centre when these data are used within a publication." The WDCGG requests data users to make appropriate acknowledgements. Data users can refer to the GAW Station Information System (GAWSIS) found at the GAW website (http://www.wmo.ch/web/arep/gaw/gaw_home.html) or the WDCGG website for details on GAW country contacts, measurements being made, and principal investigators. The information at the World Data Centres and GAWSIS is kept updated in cooperation with the WMO Secretariat.

Finally, the WDCGG would like to thank all data contributors worldwide, including those involved in on-site measurements, for their efforts to maintain the observational programme and for continuous provision of data.

Mailing address:
WMO World Data Centre for Greenhouse Gases (WDCGG)
c/o Japan Meteorological Agency
1-3-4, Otemachi, Chiyoda-ku, Tokyo 100-8122, Japan
E-mail: wdcgg@met.kishou.go.jp
Telephone: +81-3-3287-3439
Facsimile: +81-3-3211-4640
Web Site: http://gaw.kishou.go.jp/wdcgg.html

2. Analysis

The WDCGG collects, archives and provides observational data on the mole fractions of greenhouse gases, and publishes diagnostic information on greenhouse gases based on the reported data.

For CO_2, CH_4 and CO, long-term trends and seasonal variations in their mole fractions are analyzed for presentation as global and latitudinal means. For N_2O, only global long-term trends are presented. For surface O_3, global long-term trends are not analyzed due to an uneven geographical distribution of the stations. For halocarbons, NO_x and SO_2, only time series of monthly mean mole fractions are presented due to the small number of reporting sites.

The analyses utilize ppm, ppb, and ppt as units, rather than the SI units of μmol/mol, nmol/mol, and pmol/mol, respectively.

The following sections summarize the methods of analysis for CO_2, CH_4, CO and N_2O. The details of the global analysis methods for CO_2, CH_4, and N_2O are provided in the *Technical Report of Global Analysis Method for Major Greenhouse Gases by the World Data Centre for Greenhouse Gases*, published as a GAW technical report (WMO, 2009).

(1) Site selection

For CO_2, CH_4 and N_2O, the diagnostic analyses, such as global, hemispheric and zonal means, are based on data from sites that have adopted a standard scale traceable to the Primary Standard designated under GAW. In addition, these analyses utilize data on other standard scales that are convertible to the Primary Standard through a proven equation.

Selection of observation sites for CO_2, CH_4 and CO, which are sensitive to local sources and sinks, have also been based on their ability to provide data representing a reasonably large geographical area. These sites have been selected objectively using data measured in a reasonably scattered distribution in each latitudinal zone. Only those sites that provide annual mean mole fractions falling within a range of $\pm 3\sigma$ from a curve fitted to the LOESS model curve (Cleveland *et al.*, 1988) have been selected, by rejecting outliers in an iterated manner.

The sites selected according to the above criteria are marked with asterisks in Plate 3.1 for CO_2, Plate 4.1 for CH_4, Plate 5.1 for N_2O and Plate 8.1 for CO.

(2) Analysis of long-term trends

The mole fractions of greenhouse gases over time, measured in background conditions, represent an integration of variations on different time scales. The two major components are seasonal variation and long-term trend. Various attempts have been made to delineate measured data into these two components, including objective curve fitting (Keeling *et al.*, 1989), digital filtering (Thoning *et al.*, 1989; Nakazawa *et al.*, 1991), or both (Conway *et al.*, 1994; Dlugokencky *et al.*, 1994).

In this report, seasonal variations derived from components of Fourier harmonics and long-term trends are extracted by low-pass filtering with a cut-off frequency of 0.48 cycles/year for each selected site. Details are described in WDCGG Data Summary No. 22 (2000).

(3) Estimation for missing periods and gaps

The number and distribution of sites used for trend analysis during the analysis period should be kept as constant as possible to avoid the effects of changes in the availability of data. However, only a small number of sites provide data throughout the whole analysis period; others may cover the period insufficiently or have gaps. To use as many sites as possible, missing values are estimated for the calculation of zonal means, using interpolation and extrapolation as described below.

For the former, the gaps are interpolated linearly based on the data, by subtracting the seasonal variation calculated from the longest consecutive period of data with Lanczos filters (Duchon, 1979). The subtracted variation is added back to the data to obtain estimated mole fractions in a single sequence.

For the latter, long-term trends calculated from the interpolated series of data are extrapolated based on zonal mean growth rates calculated from other sites in the same latitudinal zone. The seasonal variation is added to the extrapolated long-term trend to obtain estimated mole fractions for the whole analysis period.

(4) Calculation of global, hemispheric and zonal means

Zonal means are calculated by determining the arithmetic average of the mole fractions in each latitudinal zone, based on consistent datasets derived as above.

Global and hemispheric means are calculated as the weighted averages of the zonal means taking account of the area of each latitudinal zone.

Deseasonalized long-term trends and growth rates for the globe, each hemisphere and each latitudinal zone are calculated from the global, hemispheric and zonal means using the low-pass filter mentioned above.

3.

CARBON DIOXIDE

(CO_2)

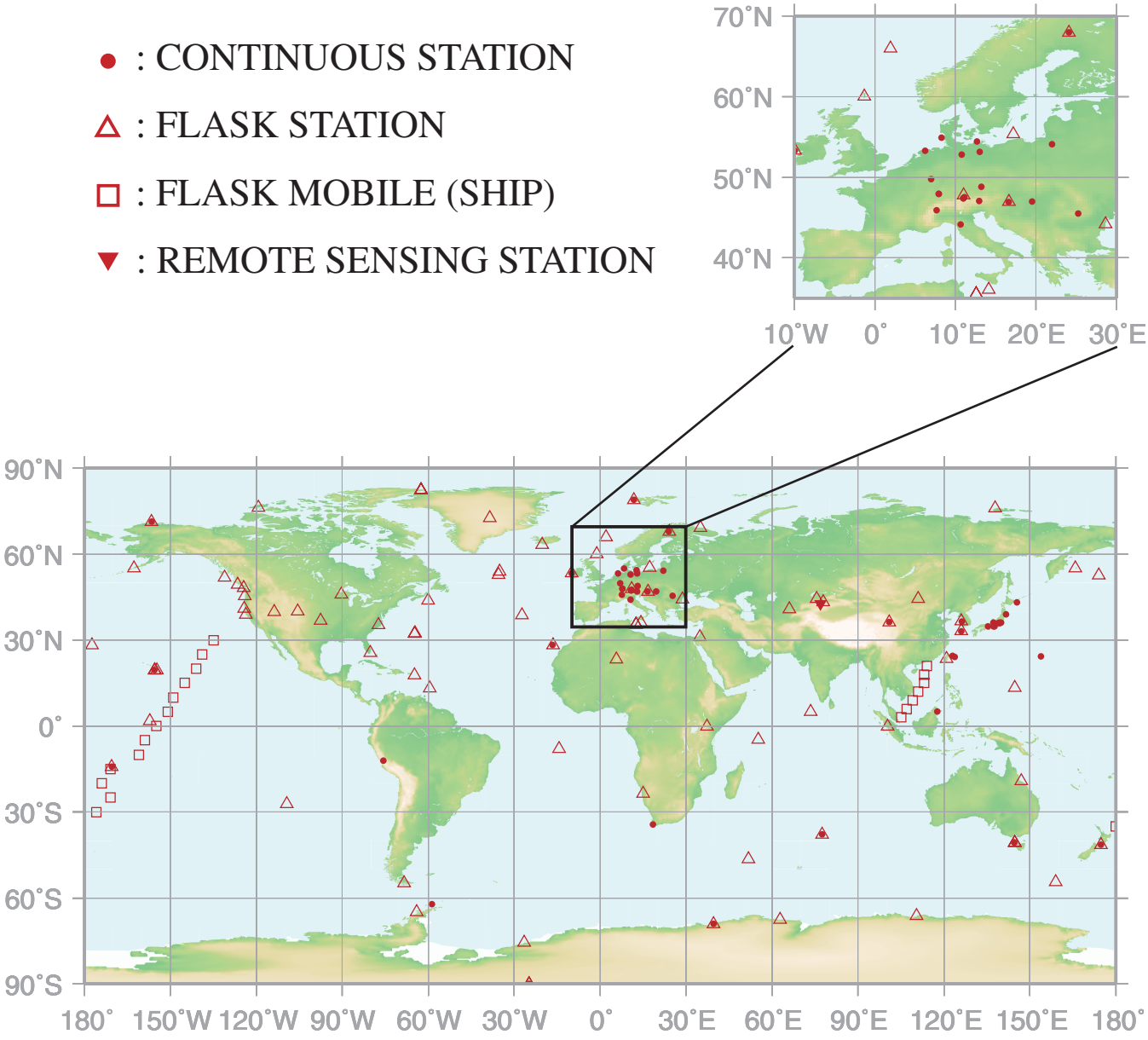

This map shows locations of the stations that have submitted data for monthly mean mole fraction.

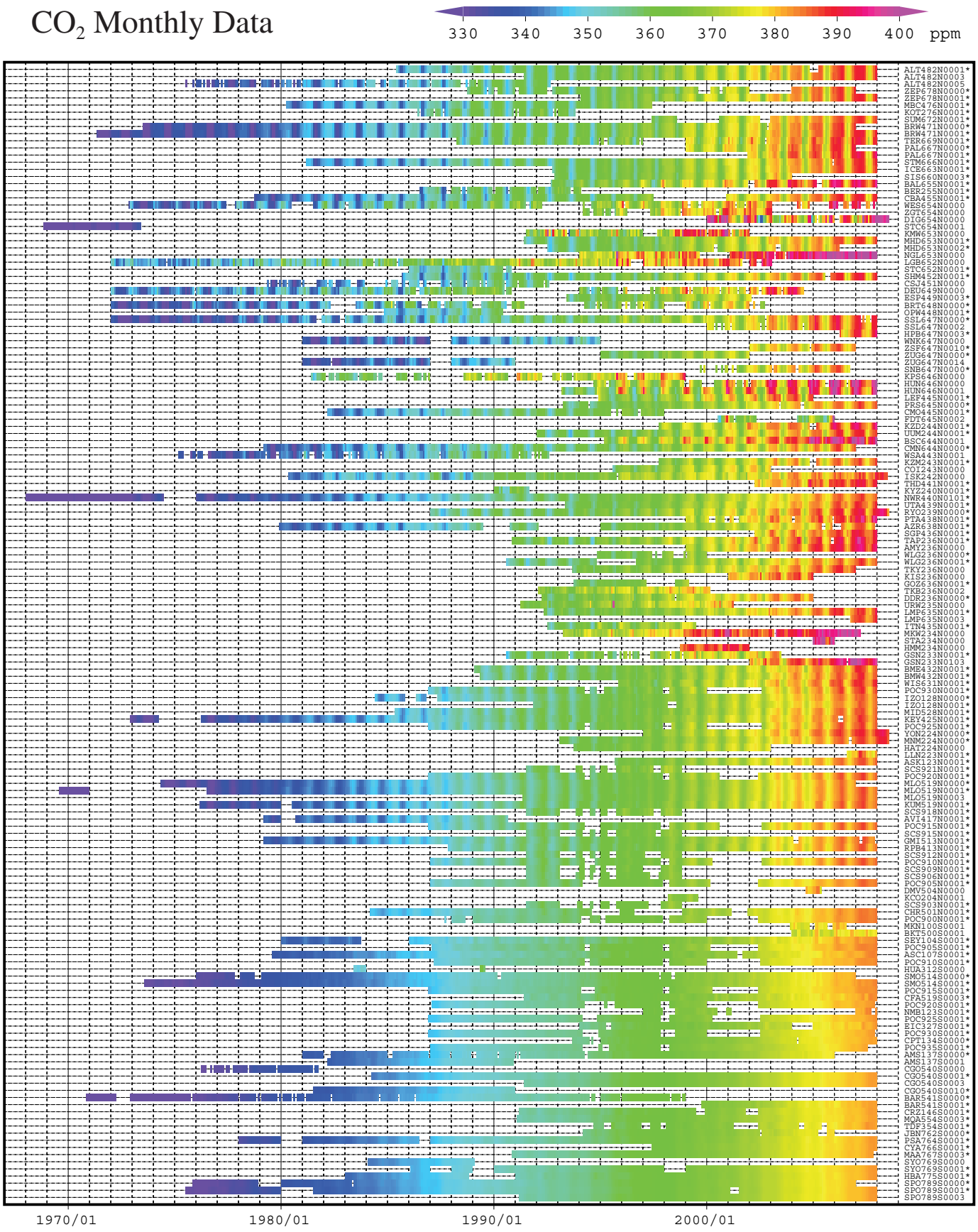

Plate 3.1 Monthly mean CO_2 mole fractions that have been reported to the WDCGG. The mole fractions are illustrated in different colors. The sites are listed in order from north to south. In the case where data are reported for two or three different altitudes, only the data at the highest altitudes are illustrated. In the case where monthly means are not reported, the WDCGG calculates them from hourly or other mole fractions reported to the WDCGG by simple arithmetic mean. The data from the sites with an asterisk at the end of the station index are used for the analysis shown in Plate 3.2. (see Chapter 2)

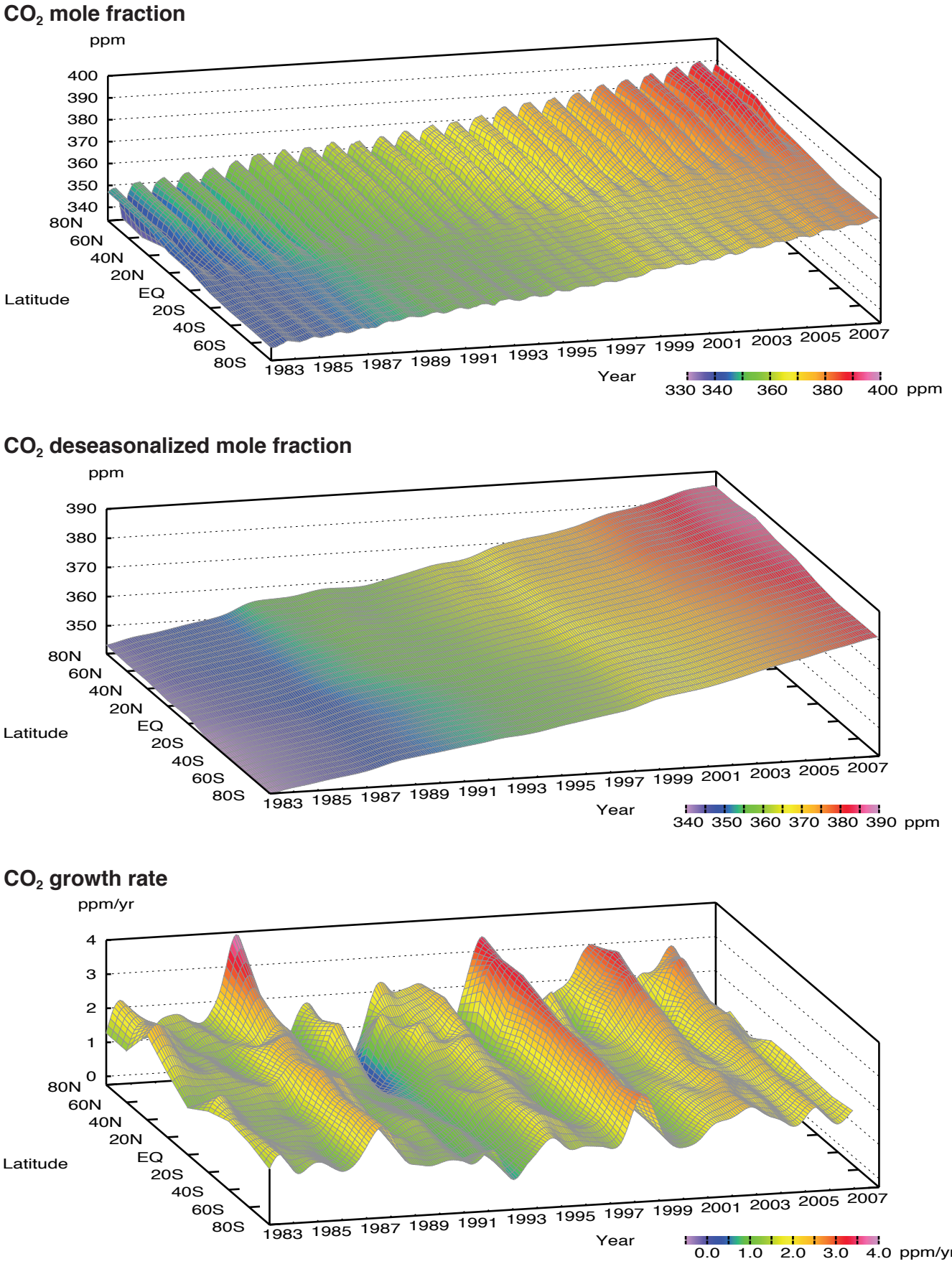

Plate 3.2 Variation of zonally averaged monthly mean CO_2 mole fractions (top), deseasonalized long-term trends (middle), and growth rates (bottom). The zonally averaged mole fractions are calculated for each 20° zone. The deseasonalized trends and growth rates are derived as described in Chapter 2.

3. Carbon Dioxide (CO_2)

Basic information on CO_2 with regard to environmental issues

Carbon dioxide (CO_2) has strong absorption bands in the infrared region and is the biggest contributor to the greenhouse effect. CO_2 accounted for 63% of the radiative forcing caused by the increase in well-mixed greenhouse gases from 1750 to 2005 (IPCC, 2007).

The balance between its emission and absorption at the surface of the Earth or oceans determines the mole fraction of CO_2 in the atmosphere. About 762 gigatonnes of carbon are present in the atmosphere as CO_2. Carbon in the atmosphere is exchanged with two other large reservoirs, the terrestrial biosphere and the oceans. CO_2 exchanges between the atmosphere and terrestrial biosphere occur mainly through absorption by photosynthesis and emission from the respiration of plants and the decomposition of organic soils. These biogenic activities vary seasonally, resulting in large seasonal variations in the level of CO_2. CO_2 is transported between the atmosphere and oceans in a direction determined by the relative CO_2 mole fraction, and varying by time and place.

The current mole fractions of atmospheric CO_2 far exceed pre-industrial values, dating back 650,000 years (Solomon *et al*., 2007). Based on the results of ice core studies, the mole fraction of atmospheric CO_2 in pre-industrial times was about 280 ppm (IPCC, 2007). The emission of CO_2 due to human activities has increased since the beginning of the industrial era, and been distributed into the atmosphere, oceans and terrestrial biosphere. The global carbon cycle, which is comprised mainly of CO_2, is not fully understood. About half of anthropogenic CO_2 emissions have remained in the atmosphere, the rest being removed by sinks, including the terrestrial biosphere and oceans. However, the amount of CO_2 removed from the atmosphere by sinks varies greatly over time (Figure 3.1).

Carbon isotopic studies have demonstrated the importance of the terrestrial biosphere and oceans as sources and sinks (Francey *et al.*, 1995; Keeling *et al.*, 1995; and Nakazawa *et al.*, 1993, 1997a). In contrast, the atmospheric content of O_2 is dependent mainly on its removal by the burning of fossil fuels and on its release from the terrestrial biosphere. Therefore, the uptake of carbon by the terrestrial biosphere and oceans can be estimated from the combination of measurements of O_2 (O_2/N_2) and CO_2 (IPCC, 2001). Solomon *et al*., (2007) showed that the oceans and the terrestrial biosphere absorb about 31% and 12%, respectively, of the CO_2 emitted from the burning of fossil fuels in 2000–2005, while the remaining 57% contributed to annual increases in CO_2 level in the atmosphere.

Large amounts of CO_2 are exchanged among these reservoirs, and the global carbon cycle is coupled with the climate system on seasonal, yearly and decadal time scales. Accurate understanding of the global carbon cycle is essential for the estimation of future CO_2 mole fractions in the atmosphere.

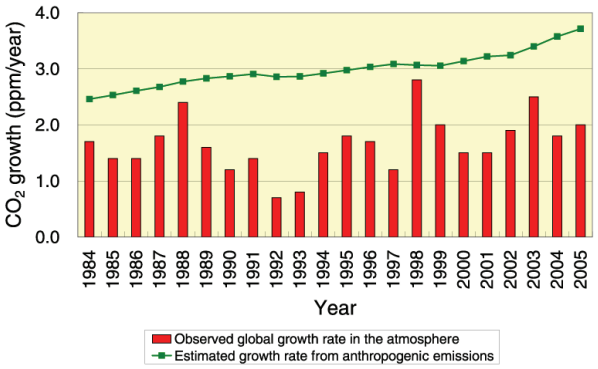

Fig. 3.1 . Annual mean growth rates of CO_2 in the atmosphere calculated from observational data (red column) and from data for anthropogenic emissions (green curve). The emissions were calculated by CDIAC based on United Nations Energy Statistics, and the observed growth rates were calculated by the WDCGG. The observational CO_2 abundance is expressed as mole fraction with respect to dry air, while the CO_2 amount calculated from anthropogenic emissions is based on the atmosphere including water vapor usually in a mole fraction less than 1%.

The observation sites that submitted data for CO_2 to the WDCGG are shown on the map at the beginning of this chapter. They include *in situ* stations performing continuous measurements as well as flask-sampling stations, including those in the NOAA/ESRL/GMD cooperative air sampling network. In addition to such fixed stations, mobile stations on ships and aircraft and other stations observing on an event basis report their data to the WDCGG (see Appendix: LIST OF OBSERVATION STATIONS).

Annual variations in the mole fraction of CO_2 in the atmosphere

All the monthly mean mole fractions of CO_2 that have been reported to the WDCGG are shown in Plate 3.1, with mole fraction levels illustrated in different colours. Global, hemispheric and zonal mean mole fractions were analysed based on data from selected stations in background conditions (see the caption to Plate 3.1). Latitudinally averaged mole fractions of atmospheric CO_2, together with their deseasonalized components and growth rates, are shown as three-dimensional representations in Plate 3.2. They

indicate that the seasonal variations in mole fraction are large in northern high and mid-latitudes, but are indistinct in the Southern Hemisphere; the increases in the Northern Hemisphere, which precede those in the Southern Hemisphere, propagate to the latter, and the interannual variation in growth rate is large in the Northern Hemisphere.

Figure 3.2 shows global monthly mean mole fractions and their growth rates from 1983 to 2007. The global average mole fraction reached a new high in 2007 at 383.1 ppm, 137% of the pre-industrial level. The increase from 2006 to 2007 was 1.9 ppm, larger than the average annual increase for the 1990s (about 1.5 ppm/yr).

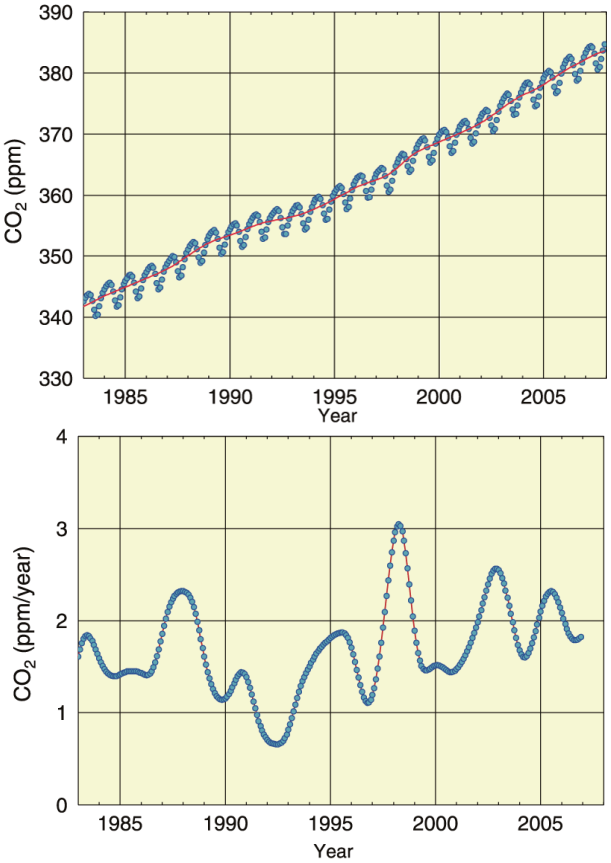

Fig. 3.2 Global monthly mean mole fractions of CO_2 from 1983 to 2007, with deseasonalized long-term trends shown as a red line (top) and their growth rates (bottom).

The average global growth rate for 1997–2007 was 2.00 ppm/year. There were large interannual variations of 3.1 ppm/year in April 1998 and 0.7 ppm/year in June 1992. Growth rates exceeding 2 ppm/year were seen in 1987/1988, 1997/1998, 2002/2003 and 2005.

Figure 3.3 shows monthly mean mole fractions and long-term trends from 1983 to 2007 for each 30° latitudinal zone, indicating clear long-term increases in both hemispheres and seasonal variations in the Northern Hemisphere.

As shown in Figure 3.4, the growth rates for each 30° latitude zone fluctuated between –0.3 and 3.5 ppm/year, with relatively large interannual variabilities in northern high latitudes. The high growth rates in 1987/1988, 1997/1998, 2002/2003 and 2005 were observed for all 30° latitude zones, while negative rates were recorded in northern high latitudes in 1992.

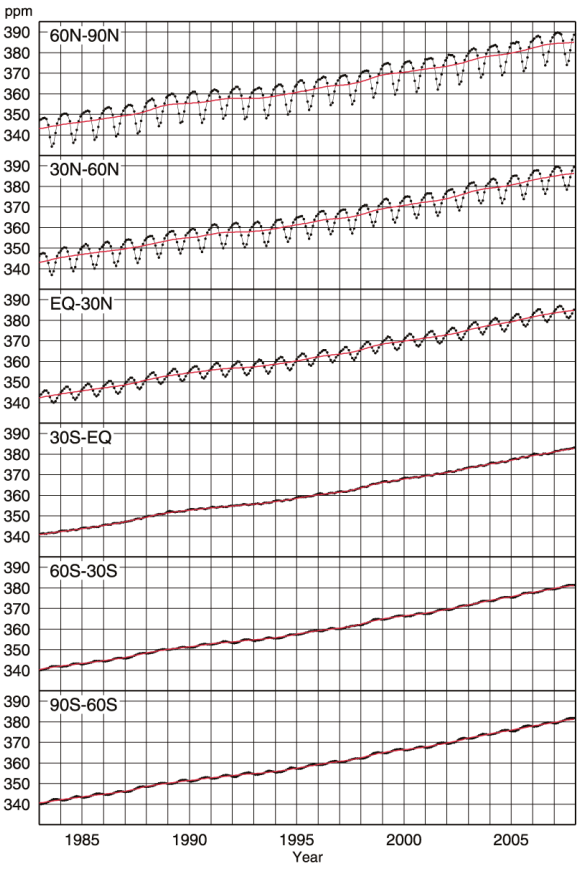

Fig. 3.3 Monthly mean mole fractions of CO_2 from 1983 to 2007 for each 30° latitudinal zone (dots) and their deseasonalized long-term trends (red lines).

Changes in growth rate are known to be associated with El Niño-Southern Oscillation (ENSO). The El Niño events in 1982/1983, 1986–1988, 1991/1992, 1997/1998 and 2002/2003 coincided with high growth rates of CO_2, with an exception in 1992. The high growth rates in 2005, without El Niño events, may be related to the global high temperature, especially in the Northern Hemisphere. The growth rates of CO_2 observed by aircraft at high altitudes (8–13 km) over the Pacific Ocean also have a similar relationship with ENSO (Matsueda *et al.*, 2002). During El Niño events, the up-welling of CO_2-rich ocean water in the eastern equatorial Pacific was suppressed, resulting in reduced CO_2 emissions from this area. In contrast, El Niño events induce high temperature anomalies in many areas, particularly in the Tropics, resulting in increased CO_2 emissions from the terrestrial biosphere through the enhanced respiration of plants and

activated decomposition of organic matter in soil (Keeling *et al.*, 1995). This effect is enhanced by the suppressed plant photosynthesis in areas of anomalously low precipitation, particularly in the Tropics. These oceanic and terrestrial processes during El Niño events have opposite effects. However, Dettinger and Ghil (1998) suggested that the former was limited to the eastern equatorial Pacific, while the latter was seen more globally. Thus, the global growth rate in the mole fraction of CO_2 responds almost synchronously to changes in the terrestrial biosphere due to global temperature variations associated with El Niño events.

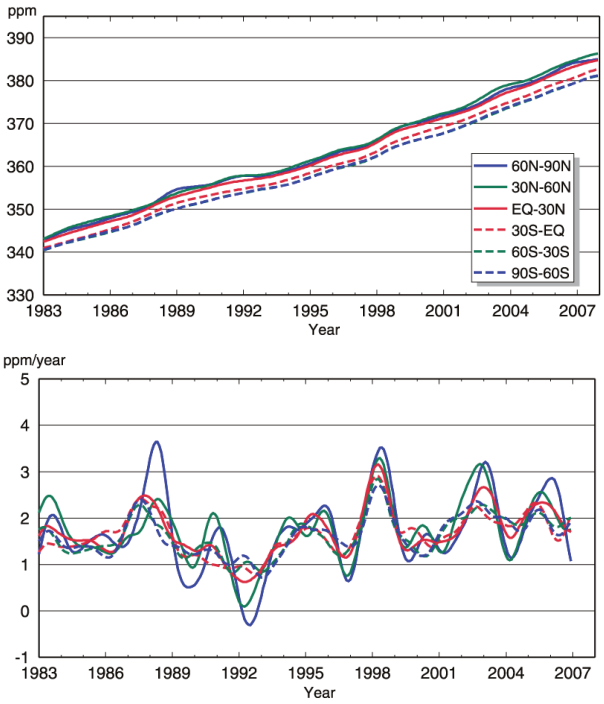

Fig. 3.4 Long-term trends in the mole fraction of CO_2 for each 30° latitudinal zone (top) and their growth rates (bottom) .

Carbon isotope (^{13}C) studies have also shown that atmospheric CO_2 variations accompanying El Niño events are related to the flux between the terrestrial biosphere and atmosphere, rather than that between the oceans and atmosphere (Keeling *et al.*, 1989; Nakazawa *et al.*, 1993; Morimoto *et al.*, 2000). The El Niño event in 1997/1998, which was one of the most severe in the 20th century, brought about high temperatures and low precipitation on a global scale (WMO, 1999b), resulting in frequent wildfires and drought in Southeast Asia. Such meteorological conditions perturbed the global carbon cycle, and are considered to have intensified CO_2 emission from the terrestrial biosphere. However, an exceptionally low CO_2 growth rate occurred during the El Niño event in 1991/1992.

The injection of 14–20 Mt of SO_2 aerosols into the stratosphere by the Mt. Pinatubo eruption in June 1991 affected the radiation budget and atmospheric circulation (Hansen *et al.*, 1992; Stenchikov *et al.*, 2002), and resulted in a drop in global temperature. Angert *et al.*, (2004) suggested that the low CO_2 growth rate observed during this El Niño event was due to reduced CO_2 emissions caused by consequent changes in the respiration of terrestrial vegetation and the decomposition of organic matter (Conway *et al.*, 1994; Lambert *et al.*, 1995; Rayner *et al.*, 1999), and by enhanced CO_2 absorption due to intensive photosynthesis caused by an increase in diffuse radiation (Gu *et al.*, 2003).

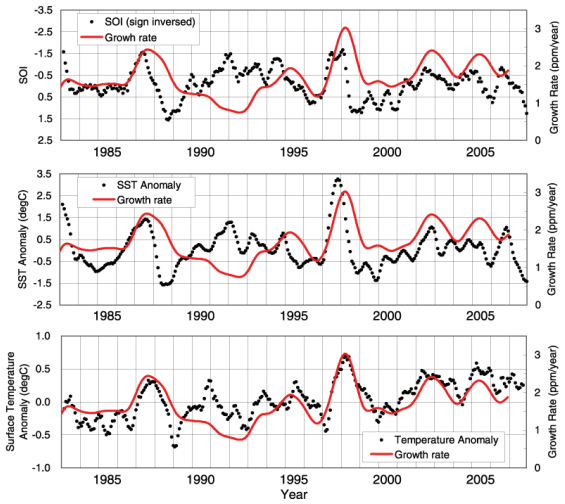

Fig. 3.5 Time series of CO_2 growth rates in the Tropics (30°N–30°S), compared with the Southern Oscillation Index with inversed sign (top), SST anomaly in the eastern equatorial Pacific (5°N–5°S, 150°W–90°W) (middle) and anomaly in temperature on land in the Tropics calculated from JRA-25 reanalysis data (bottom). The red lines and black dots show the growth rates and compared values respectively expressed as running mean over 5 months.

Figure 3.5 shows time series of the growth rates of CO_2 in the Tropics (within 30° from 1983 to 2006), the Southern Oscillation Index (SOI), the Sea Surface Temperature (SST) anomaly in the eastern equatorial Pacific (5°N–5°S, 150°W–90°W) and the temperature anomaly on land in the Tropics calculated from data of Japanese Re-Analysis 25 years (JRA-25: Onogi *et al.*, 2007). The data for SOI and SST are provided by the WMO DDBs (Distributed Data Bases). In the figure, values for SOI, SST anomaly and temperature anomaly are expressed as running means over five months to extract seasonal variation. The growth rate in the Tropics corresponded with the SOI and SST anomalies, with a certain time lag, with an exception observed during 1992. The growth rate also corresponded to the temperature anomaly on land in the Tropics, including 1992. These results suggest that the growth rate of CO_2 in the Tropics is related to ENSO events and more closely to temperature anomalies on tropical

land, indicating a strong effect of the tropical biosphere on the mole fraction of CO_2 in the Tropics.

Seasonal cycle in the level of CO_2 in the atmosphere

Figure 3.6 shows average seasonal cycles in the mole fraction of CO_2 for each 30° latitudinal zone. The seasonal cycles are clearly large in amplitude in northern high and mid-latitudes and small in the Southern Hemisphere. Oceanic uptake (Ramonet *et al.*, 1996) and biomass burning (Wittenberg *et al.*, 1998) are thought to influence the seasonal variation. However, these large seasonal cycles in the Northern Hemisphere are characterized by rapid decreases from June to August and large returns from September to December. They result from the activity of the terrestrial biosphere, *i.e.*, absorption of CO_2 by photosynthesis, and emission by the respiration of vegetation and the decomposition of organic matter by microbes in soil (*e.g.*, Nakazawa *et al.*, 1997b).

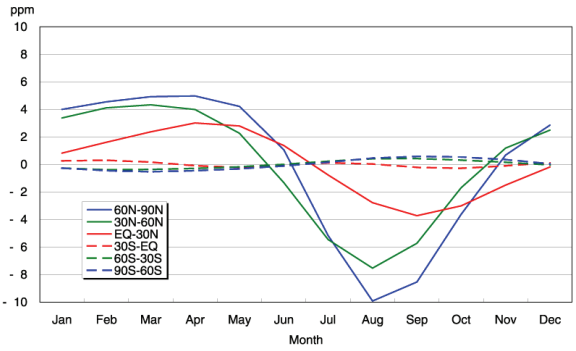

Fig. 3.6 Average seasonal cycles in the mole fraction of CO_2 for each 30° latitudinal zone obtained by subtracting long-term trends.

In northern high and low latitudes, the mole fractions of CO_2 reach their maximum with a lag of one or two months. The minimum values appear in August in northern high and mid-latitudes and in September in northern low latitudes. The peak in low latitudes is delayed because it takes time for the seasonal variation in high latitudes to reach low latitudes (Tanaka *et al.*, 1987), and the seasonal cycle in the activity of the terrestrial biosphere in low latitudes lags behind that in mid-latitudes due to the timing of wet and dry seasons (Nemry *et al.*, 1996).

In the Southern Hemisphere, seasonal variations show small amplitudes with a half-year delay due to small amounts of net emission and absorption by the terrestrial biosphere. Seasonal variations in both northern and southern mid-latitudes are apparently superimposed in southern low latitudes (0–30°S). The direct influence of sources and sinks in the Southern Hemisphere may be partially cancelled by the propagation of an antiphase variation from the Northern Hemisphere.

Figure 3.7 shows latitudinal distributions of the mole fractions of CO_2 in January, April, July and October 2007. Latitudes around 30°N were positive, and the mole fractions increased towards higher latitudes in January and April, and decreased towards higher latitudes in July, corresponding to the large seasonal variation in northern high and mid-latitudes.

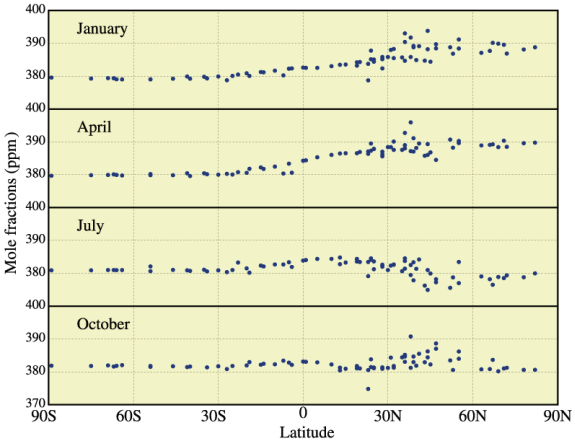

Fig. 3.7 Latitudinal distributions of the monthly mean mole fractions of CO_2 in January, April, July and October 2007.

Annual variation in the level of CO_2 in the upper atmosphere

Since 1993, the Meteorological Research Institute of JMA has measured trace gases, including CO_2, at altitudes of 8–13 km over the western Pacific using commercial flights between Japan and Australia in cooperation with Japan Airlines Foundation, the Ministry of Land, Infrastructure, Transport and Tourism, and Japan Airlines, and has submitted these observational data to the WDCGG. Figure 3.8 shows time series of the mole fraction of CO_2 in the upper air. The trends are obtained by linear interpolation, as described in Chapter 2. The increasing mole fractions of CO_2 along the entire route, as well as their seasonal variations in the Northern Hemisphere, were similar to those on the surface, but the amplitudes of the seasonal variations were smaller.

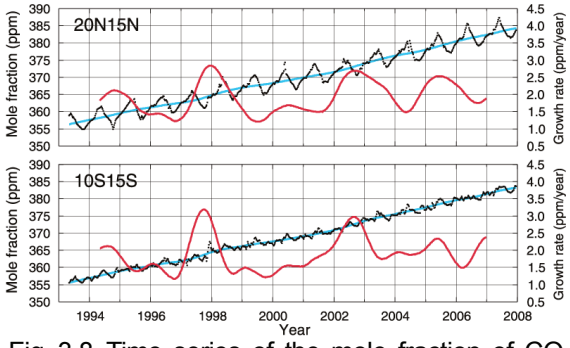

Fig. 3.8 Time series of the mole fraction of CO_2 (dots), with their deseasonalized trends (blue lines) and growth rates (red lines), observed at altitudes of 8–13 km over the western Pacific in the latitudinal zones of 15–20°N and 10–15°S.

4.

METHANE

(CH_4)

● : CONTINUOUS STATION

△ : FLASK STATION

□ : FLASK MOBILE (SHIP)

▼ : REMOTE SENSING STATION

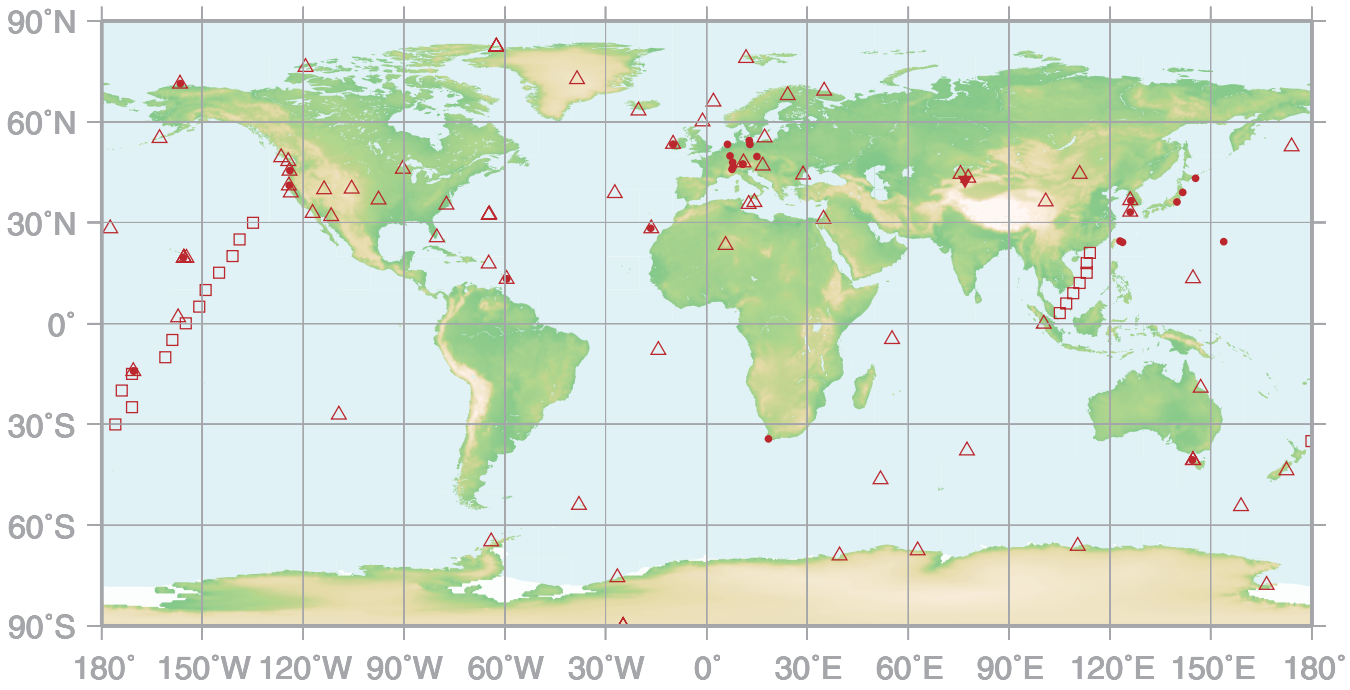

This map shows locations of the stations that have submitted data for monthly mean mole fraction.

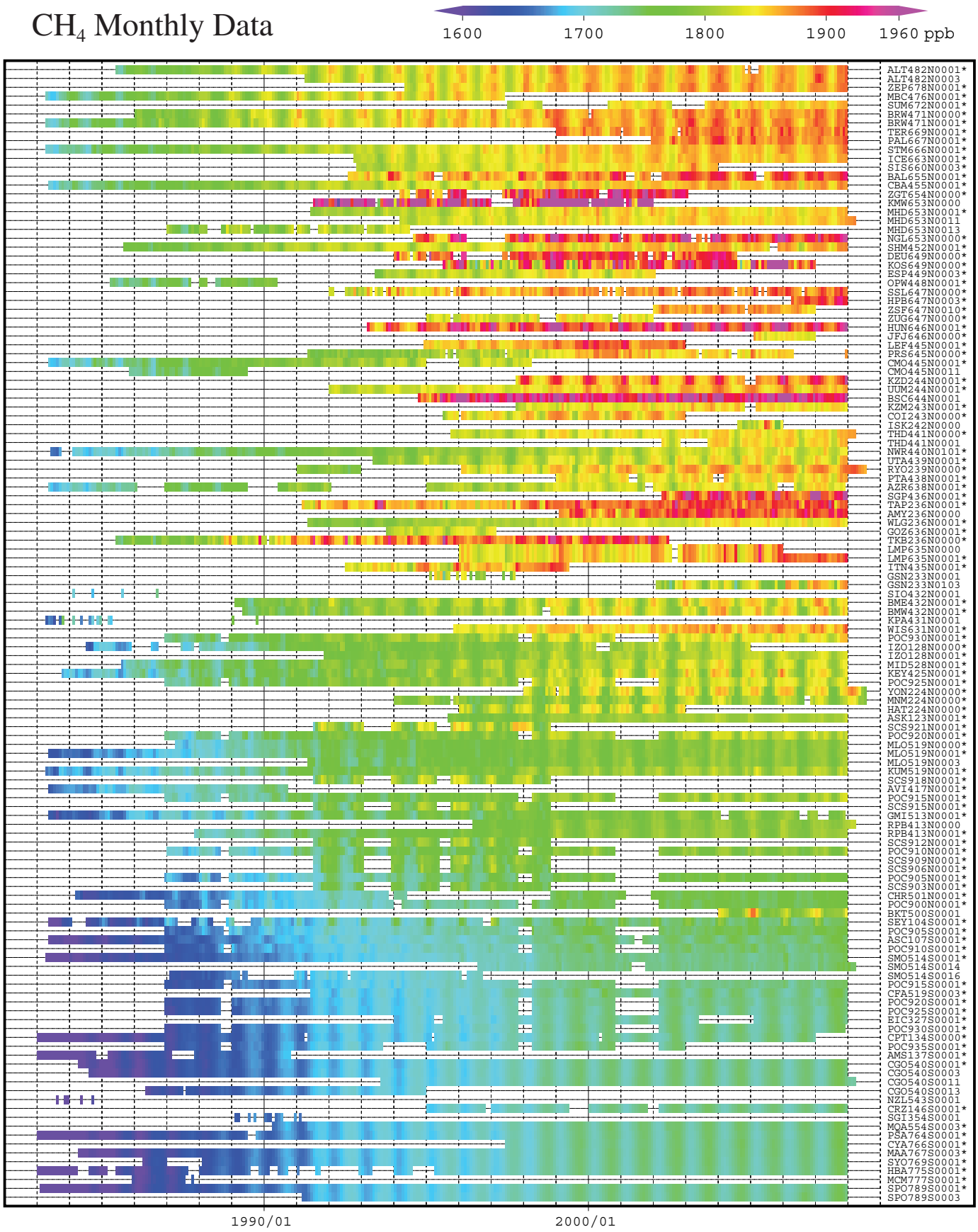

Plate 4.1 Monthly mean CH_4 mole fractions that have been reported to the WDCGG. The mole fractions are illustrated in different colors. The sites are listed in order from north to south. In the case where data are reported for two or three different altitudes, only the data at the highest altitudes are illustrated. In the case where monthly means are not reported, the WDCGG calculates them from hourly or other mole fractions reported to the WDCGG by simple arithmetic mean. The data from the sites with an asterisk at the end of the station index are used for the analysis shown in Plate 4.2. (see Chapter 2)

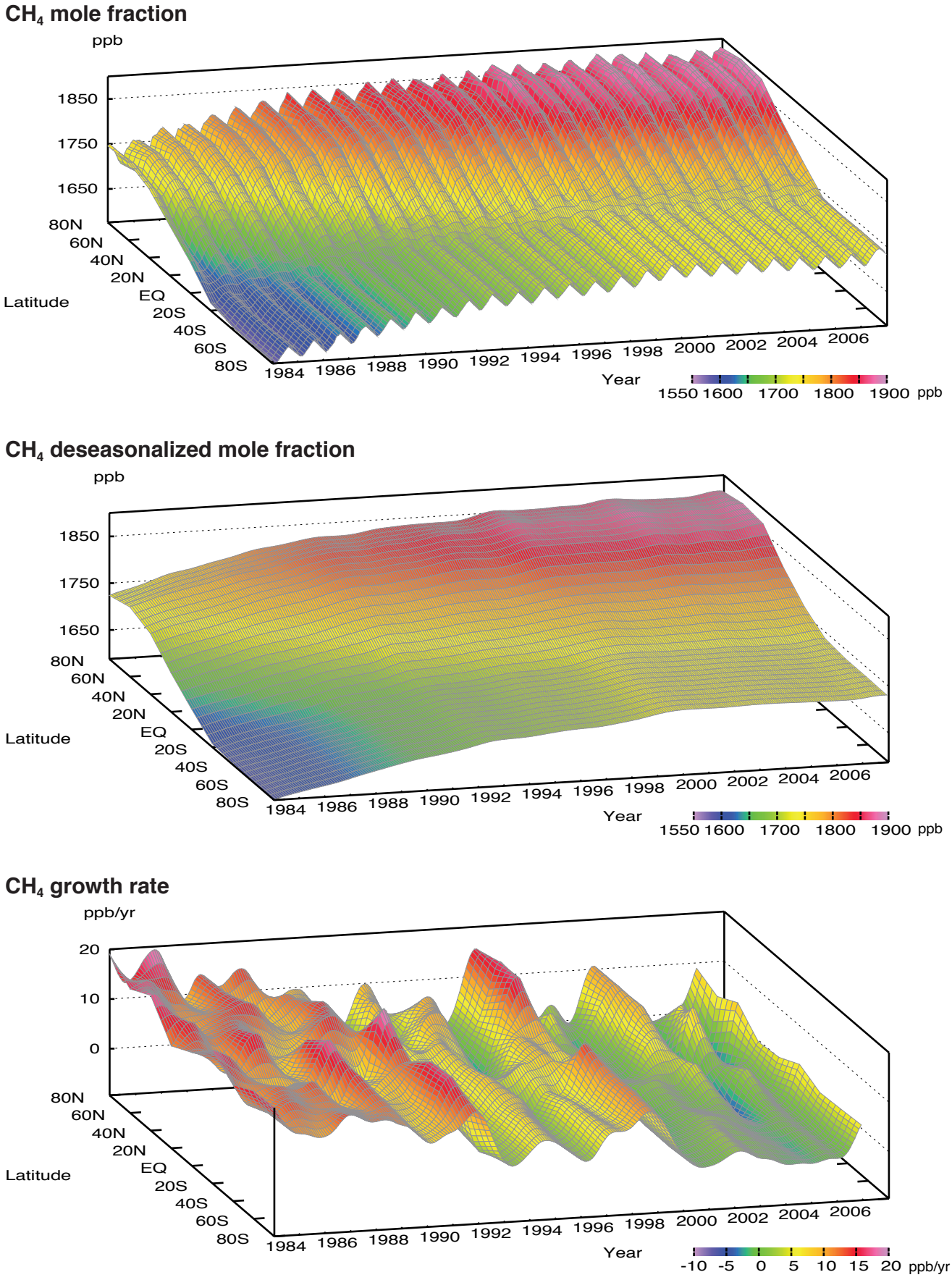

Plate 4.2 Variation of zonally averaged monthly mean CH_4 mole fractions (top), deseasonalized long-term trends (middle), and growth rates (bottom). The zonally averaged mole fractions are calculated for each 20° zone. The deseasonalized trends and growth rates are derived as described in Chapter 2.

4. Methane (CH_4)

Basic information on CH_4 with regard to environmental issues

Methane (CH_4) is the second most significant greenhouse gas, but has been estimated to have a 23 times greater global warming potential per molecule over a 100 year horizon than CO_2. Between 1750 and 2005, CH_4 accounted for 18% of the radiative forcing caused by the increase in well-mixed greenhouse gases (IPCC, 2007).

Analyses of air trapped in ice cores from Antarctica and the Arctic revealed that the current atmospheric CH_4 mole fraction is the highest over the last 650,000 years (Solomon *et al.*, 2007b). The mole fraction of CH_4 remained steady at 700 ppb from 1000 A.D. until the start of the industrial era (Etheridge *et al.*, 1998), after which it began to increase. The rate of increase has been small over the last few years. Measurements in ice cores from the Antarctica and Greenland have shown that the difference in CH_4 mole fractions between the Northern and Southern Hemispheres ranged from 24–58 ppb between 1000 and 1800 A.D. (Etheridge *et al*., 1998), but is now as high as about 150 ppb (see Fig. 4.3), reflecting more emissions in the Northern Hemisphere, where there are major anthropogenic sources.

CH_4 is emitted by both natural and anthropogenic sources, including natural wetlands, oceans, landfills, rice paddies, enteric fermentation, gas drilling and biomass burning. Denman *et al.* (2007) estimated the global emission to be 582 teragrams (Tg) CH_4 per year, with more than 60% related to anthropogenic activities. CH_4 is destroyed by reaction with hydroxyl radicals (OH) in both the troposphere and stratosphere, and by reaction with chlorine atoms and O (^{1}D), an excited state of oxygen, in the stratosphere. CH_4 is one of the most important sources of water vapour in the stratosphere and has an atmospheric lifetime of about 12 years. However, the mole fraction of OH radicals is affected by ambient temperature and humidity. In addition, emissions from some sources are dependent on air temperature. Furthermore, Keppler *et al*. (2006) estimated that living plants and plant litter emit 62–236 and 1–7 Tg of methane per year, respectively. More information regarding sources and sinks of CH_4 must be collected to better estimate the budget of atmospheric CH_4.

The observational sites that have submitted data for CH_4 to the WDCGG are shown on the map at the beginning of this chapter.

Annual variation in the level of CH_4 in the atmosphere

All the monthly mean mole fractions of CH_4 that have been reported to the WDCGG are shown in Plate 4.1, with the mole fraction levels illustrated in different colours. Global, hemispheric and zonal mean mole fractions have been analysed based on data from selected stations in background conditions (see the caption for Plate 4.1). Latitudinally averaged atmospheric CH_4 mole fractions, together with their deseasonalized components and growth rates, are shown as three-dimensional representations in Plate 4.2. They indicate that the seasonal variations in mole fraction are larger in the Northern Hemisphere than in the Southern Hemisphere and that the increase in the Northern Hemisphere expands to the Southern Hemisphere. The growth rates vary on a global scale. These features are similar to those for CO_2 (see Section 3). A large latitudinal gradient in CH_4 mole fraction exists from the northern mid-latitudes to the Tropics, suggesting major sources in high and middle northern latitudes and sinks in the Tropics, where the mole fraction of OH radicals is higher.

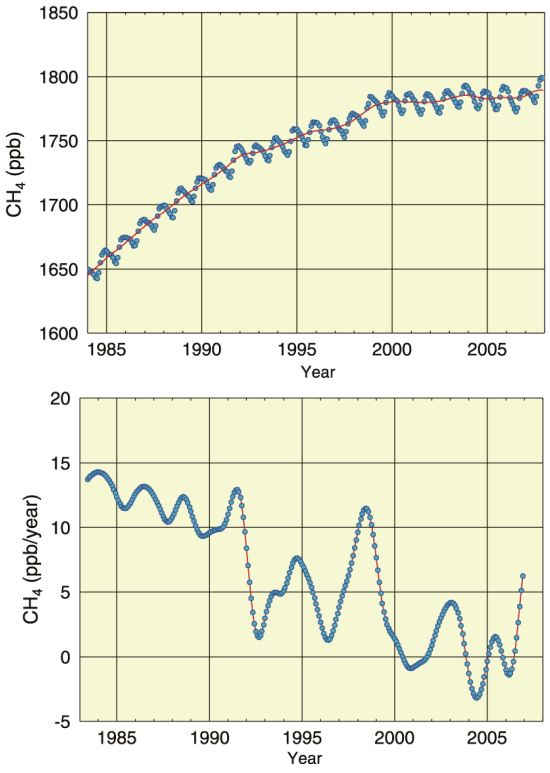

Fig. 4.1 Global monthly mean mole fractions of CH_4 from 1984 to 2007 with deseasonalized long-term trends in red line (top) and their growth rates (bottom).

Figure 4.1 shows global monthly mean mole fractions and the global growth rate from 1984 to 2007. The mean mole fraction was 1789 ppb in 2007, an increase of 6 ppb since 2006. This increase is the largest since 1998. Between 1997 and 2007, the average growth rate was 2.7 ppb/year. The current

mole fraction is 256% of its pre-industrial level. Figure 4.2 shows monthly mean mole fractions from 1984 to 2007 for each 30° latitudinal zone. The seasonal variation is small in the latitudinal zone between the equator and 30°S.

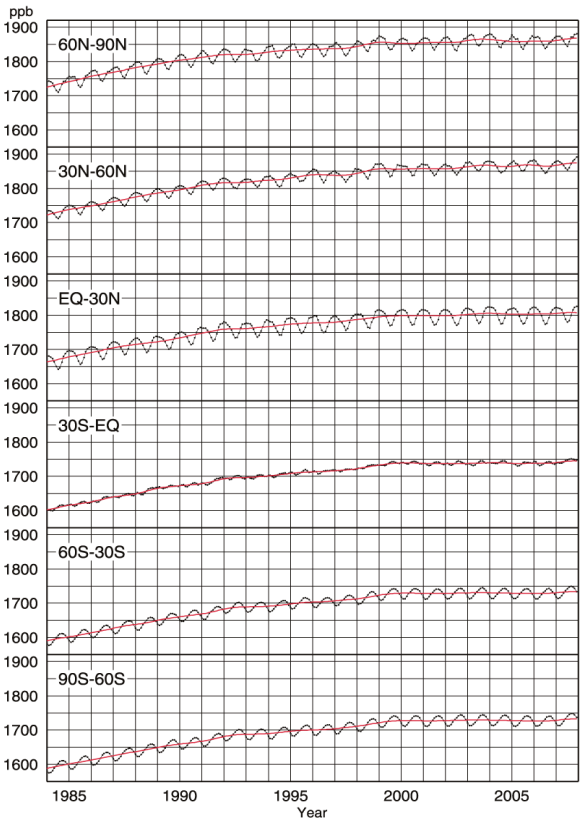

Fig. 4.2 Monthly mean mole fractions of CH_4 from 1984 to 2007 for each 30° latitudinal zone (dots) and their deseasonalized long-term trends (red lines) .

Figure 4.3 shows deseasonalized long-term trends for each 30° latitudinal zone and their growth rates. The deseasonalized long-term trends are distinguished by high mole fractions in the northern high and mid-latitudes and low mole fractions in southern latitudes. In the 1990s, these growth rates clearly decreased in all latitudinal zones. The growth rates in the Southern Hemisphere and the northern subtropics were elevated in 1991, but the global growth rate fell to about 1 ppb/year around 1992 and 1996. In 1998, the global growth rate increased to about 12 ppb/year, particularly in northern high and mid-latitudes, where the growth rates were over 15 ppb/year. In 2000 and 2001, the global growth rate decreased to around –1 ppb/year. Around 2002/2003, the growth rates increased in the Northern Hemisphere, especially in northern high and mid-latitudes where it reached about 10 ppb/year. The global growth rate was –3 ppb/year in 2004 and 1 ppb/year in 2005. Despite the large growth rates in 1998 and 2002/2003, during El Niño events, the global mean mole fraction was relatively stable between 1999 and 2006. However, the growth rates during 2007 increased significantly throughout the entire monitoring network (Rigby, *et al.*, 2008).

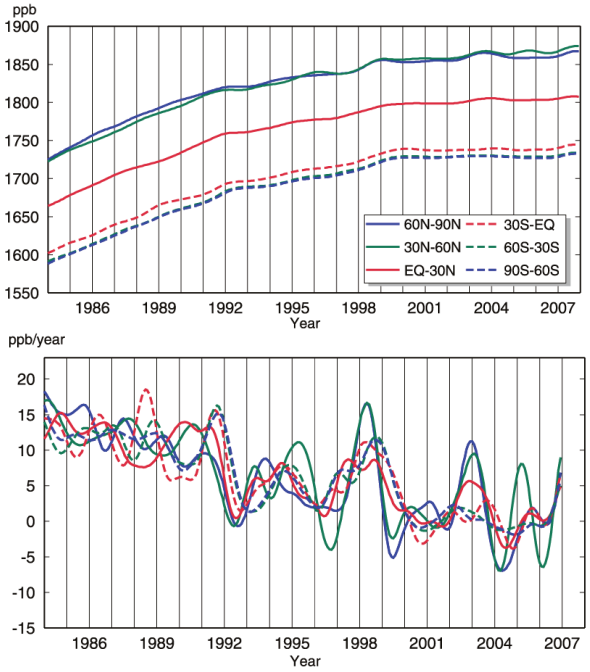

Fig. 4.3 Long-term trends in the mole fraction of CH_4 for each 30° latitudinal zone (top) and their growth rates (bottom).

Bekki and Low (1997) suggested that high temperatures result in increased CH_4 emissions from wetlands and enhanced destruction of CH_4 by increased OH radical levels. The relationship between the global growth rate and temperature anomalies showed that the former exceeds the latter globally. Based on a study of the relationship between CH_4 mole fractions in ice cores or firn layers and global temperature anomalies, Etheridge *et al.* (1998) suggested that high CH_4 growth rates follow high global temperatures. Figure 4.4 shows interannual variations in global mean growth rate and global surface temperature anomaly. The global CH_4 growth rate fluctuations are overlaid by global mean temperature anomalies for the period 1990–1998. Outside this period, however, the interannual variations in global mean growth rate may have been caused by factors other than global temperature anomalies.

The large increase in CH_4 growth rate in 1991 may have been caused by decreased levels of OH radicals due to reduced UV radiation as a result of the eruption of Mt. Pinatubo in 1991 (Dlugokencky *et al.*, 1996) and the subsequent decrease in 1992 may have been attributed to increased OH radicals as a result of the stratospheric ozone depletion following this eruption (Bekki *et al.*, 1994). However, an analysis of monsoon activity suggested that these changes may have been caused by decreased emission from wetlands and rice paddy fields due to low temperatures, and more

abundant decomposition due to dryness (Lelieveld *et al.*, 1998). Observations of carbon isotopes, however, have suggested that the decrease in 1992 may have been caused by a reduction in biomass burning in low latitudes (Lowe *et al.*, 1997).

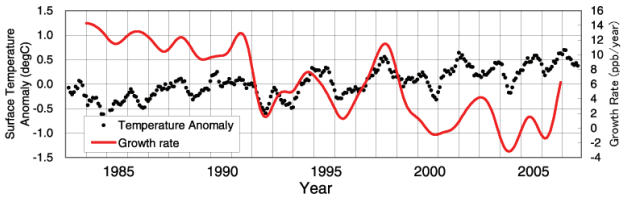

Fig. 4.4 Time series of the global mean growth rates of CH_4, compared with temperature anomalies on land from JRA-25 reanalysis data (Onogi *et al*., 2007). The solid line and dots show the growth rates and temperature anomalies respectively, expressed as running means over 5 months.

In 1998, the growth rates were high in all latitudes, which may have been due to increased emissions in northern high latitudes and tropical wetlands caused by high temperatures and increased precipitation, as well as by biomass burning in boreal forests, mainly in Siberia (Dlugokencky *et al.*, 2001). In contrast, Morimoto *et al.* (2006) estimated from isotope observations that the contribution of biomass burning to the increase in 1998 was about a half that of wetlands. The growth rates decreased afterward, but increased again upon occurrence of the El Niño event of 2002 /2003.

The cause of this long-term decreasing trend in CH_4 growth rate since 1991 remains unresolved. Lelieveld *et al*. (1998) noted that decreased global emissions of CH_4 led to a reduced CH_4 growth rate in the 1990s. Bousquet *et al.* (2006) have indicated that the decreased growth rate in the 1990s was caused by reduced emissions from anthropogenic sources, but that an increase in anthropogenic emissions may have been offset by a reduction in emissions from wetlands after 1999. Using a global tropospheric chemical transport model, however, Fiore *et al.* (2006) showed that the decrease in CH_4 growth rate resulted from an increase in tropospheric OH and lower tropospheric warming, accelerating CH_4 destruction by OH radicals. Thus, enhanced convective activity and subsequent production of NOx by lightning increases OH radicals in the troposphere.

Seasonal cycle in the level of CH_4 in the atmosphere

Figure 4.5 shows seasonal cycles in the mole fraction of CH_4 for each 30° latitudinal zone. The seasonal cycles are driven mainly by reaction with OH radicals, a major CH_4 sink in the atmosphere. These cycles are also affected by the degree and timing of CH_4 emission from sources such as wetlands and biomass burning along with its transportation. The seasonal cycles are large in amplitude in the Northern Hemisphere. Unlike CO_2, amplitudes were also large in southern high and mid-latitudes. Seasonally, both hemispheres showed minima in summer and maxima in winter. The seasonal variation in the mole fraction of CH_4 is almost consistent with that of OH radicals reacting with CH_4. Southern low latitudes have a distinct antiphase annual component superimposing the annual component of the seasonal cycle arising from southern mid-latitudes. The maximum in the former component occurs in boreal winter due to the interhemisphere transportation of CH_4 from the Northern Hemisphere. This phenomenon is observed at stations located in the western Indian Ocean, *e.g.,* Mahe Island in the Seychelles, and in the western and central equatorial Pacific, *e.g.,* Cape Matatula in American Samoa.

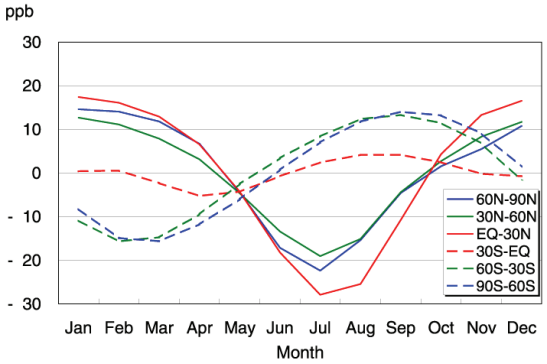

Fig. 4.5 Average seasonal cycles in the mole fraction of CH_4 for each 30° latitudinal zone obtained by subtracting long-term trends.

5.

NITROUS OXIDE

(N_2O)

● : CONTINUOUS STATION

△ : FLASK STATION

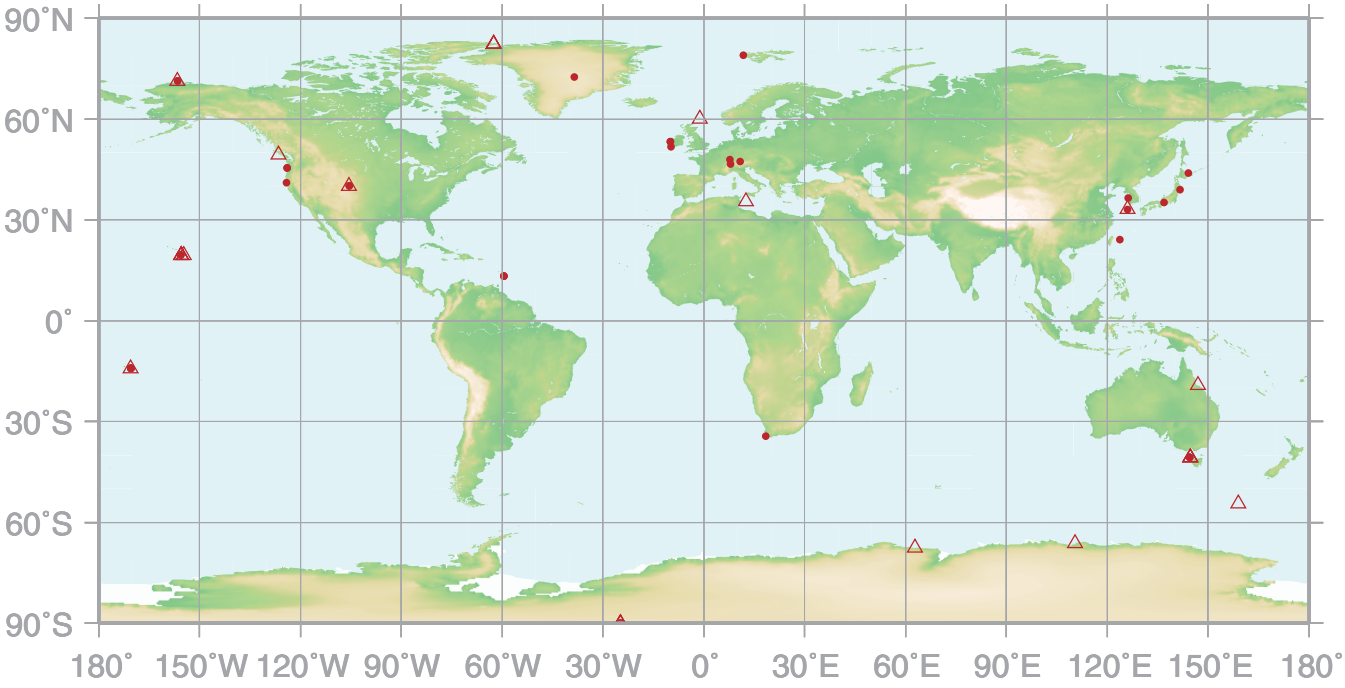

This map shows locations of the stations that have submitted data for monthly mean mole fraction.

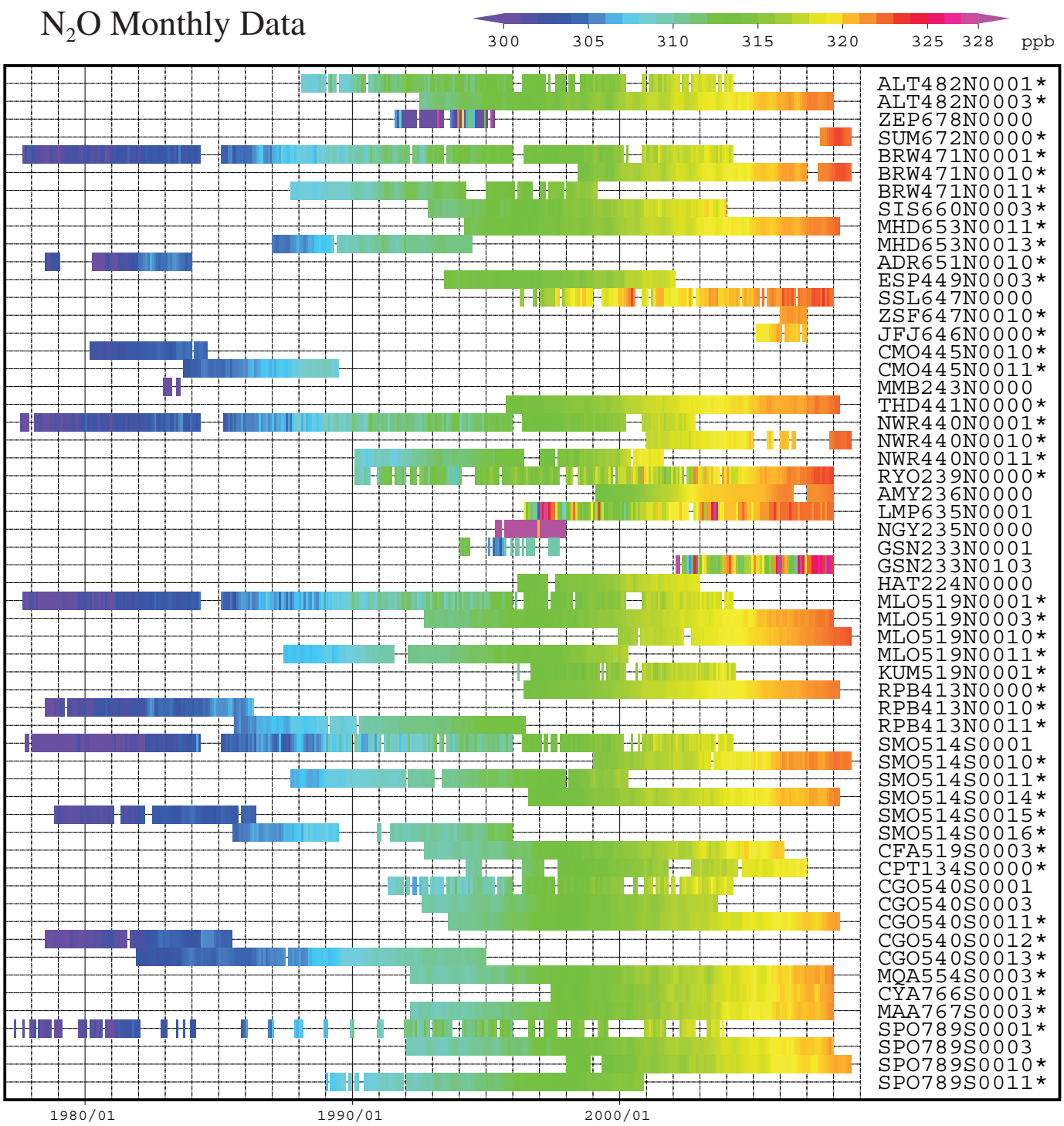

Plate 5.1 Monthly mean N_2O mole fractions that have been reported to the WDCGG. The mole fractions are illustrated in different colors. The sites are listed in order from north to south. The data from the sites with an asterisk at the end of the station index are used for the analysis shown in Plate 5.1. (see Chapter 2)

5. Nitrous Oxide (N_2O)

Basic information on N_2O with regard to environmental issues

Nitrous oxide (N_2O) is a relatively stable greenhouse gas in the troposphere with an "adjustment-time" of 114 years. Radiative forcing due to the increase of N_2O from 1750 to 2005 is estimated at 0.16 W/m^2, which is 6% of that of all long-lived and globally mixed greenhouse gases (IPCC, 2007). The mole fraction of N_2O in the atmosphere has increased steadily from about 270 ppb in pre-industrial times to a current value 19% higher.

N_2O is emitted into the atmosphere from natural and anthropogenic sources, including the oceans, soil, combustion of fuels, biomass burning, use of fertiliser and various industrial processes. One third of the total amount of emission has been attributed to anthropogenic sources. N_2O is removed from the atmosphere mainly by photo-dissociation in the stratosphere. However, the estimated amounts from sources and sinks have not yet been determined.

Annual variation of N_2O levels in the atmosphere

The observation sites that have submitted data for N_2O to the WDCGG are shown on the map at the beginning of this chapter. All the monthly mean mole fractions of N_2O that have been submitted to the WDCGG are shown in Plate 5.1, with the various mole fraction levels illustrated in different colours. The data submitted to the WDCGG show that N_2O mole fractions are increasing in both hemispheres. Figure 5.1 shows global monthly mean mole fractions from 1980 to 2007 and their long-term trends. The global mean mole fraction reached a new high of 320.9 ppb in 2007, an increase of 0.8 ppb over the year before. This value is 119% of the pre-industrial level. The mean growth rate of the global mean mole fraction during the period 1997–2007 was 0.77 ppb/year.

At some stations, the growth rates, defined as a difference in mole fraction from the year before, decreased considerably between 1991 and 1993, but were then similar to those observed in the 1980s. This may have been due to a decreased use of nitrogen-based fertilisers, lower biogenic emissions and larger stratospheric losses caused due to volcanic eruption-induced changes in the atmospheric circulation (IPCC, 2001).

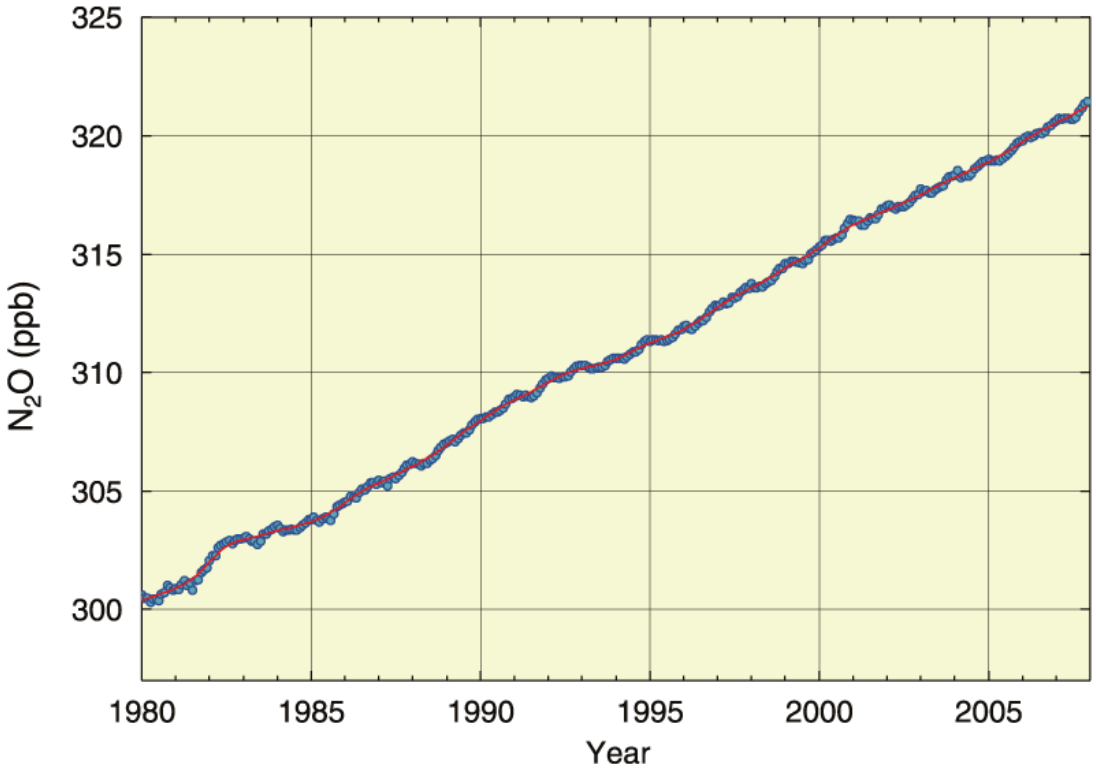

Fig. 5.1 Global monthly mean mole fractions of N_2O from 1980 to 2007 (dots) and their deseasonalized long-term trends (lines).

6.

HALOCARBONS AND OTHER HALOGENATED SPECIES

● : CONTINUOUS STATION

△ : FLASK STATION

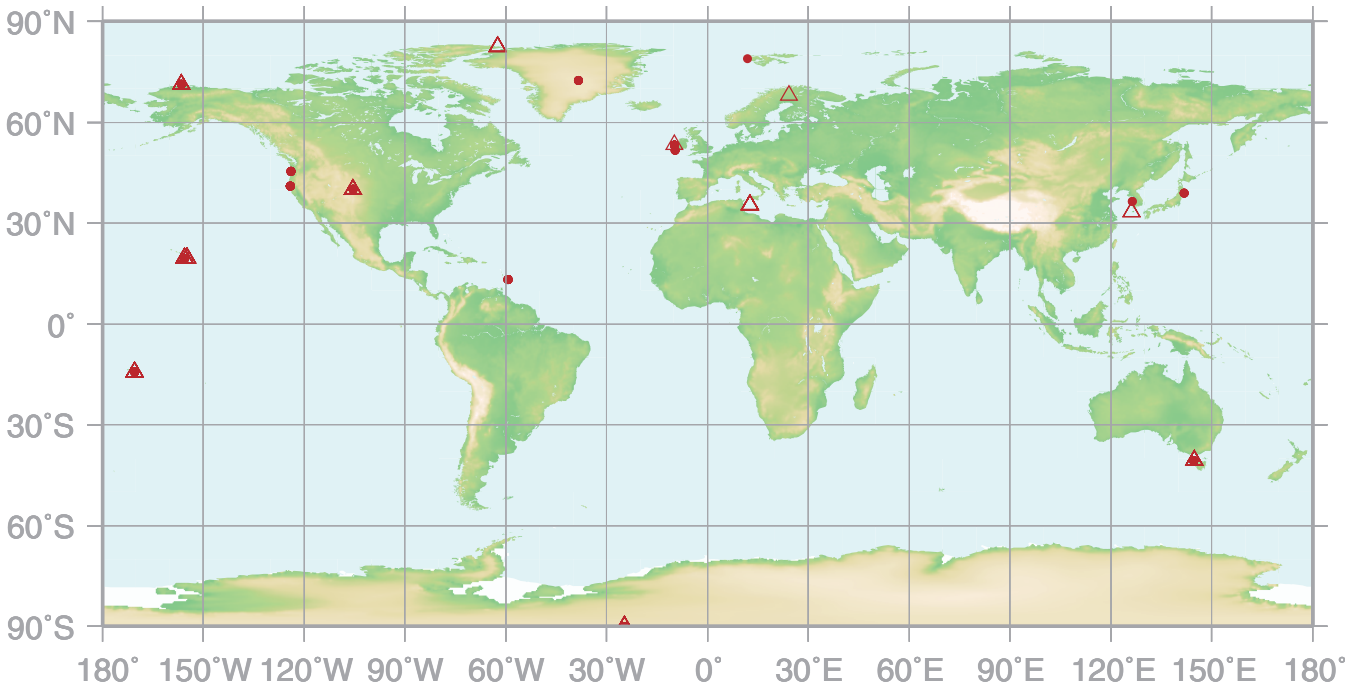

This map shows locations of the stations that have submitted data for monthly mean mole fraction.

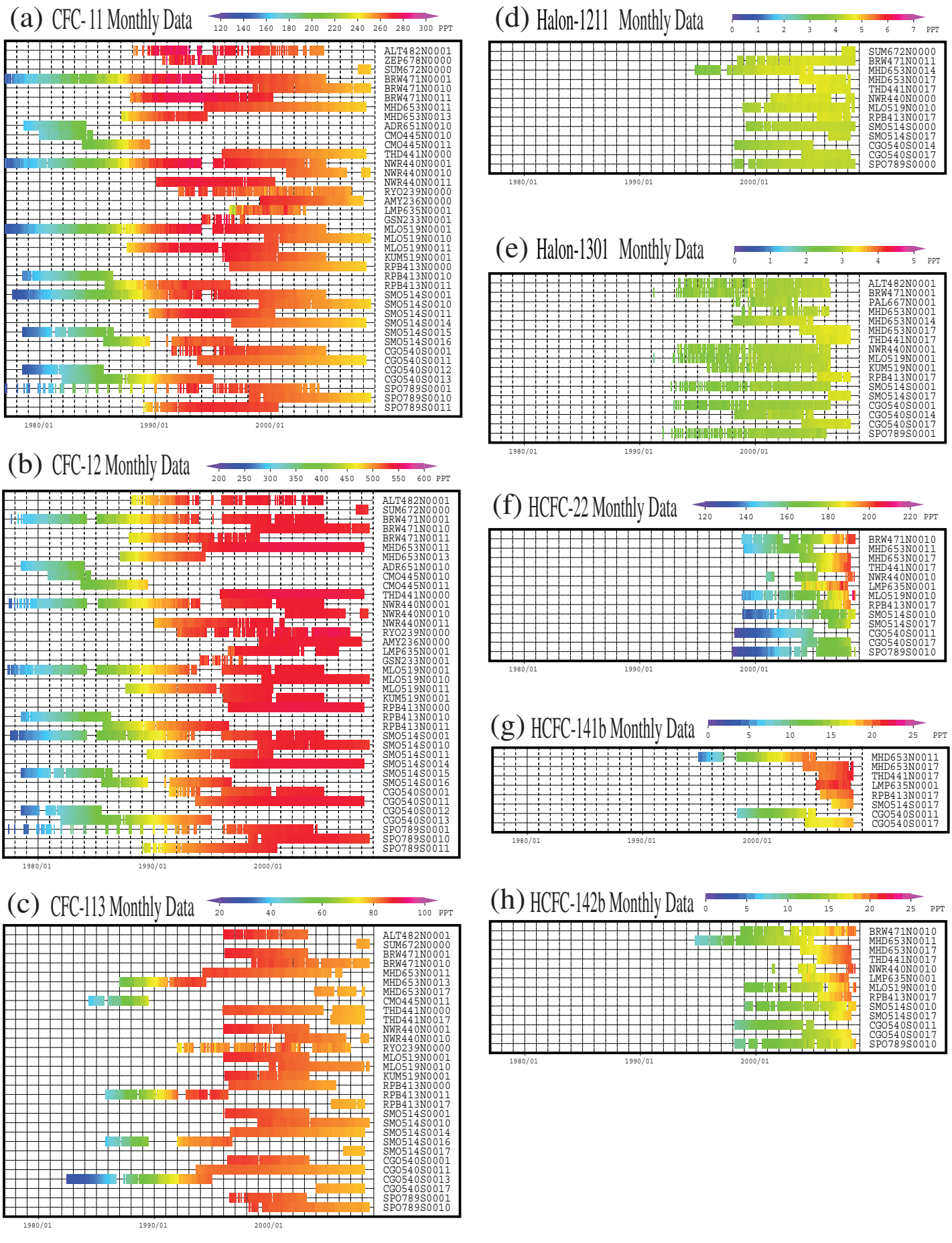

Plate 6.1 Monthly mean (a) CFC-11, (b) CFC-12, (c) CFC-113, (d) Halon-1211, (e) Halon-1301, (f) HCFC-22, (g) HCFC-141b, (h) HCFC-142b mole fractions that have been reported to the WDCGG. The mole fractions are illustrated in different colors. The sites are listed in order from north to south.

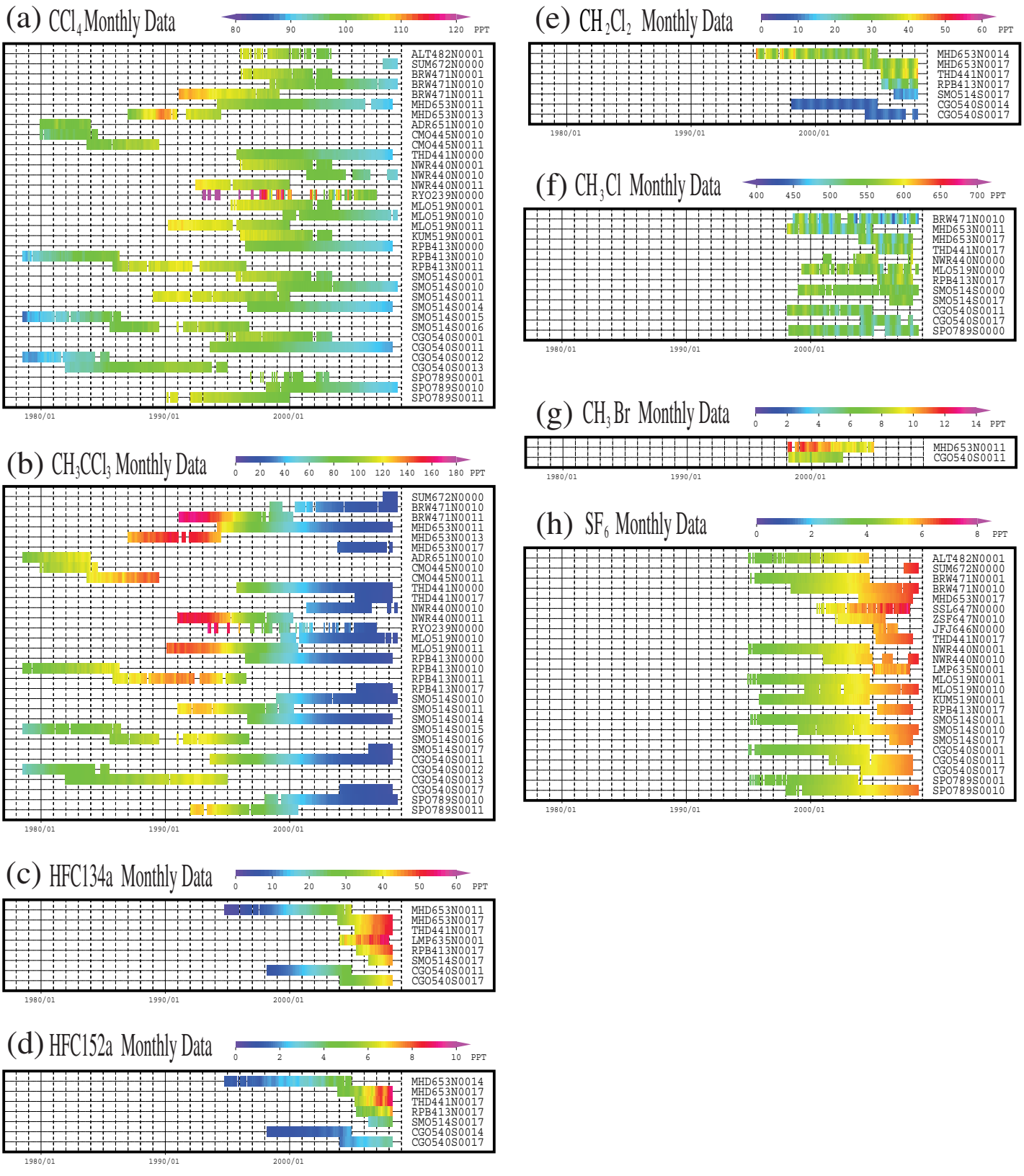

Plate 6.2 Monthly mean (a) CCl_4, (b) CH_3CCl_3, (c) HFC134a, (d) HFC152a, (e) CH_2Cl_2, (f) CH_3Cl, (g) CH_3Br, (h) SF_6 mole fractions that have been reported to the WDCGG. The mole fractions are illustrated in different colors. The sites are listed in order from north to south.

6. Halocarbons and Other Halogenated Species

Basic information on halocarbons with regard to environmental issues

Halocarbons are carbon compounds containing one or more halogens, *i.e.*, fluorine, chlorine, bromine or iodine, and are mostly industrial products. Chlorofluorocarbons (CFCs) are halocarbons containing fluorine and chlorine, and halons are halocarbons containing bromide and other halogen atoms, but not hydrogen, while hydrochlorofluorocarbons (HCFCs) contain hydrogen. Carbon tetrachloride (CCl_4) and methyl chloroform (CH_3CCl_3) are produced industrially, while methyl chloride (CH_3Cl) and methyl bromide (CH_3Br) have natural sources. Although the mole fractions of the halocarbons are relatively low in the atmosphere, most have high global warming potentials. The halocarbons have been shown to account for 13% of the radiative forcing caused by the increased levels of globally mixed long-lived greenhouse gases from 1750 to 2005 (IPCC, 2007a).

The halocarbons are clear, odourless and innocuous substances, which are readily gasified and liquefied and have low surface tension. Thus, they were commonly used as refrigerants, propellants and detergents for semiconductors, resulting in a rapid increase in their mole fraction in the atmosphere until the mid-1980s. Halocarbons containing chlorine and bromine led to the depletion of the ozone layer. Since the mid-1990s, the Montreal Protocol on Substances that Deplete the Ozone Layer and its Adjustments and Amendments has progressively increased the regulation of the production, consumption and trade of ozone-depleting compounds.

A decrease in stratospheric ozone leads to a cooling of the lower stratosphere. However, an increase in halocarbons has a net positive radiative forcing on global warming because their positive direct radiative forcing exceeds their negative indirect radiative forcing associated with ozone depletion (WMO, 1999a).

The CFCs are dissociated mainly by ultraviolet radiation in the stratosphere, and their lifetimes are generally long (*e.g.*, about 50 years for CFC-11). However, the HCFCs and CH_3CCl_3, which contain hydrogen, react with hydroxyl radicals (OH) in the troposphere and have relatively short lifetimes (*e.g.*, about 5 years for CH_3CCl_3). As the reaction with OH in the troposphere is a major sink for CH_3CCl_3, global measurements of CH_3CCl_3 provide an accurate estimate of the global mole fraction of OH (Prinn *et al.*, 2001).

The Kyoto Protocol to the United Nations Framework Convention on Climate Change (UNFCCC), which entered into force on 16 February 2005, specifies carbon dioxide (CO_2), methane (CH_4), nitrous oxide (N_2O), hydrofluorocarbons (HFCs), perfluorocarbons (PFCs) and sulphur hexafluoride (SF_6) as targets for quantified emission limitation and reduction commitments. PFCs, HFCs and SF_6, which have not been regulated by the Montreal Protocol, are very effective greenhouse gases, and even small amounts in the atmosphere may contribute significantly to global warming (IPCC, 2007a). HFCs were developed as replacements for CFCs (IPCC/TEAP, 2005) and SF_6 is produced as an electrical insulant (IPCC, 2007a).

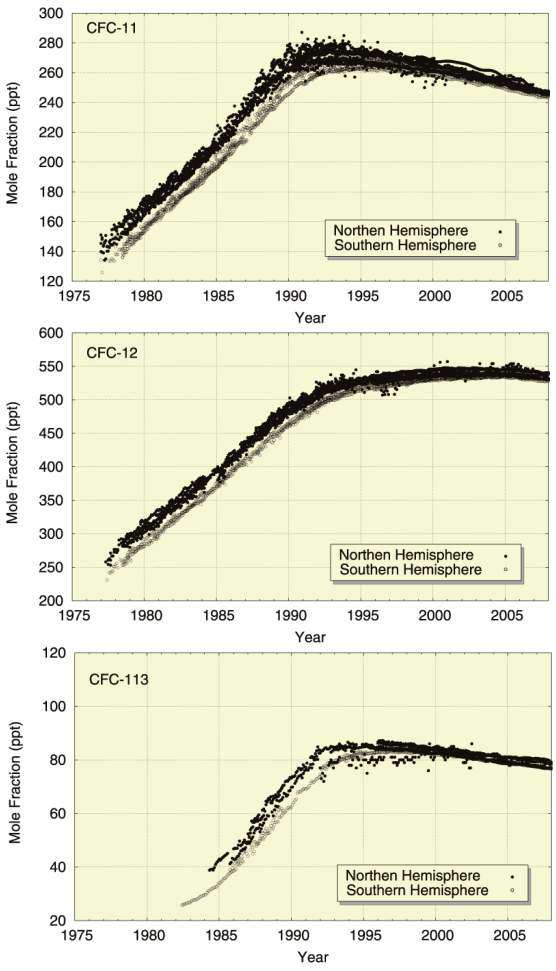

Fig. 6.1 Time series of then monthly mean mole fractions of CFC-11, CFC-12 and CFC-113. Solid circles show mole fractions measured in the Northern Hemisphere and open circles show mole fractions in the Southern Hemisphere. All data reported to the WDCGG are shown.

Annual changes in the levels of halocarbons in the atmosphere

The map at the beginning of this chapter shows observational sites that have submitted data on

halocarbons and other halogenated species to the WDCGG, and Plates 6.1 and 6.2 show all the monthly mean mole fractions of these gases submitted to the WDCGG. The figures below plot all monthly data reported to the WDCGG. There are discrepancies in the absolute mole fractions for several different stations, suggesting that these stations may have adopted different standard scales. Observational data based on identical standard scales revealed that the differences in the mole fractions between the two hemispheres were large in the 1980s for all compounds except HCFCs but have since narrowed.

Figure 6.1 shows monthly mean mole fractions of CFC-11 (CCl_3F), CFC-12 (CCl_2F_2) and CFC-113 (CCl_2FCClF_2) over time. The mole fractions of CFC-11 were at a maximum around 1992 in the Northern Hemisphere, followed by a maximum about one year later in the Southern Hemisphere. The mole fractions of CFC-113 were at a maximum around 1992 in the Northern Hemisphere and around 1997 in the Southern Hemisphere. The mole fractions of these gases have since been decreasing slowly in both hemispheres. The mole fractions of CFC-12 may have peaked in 2003 (IPCC, 2007).

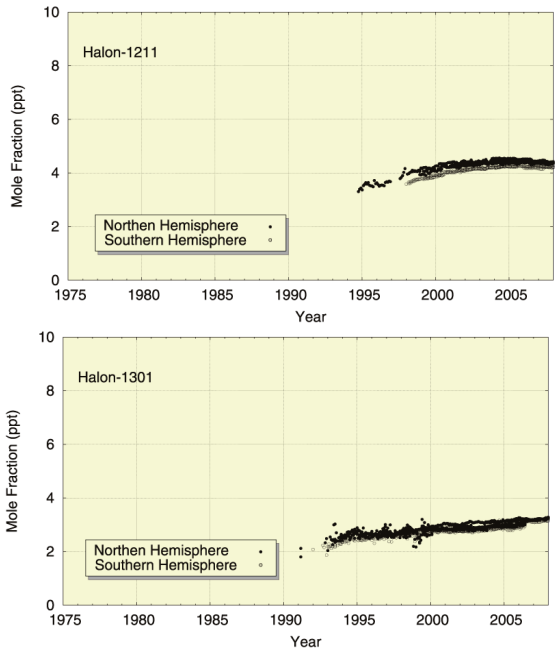

Fig. 6.2 Time series of monthly mean mole fractions of Halon-1211 ($CBrClF_2$) and Halon-1301 ($CBrF_3$). Solid circles show mole fractions measured in the Northern Hemisphere and open circles show mole fractions in the Southern Hemisphere. All data reported to the WDCGG are shown.

Figure 6.2 shows time series of the monthly mean mole fractions of Halon-1211 ($CBrClF_2$) and Halon-1301 ($CBrF_3$). The mole fractions of Halon-1211 and Halon-1301 are increasing, but their growth rates have decelerated.

Figure 6.3 shows time series of the mole fractions of HCFC-22 ($CHClF_2$), HCFC-141b (CH_3CCl_2F) and HCFC-142b (CH_3CClF_2). The mole fractions of these gases increased significantly during the 2000s (IPCC/TEAP, 2005) as a result of continued use as substitutes for CFCs. According to the special report from the Intergovernmental Panel on Climate Change (IPCC) and the Technology and Economic Assessment Panel (TEAP) of the United Nations Environment Programme (UNEP), the HCFCs are increasing rapidly, at annual rates of 3–7%, despite their small mole fractions (IPCC/TEAP, 2005).

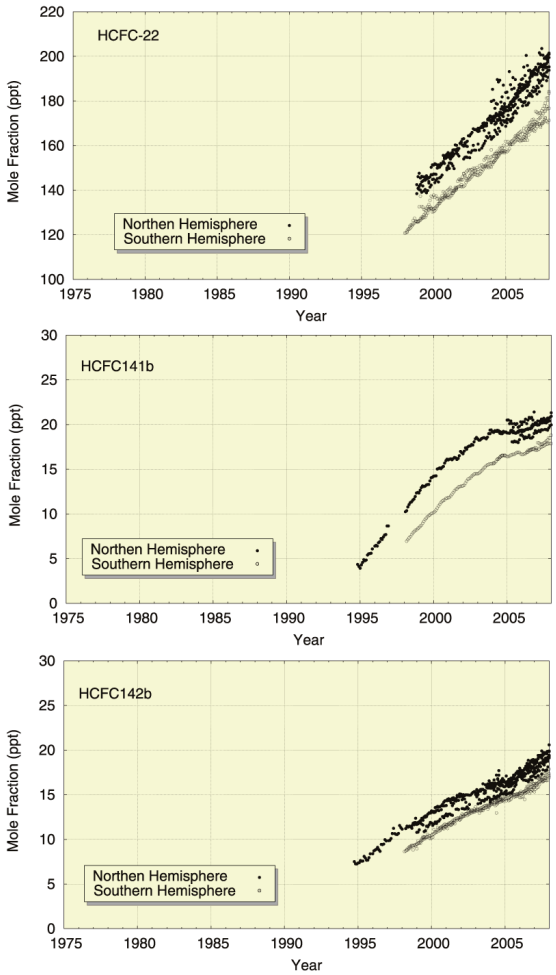

Fig. 6.3 Time series of the monthly mean mole fractions of HCFC-22, HCFC-141b, and HCFC-142b. Solid circles show mole fractions measured in the Northern Hemisphere and open circles show mole fractions in the Southern Hemisphere. All data reported to the WDCGG are shown.

Figure 6.4 shows time series of the mole fractions of CCl_4 and CH_3CCl_3. The mole fractions of CCl_4 in both hemispheres were at a maximum around 1991. The mole fractions of CH_3CCl_3 were at a maximum around 1992 in the Northern Hemisphere and around 1993 in the Southern Hemisphere. The mole fractions of these gases have since been decreasing.

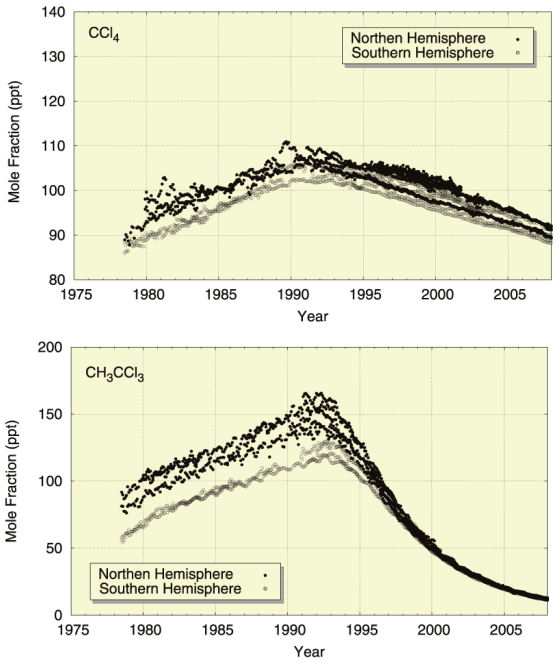

Fig. 6.4 Time series of the monthly mean mole fractions of CCl_4 and CH_3CCl_3. Solid circles show mole fractions measured in the Northern Hemisphere and open circles show mole fractions in the Southern Hemisphere. All data reported to the WDCGG are shown.

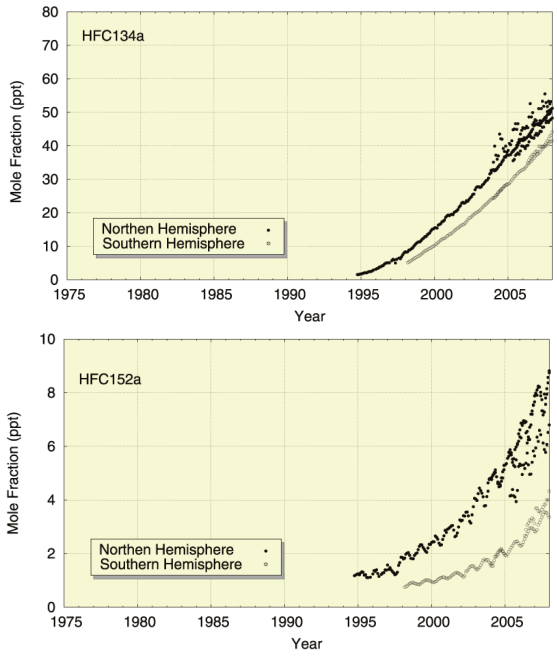

Fig. 6.6 Time series of the monthly mean mole fractions of HFC-134a and HFC-152a. Solid circles show mole fractions measured in the Northern Hemisphere and open circles show mole fractions in the Southern Hemisphere. All data reported to the WDCGG are shown.

Figure 6.5 shows time series of the monthly mean mole fractions of methylene chloride (CH_2Cl_2), methyl chloride (CH_3Cl) and methyl bromide (CH_3Br). The mole fractions of CH_3Br peaked in 1999 and have declined since as a result of the regulation under the Montreal Protocol (WMO, 2007c). The mole fractions of CH_3Cl have remained steady after 1980, although there is large interannual variability.

Figure 6.6 shows time series of the monthly mean mole fractions of HFC-134a (CH_2FCF_3) and HFC-152a (CH_3CHF_2). The mole fractions of HFC-134a and HFC-152a are increasing rapidly. The growth rates of HFC-134a are an average of almost 20%/year since 2000 (IPCC/TEAP, 2005), and the mole fractions of HFC-152a have increased approximately 17%/year (WMO, 2007c). The increasing trends of these gases are larger in the Northern Hemisphere, suggesting that predominant sources are located there (IPCC, 2007).

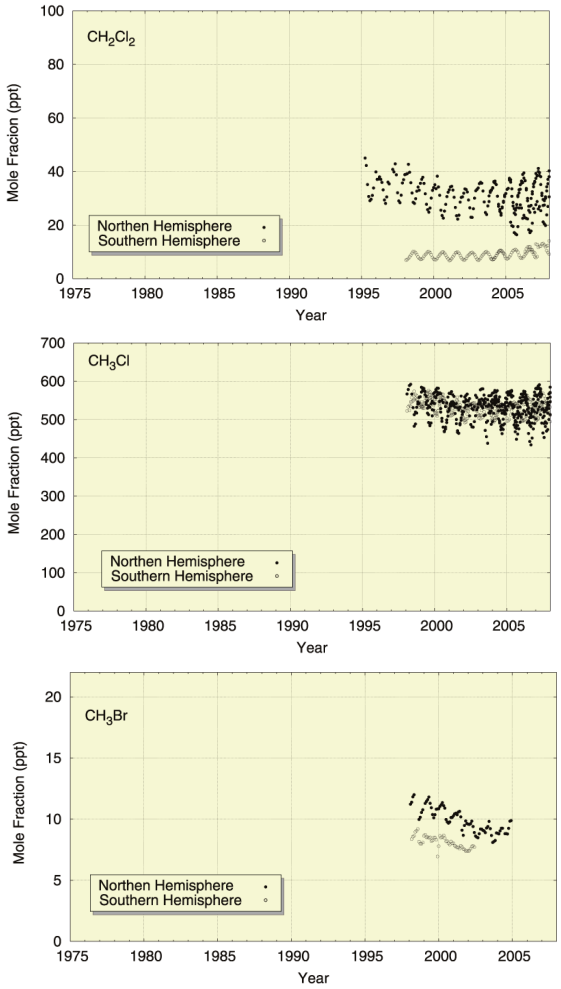

Fig. 6.5 Time series of the monthly mean mole fractions of CH_2Cl, CH_3Cl and CH_3Br. Solid circles show mole fractions measured in the Northern Hemisphere and open circles show mole fractions in the Southern Hemisphere. All data reported to the WDCGG are shown.

Figure 6.7 shows time series of the monthly mean mole fractions of SF_6. The mole fractions of SF_6 are

increasing at a rate of about 5%/year, but the growth rates have been slightly lower over the last few years (IPCC/TEAP, 2005).

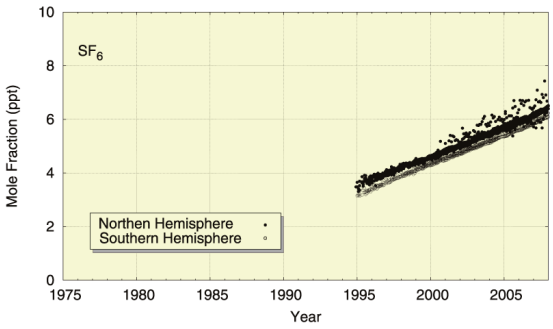

Fig. 6.7 Time series of the monthly mean mole fractions of SF_6. Solid circles show mole fractions measured in the Northern Hemisphere and open circles show mole fractions in the Southern Hemisphere. All data reported to the WDCGG are shown.

7.

Surface OZONE

(O_3)

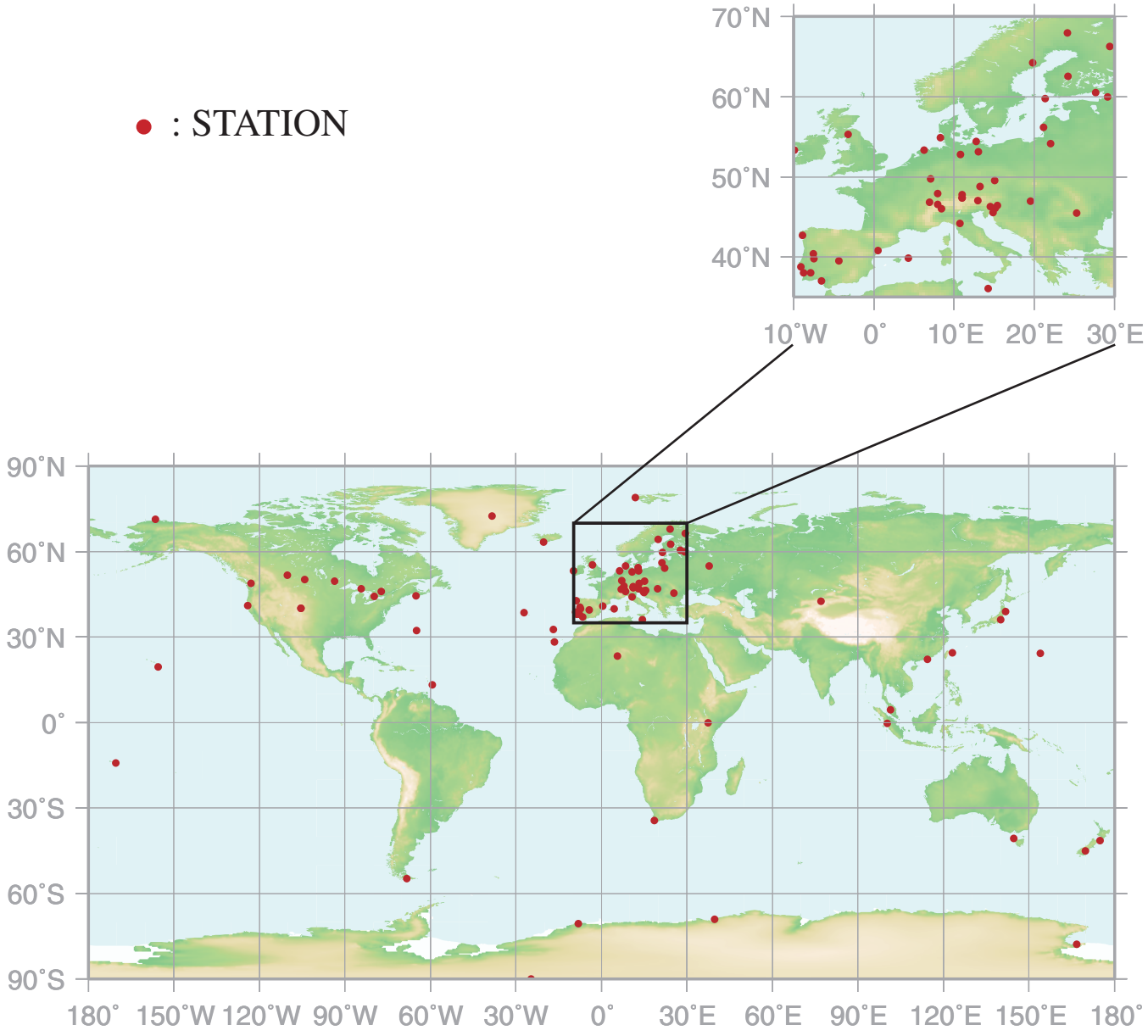

This map shows locations of the stations that have submitted data for monthly mean mole fraction.

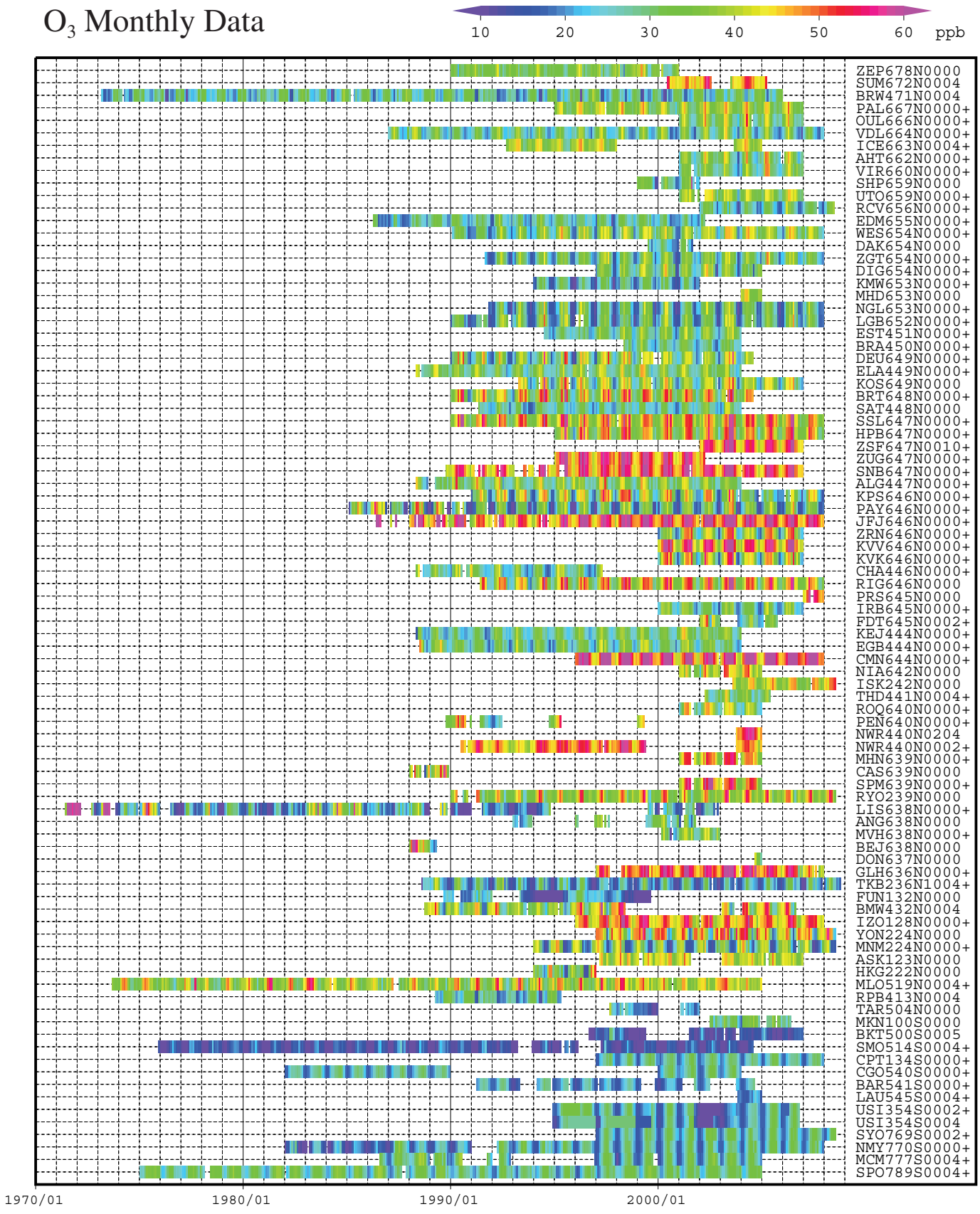

Plate 7.1 Monthly mean O_3 mole fractions that have been reported to the WDCGG. The mole fractions are illustrated in different colors. The sites are listed in order from north to south. The stations with a cross incidental (+) at the end of the station index provide data of a single-peak type as shown in Fig 7.1.

7. Surface Ozone (O_3)

Basic information on surface ozone (O_3) with regard to environmental issues

Ozone (O_3) in the atmosphere exists mostly in the stratosphere, with less than 10% in the troposphere. However, O_3 in the troposphere plays an important role in the atmospheric environment through radiative and chemical processes. O_3 absorbs UV radiation in the stratosphere and thus influences the vertical profile of temperature and circulation in the stratosphere. It also absorbs IR radiation as one of the greenhouse gases in the troposphere. The latter effect is more significant in the upper troposphere, and tropospheric O_3 is the third most important greenhouse gas after CO_2 and CH_4 (Denman *et al.*, 2007). Tropospheric O_3 in the northern extratropics was the greatest contributor to global warming during the 20th century, and increases in tropospheric O_3 from industrialization in developing countries was found to contribute to accelerated warming in the Tropics during the latter half of the century (Shindell *et al*., 2006). Furthermore, through reaction with water vapour under UV radiation, O_3 produces OH radicals, which control atmospheric mole fractions of many greenhouse gases, such as CH_4, through chemical reactions.

Tropospheric O_3 is estimated to have increased 38% since pre-industrial times (Denman *et al.*, 2007). The observational results at high altitudes around 1990, compared with those from the end of the 19th century to the first half of 20th century, show alarming global increases in tropospheric ozone in urban areas (Staehelin *et al.*, 1994). However, ozonesonde measurements in the troposphere show stable or decreasing trends in northern mid-latitudes (Oltmans *et al*., 2006).

Tropospheric O_3 originates from intrusion from the stratosphere and photochemical production. Major intrusions occur during tropopause folding events associated with low-pressure activity in high and mid-latitudes and by unstable mixing around the tropopause associated with cold vortexes. Such intrusions occur around meandering parts of the jet stream. Photochemical production of O_3 occurs when nitrogen oxides react with carbon monoxide (CO) or non-methane hydrocarbons under solar radiation (these substances are called "O_3 precursors"). At the same time, O_3 is destroyed mainly through chemical reactions with OH radicals and deposition at the Earth's surface. The lifetime of tropospheric ozone varies from one or a few days in the boundary layer to a few tens of days or even a few months in the free troposphere.

In the middle troposphere, the mole fractions of O_3 are high in high and mid-latitudes in both hemispheres, and low in the Tropics over the Atlantic (Marenco and Said, 1989) and Pacific (Tsutsumi *et al.,* 2003) Oceans. The localised sources and generally short lifetime of surface O_3 make its distribution localised and time-variant.

Annual variation in the level of surface O_3

The observational sites that have submitted data for surface O_3 to the WDCGG are shown on the map at the beginning of this chapter. The monthly mean mole fractions of O_3 that have been reported from observational sites around the world are shown in Plate 7.1, with different mole fraction levels illustrated in different colours. Data for the mole fractions of surface O_3 are reported in two different units, *i.e.*, mole fraction (ppb) and weight per volume ($\mu g/m^3$) at 25°C. The latter is converted to the former using the formula:

$$X_p\,[\text{ppb}] = (R \times T / M / P_0) \times 10 \times X_g\,[\mu g/m^3]$$

where R is the molar gas constant (8.31451 [J/K/mol]),
T is the absolute temperature as reported from the station,
M is the molecular weight of O_3 (47.9982), and
P_0 is the standard pressure (1013.25 [hPa]).

The mole fraction of surface O_3 varies from station to station, but many of these stations are located in Europe. Moreover, the seasonal and interannual variation is relatively large at most stations. Therefore, it is difficult to identify a global long-term trend in the mole fraction of surface O_3.

Figures 7.1 and 7.2 show average single and multi-peak type seasonal cycles, respectively, for each 30° latitudinal zone. The stations can be divided into single- and multi-peak types of seasonal cycles in the monthly mean mole fraction of surface O_3. For the single-peak type, the peak appears in April in northern high and low latitudes and in May in northern mid-latitudes. The delayed peak in the mid-latitudes may be due to air pollution in Europe, given that most mid-latitude stations are located on this continent. Relatively high mole fractions were observed in spring at Sonnblick, Niwot Ridge, Assekrem and Mauna Loa, all of which are located high at altitudes over 2,700 m. For the multi-peak type, the second peak in the zone of 60°N–30°N around August is unclear because O_3 tends to disperse around this time.

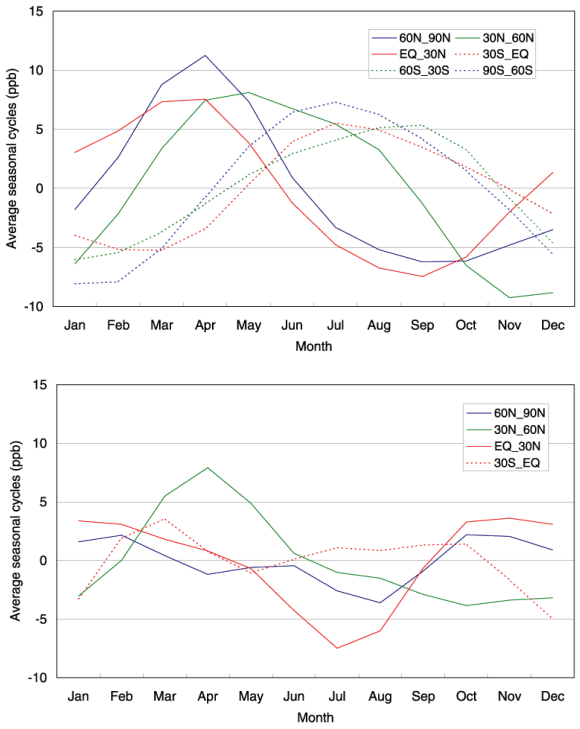

Fig. 7.2 Average seasonal cycles of a multi-peak type in the mole fraction of O_3 for each 30° latitudinal zone obtained by subtracting long-term trends.

8.

CARBON MONOXIDE

(CO)

● : CONTINUOUS STATION

△ : FLASK STATION

□ : FLASK MOBILE (SHIP)

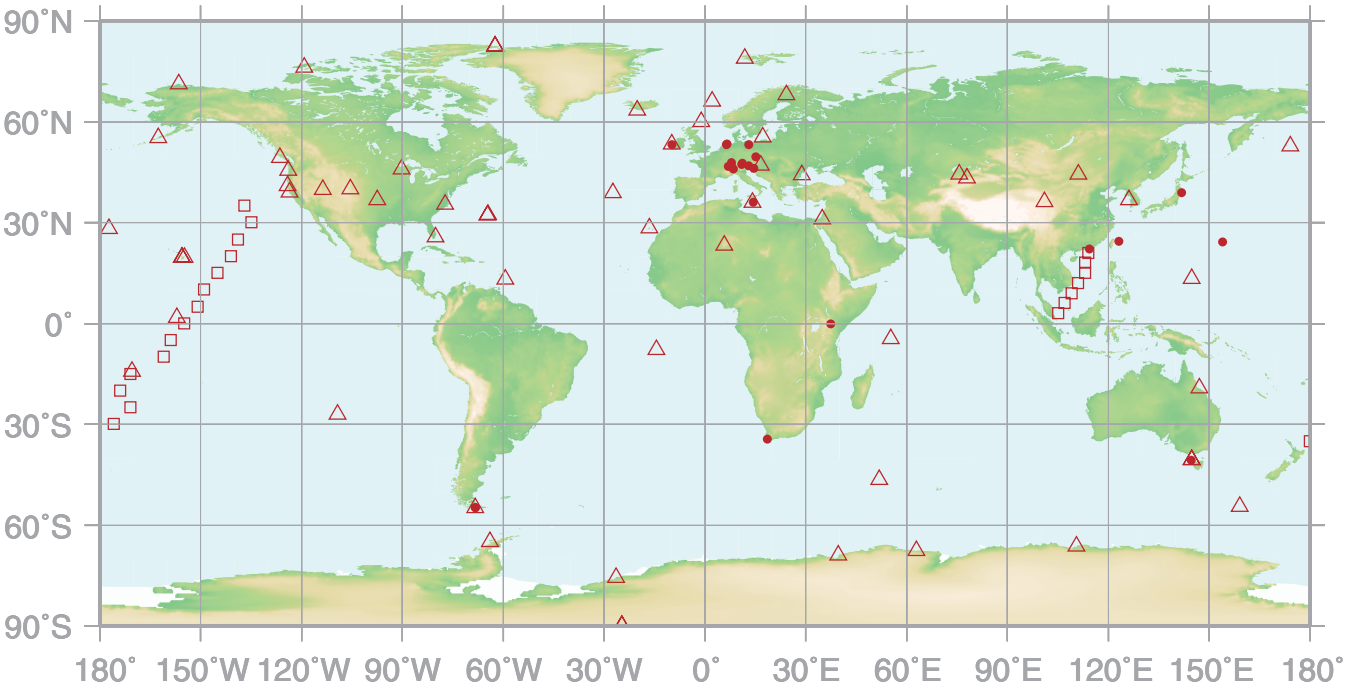

This map shows locations of the stations that have submitted data for monthly mean mole fraction.

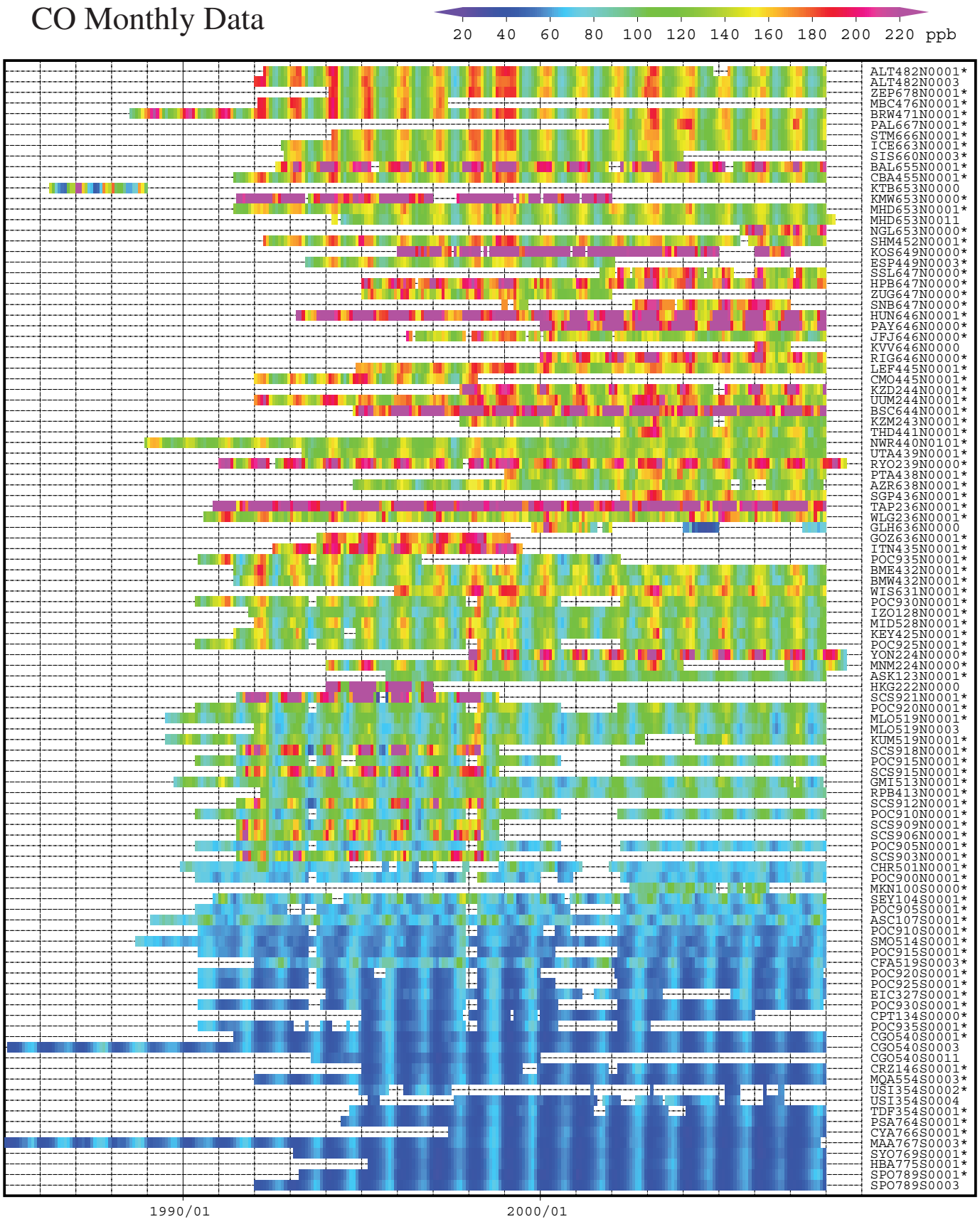

Plate 8.1 Monthly mean CO mole fractions that have been reported to the WDCGG. The mole fractions are illustrated in different colors. The sites are listed in order from north to south. The data from the sites with an asterisk at the end of the station index are used for the analysis shown in Plate 8.2. (see Chapter 2)

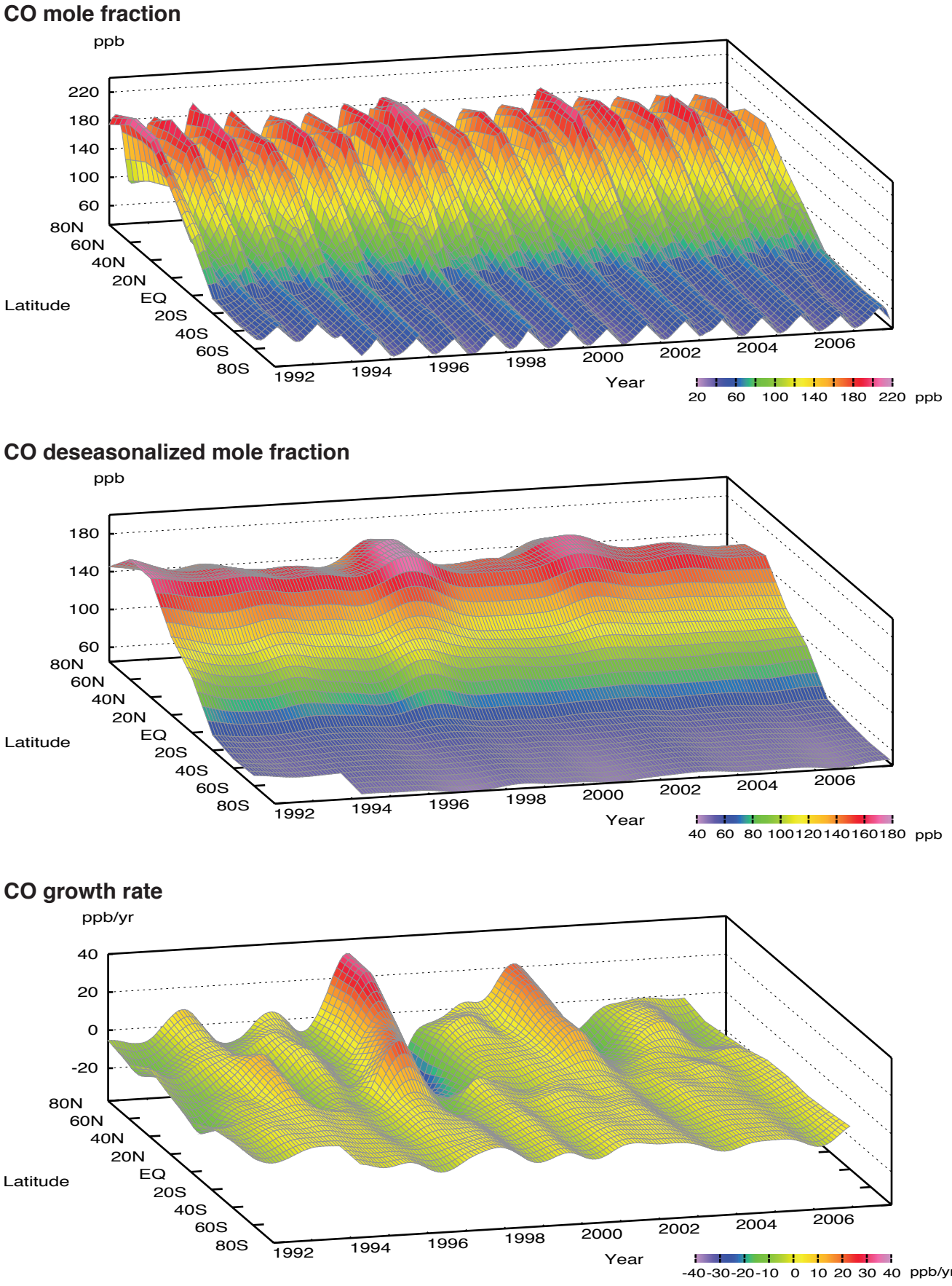

Plate 8.2 Variation of zonally averaged monthly mean CO mole fractions (top), deseasonalized long-term trends (middle), and growth rates (bottom). The zonally averaged mole fractions are calculated for each 20° zone. The deseasonalized trends and growth rates are derived as described in Chapter 2.

8. Carbon Monoxide (CO)

Basic information on CO with regard to environmental issues

Carbon monoxide (CO) is not a significant greenhouse gas; it absorbs little infrared radiation from the Earth. However, CO influences oxidation in the atmosphere through interaction with hydroxyl radicals (OH), which react with methane, halocarbons and tropospheric ozone. Currently, the indirect influence of CO emission on radiative forcing has been estimated to be greater than the direct influence of N_2O (Daniel and Solomon, 1998). CO is identified in IPCC (2001) as an important indirect greenhouse gas.

Sources of atmospheric CO include fossil fuel combustion and biomass burning, along with the oxidation of natural and anthropogenic methane and non-methane hydrocarbons (NMHC). IPCC (2001) estimated a global total emission of 2,780 Tg per year. Major sinks include reactions with OH and surface deposition. The lifetime of CO in the atmosphere is relatively short (a few months), so that, unlike CO_2, anthropogenic CO emission does not lead to CO accumulation in the atmosphere. Furthermore, the uneven distribution of sources causes large spatial and temporal variations in the amount of CO. Therefore, CO has been used as a tracer of anthropogenic pollution.

Measurements of trapped air in ice cores reveal that the CO mole fraction over central Antarctica during the last two millennia was about 50 ppb, increasing to 110 ppb by 1950 in Greenland (Haan and Raynaud, 1998). Beginning in 1950, the CO mole fraction increased at a rate of 1% per year but started to decrease in the late 1980s (WMO, 1999a). Between 1991 and 2001, the global average mole fraction of CO decreased at a rate of about 0.5 ppb per year, excluding temporal enhancements from large biomass burning (Novelli *et al.*, 2003). In recent years, CO emission from large forest fires has also been widely observed. Biomass burning including forest fires is considered to account for 30% of total CO emission worldwide (Holloway *et al.*, 2000).

The global distribution and the budget of CO have been estimated using satellite observations and inverse methods (e.g. Pétron et al., 2002; Stavrakou and Müller, 2006), but the estimated anthropogenic emissions are larger than those calculated from industrial statistics (Bergamaschi *et al.*, 2000; Kasihbhatla *et al.*, 2002; Arellano Jr *et al.*, 2004).

Annual variation of CO levels in the atmosphere

The observational sites that have submitted data for CO to the WDCGG are shown on the map at the beginning of this chapter. All the monthly mean mole fractions of CO that have been reported to the WDCGG are shown in Plate 8.1, in which different mole fraction levels are illustrated in different colours. Global and zonal mean mole fractions were calculated using data from selected stations (see caption).

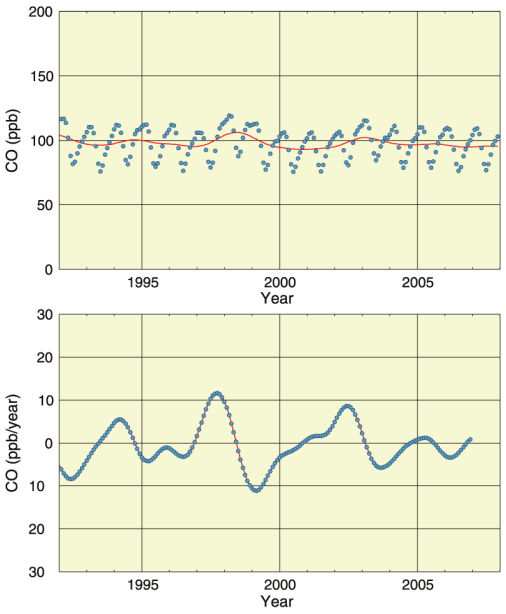

Fig. 8.1 Global monthly mean mole fractions of CO from 1992 to 2007 with deseasonalized long-term trend in red line (top) and their growth rates (bottom).

Latitudinally averaged mole fractions of CO in the atmosphere, together with their deseasonalized mole fractions and growth rates are shown in Plate 8.2 as three-dimensional representations.

Data for the mole fraction of CO are reported in various units, *i.e.*, ppb, $\mu g/m^3$-25°C, $\mu g/m^3$-20°C and mg/m^3-25°C. Units other than ppb are converted to ppb using the formulas:

$$X_p\,[ppb] = (R \times T / M / P_0) \times 10 \times X_g\,[\mu g/m^3]$$
$$X_p\,[ppb] = (R \times T / M / P_0) \times 10^4 \times X_g\,[mg/m^3]$$

where R is the molar gas constant (8.31451 [J/K/mol]),
T is the absolute temperature as reported from the station,
M is the molecular weight of CO (28.0101), and
P_0 is the standard pressure (1013.25 [hPa]).

Plates 8.1 and 8.2 show that the seasonal variation of CO is large in the Northern Hemisphere and small in the Southern Hemisphere, and that the deseasonalized mole fractions are the highest in northern mid-latitudes and the lowest in the Southern Hemisphere. These

results are consistent with the global CO distribution derived from a combination of satellite observations and computational models (Bergamaschi *et al.*, 2000; Holloway *et al.*, 2000; Clerbaux *et al.*, 2001). The latitudinal gradient of CO is large from northern mid- to southern low latitudes, and is small in the Southern Hemisphere. This is due to the presence of numerous CO sources exist in the northern mid-latitudes, combined with the destruction of CO in the Tropics, where OH radicals are abundant.

Figure 8.1 shows global monthly CO mean mole fractions and their growth rates. The growth rates were high in 1993/1994, 1997/1998 and 2002, and low in 1992 and 1998/1999. The global annual mean mole fraction was about 96 ppb in 2007, as calculated without regarding different observation scales.

Figure 8.2 shows monthly mean mole fractions of CO for each 30° latitudinal zone. Seasonal variations are seen in both hemispheres. In the Northern Hemisphere, the mole fractions are higher in winter. Amplitudes of the seasonal cycle are larger in the Northern Hemisphere than in the Southern Hemisphere.

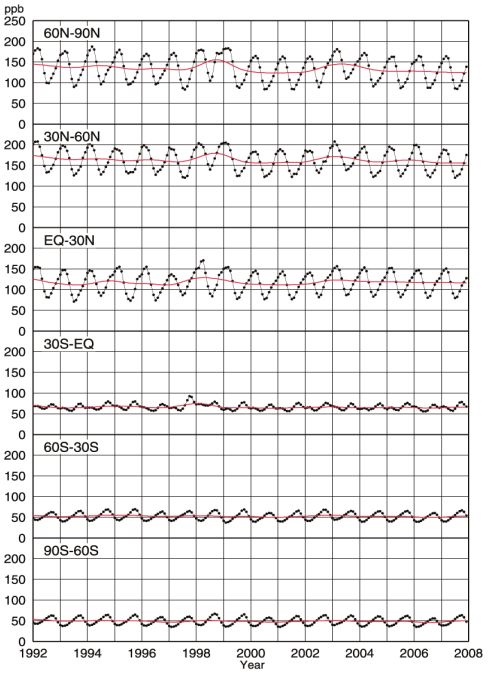

Fig. 8.2 Monthly mean mole fractions of CO from 1992 to 2007 for each 30° latitudinal zone (dots) and their deseasonalized long-term trends (red lines).

Figure 8.3 shows deseasonalized long-term trends for each 30° latitudinal zone and their growth rates. The CO mole fractions are the highest in northern mid-latitudes. Although annual variations in the atmospheric flow can influence CO mole fractions (Allen *et al.*, 1996), a negative growth rate was seen in 1992 in all latitudes. Novelli *et al.* (1998) showed a clear decline in CO mole fractions from late 1991 through mid-1993, with a subsequent recovery from mid-1993 through mid-1994. The decline in CO mole fractions almost coincided with a decrease in the growth rate of CH_4 mole fraction, most likely due to variations in their common sinks. The enhanced stratospheric ozone depletion due to increased volcanic aerosols following the eruption of Mt. Pinatubo in 1991 may have increased OH radicals, which react with both CO and CH_4 (Dlugokencky *et al.*, 1996).

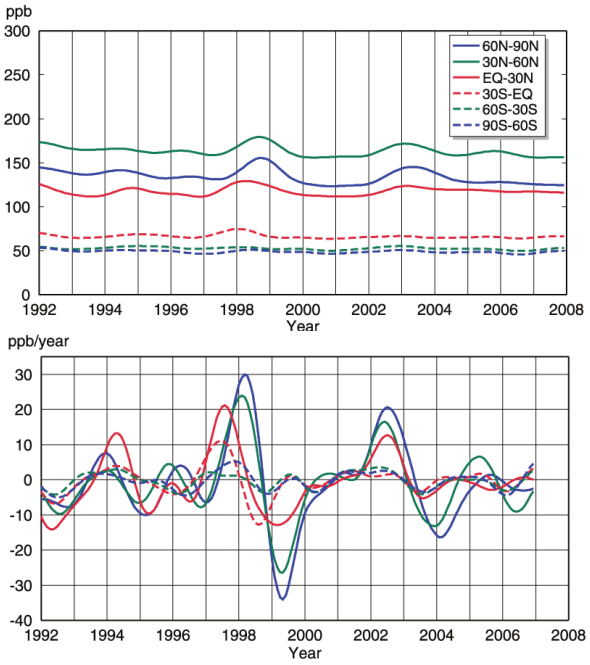

Fig. 8.3 Deseasonalized long-term trends of CO for each 30° latitudinal zone (top) and their growth rates (bottom).

Increases in CO mole fractions were observed from 1997 to 1998 in northern latitudes and in southern low latitudes. These increases were attributed to large biomass burnings around Indonesia in late 1997 and around Siberia in the summer and autumn of 1998 (Novelli *et al.*, 1998). Duncan *et al.* (2003) estimated a CO emission of 133 Tg in 1997 from biomass burning in Indonesia and Malaysia, nearly one fourth of their estimate of the global emission from biomass burning. Observations on board Japan Air Line passenger aircraft showed increased CO mole fractions over the tropical Pacific at an altitude of 10 km, and a model simulated that the biomass burning in Southeast Asia brought about this CO enhancement (Matsueda *et al.*, 1998; Matsueda *et al.*, 2002; Taguchi *et al.*, 2002).

A large-scale boreal forest fire occurred in Siberia in 1998 (Kasischke *et al.*, 1999). The burned area was estimated to be 11,000,000 hectares (ha, 10,000 square metres) by Kajii *et al.* (2002), 13,300,000 ha by Cornard et al. (2002), and 13,100,000 ha by Kasischke and Bruhwiler (2003). Based on these results, Yurganov *et al.* (2004) estimated a total emission of 148 Tg from all boreal forest fires in 1998, and

Kasischke and Bruhwiler (2003) and Duncan *et al*. (2003) estimated an emission from the boreal forest fire in Siberia in 1998 of 88–128 Tg and 69 Tg (summer only), respectively. Boreal forest fires, including those in Siberia, occur from spring to autumn every year and are of various magnitudes. The average burned area has been estimated to be 4.8 million ha by Wotawa *et al*. (2001) and 5.1 million ha by Kajii *et al*. (2002), and the average emission of CO has been estimated to be 52 Tg per year by Yurganov *et al*. (2004).

The CO mole fractions returned to normal after 1999, but the growth rates in the Northern Hemisphere increased substantially again in 2002. The latter might also be attributed to a large biomass burning. Large-scale boreal forest fires occurred in Siberia and North America from 2002 to 2003. The CO emission from these boreal forest fires was estimated to be 142 Tg (Simmonds *et al.*, 2005).

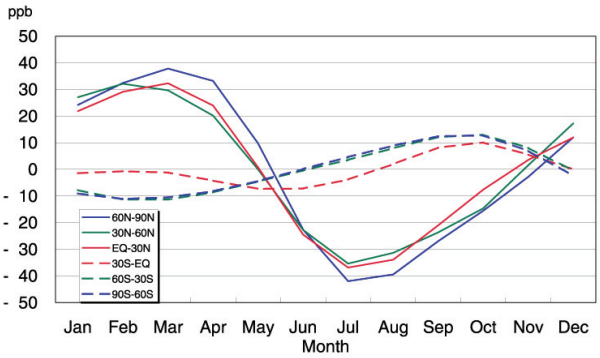

Fig. 8.4 Average seasonal cycles in the mole fraction of CO for each 30° latitudinal zone obtained by subtracting long-term trends.

Seasonal cycle in the level of CO in the atmosphere

Figure 8.4 shows average seasonal cycles in the mole fraction of CO for each 30° latitudinal zone. The seasonal cycle is mainly driven by seasonal variations in OH abundance as a CO sink. Additional factors include emission and oxidation from CO sources and large-scale transportation of CO, despite a relatively weak seasonality in emission and oxidation compared with OH abundance. This seasonality and a short lifetime of about a few months produce a sharp decrease in early summer followed by a relatively slow increase in autumn. Biannual peaks evident in the southern low latitudes may be attributed to the transportation of CO from the Northern Hemisphere.

Direct emissions from CO sources also bring about an intense seasonal variation in some cases. Novelli *et al.* (1998) showed seasonal cycles that are strongly affected by changes in emission from biomass burning in both hemispheres, using a model of two boxes representing the well-mixed northern layer and southern boundary layer. According to model simulations of global distribution of CO, seasonal variations in regional distribution reflect the strength of regional sources, including biomass burning (Bergamaschi *et al*., 2000; Holloway *et al*., 2000). Using observation data in the upper troposphere, Matsueda *et al.* (1998) showed increased CO mole fractions in the upper troposphere in southern low latitudes from October to November, which were attributed to tropical biomass burning.

9.

NITROGEN MONOXIDE (NO)

NITROGEN DIOXIDE (NO_2)

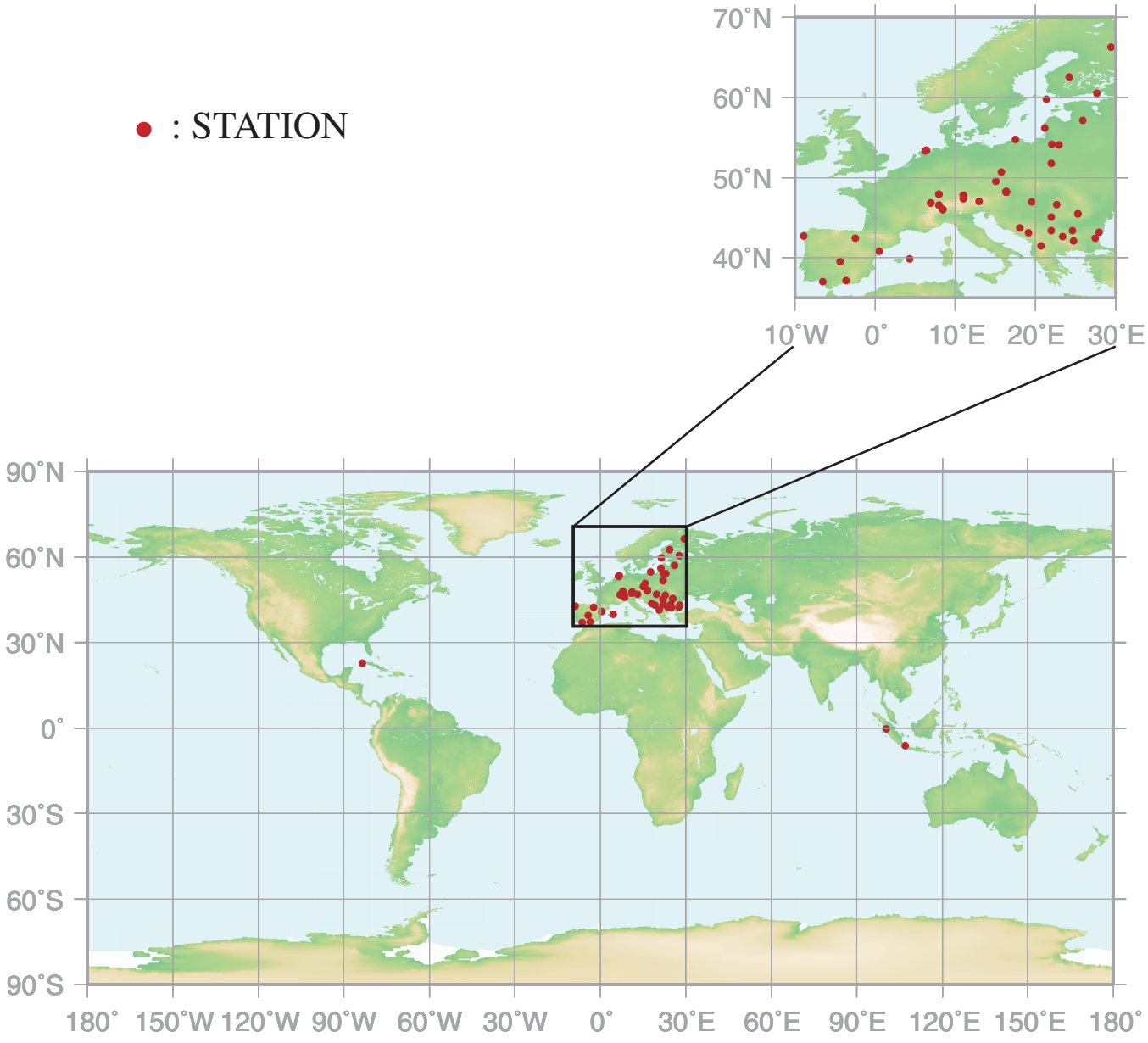

This map shows locations of the stations that have submitted data for monthly mean mole fraction.

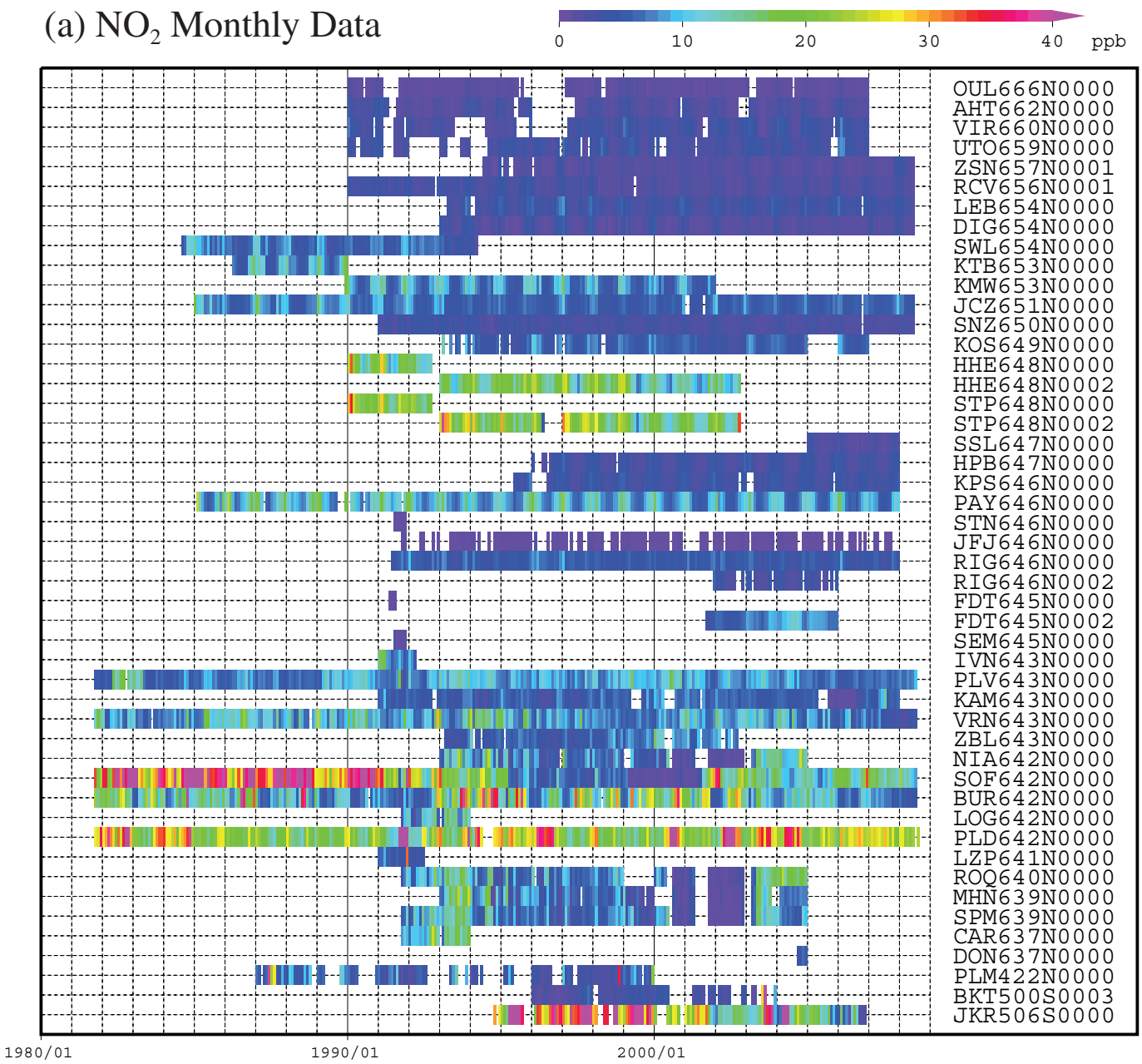

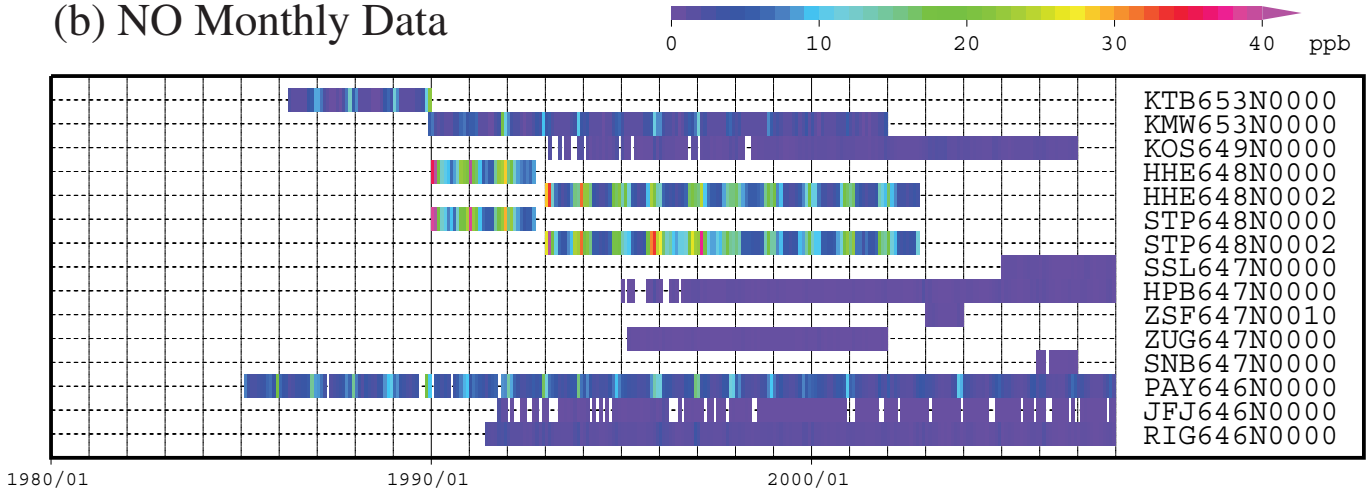

Plate 9.1 Monthly mean (a) NO_2 and (b) NO mole fractions that have been reported to the WDCGG. The mole fractions are illustrated in different colors. The sites are listed in order from north to south.

9. Nitrogen Monoxide (NO) and Nitrogen Dioxide (NO_2)

Basic information on NO and NO_2 with regard to environmental issues

Nitrogen oxides (NO_x, *i.e.*, NO and NO_2) are not greenhouse gases, but affect hydroxyl radicals (OH), which control many substances in the atmosphere such as methane (CH_4), carbon monoxide (CO) and hydrochlorofluorocarbons (HCFCs). In the presence of NO_x, CO and hydrocarbons are oxidised to produce ozone (O_3) in the troposphere, which is one of the major greenhouse gases. Thus, NO_x can influence the Earth's radiative balance and, by generating OH, alter the oxidation capacity of the atmosphere.

Sources of NO_x include fossil fuel combustion, biomass burning, lightning and soil (IPCC, 2001). The dominant sink of NO_x in the atmosphere is its conversion into nitric acid (HNO_3) and peroxyacetylnitrate (PAN), which are eventually removed by dry or wet deposition. In some cases, NO_x is removed from the atmosphere directly by dry deposition. Anthropogenic emission of NO_x is currently one of the major causes of acid rain and deposition. The NO_x mole fractions show a large variability in both space and time because of their short lifetimes and uneven source distribution.

Annual variation in the levels of NO and NO_2 in the atmosphere

The observational stations that have submitted data for NO_2 and NO to the WDCGG are shown on the map at the beginning of this chapter. Most of these stations are located in Europe.

The monthly mean mole fractions of NO and NO_2 that have been reported to the WDCGG are shown in Plate 9.1, in which different mole fraction levels are illustrated in different colours. Data for NO_x are reported in various units, *i.e.*, ppb, $\mu g/m^3$-25°C, $\mu g/m^3$-20°C, $\mu gN/m^3$-25°C and mg/m^3-25°C. Units other than ppb are converted to ppb using the formulas:

$$X_p\,[ppb] = (R \times T / M / P_0) \times 10 \times X_g\,[\mu g/m^3]$$
$$X_p\,[ppb] = (R \times T / M / P_0) \times 10^4 \times X_g\,[mg/m^3]$$
$$X_p\,[ppb] = (R \times T / M_N / P_0) \times 10 \times X_g\,[\mu gN/m^3]$$

where R is the molar gas constant (8.31451 [J/K/mol]),
T is the absolute temperature as reported from the station,
M is the molecular weight of NO (30.00614) or NO_2 (46.00554),
M_N is the atomic weight of N (14.00674), and
P_0 is the standard pressure (1013.25 [hPa]).

The localised sources and short lifetimes of NO and NO_2 make their distributions localised and variable over time. Due to the high temporal variability in the mole fraction of NO_2 at each observation site, it was difficult to identify a long-term trend. A number of stations located in southern Europe showed higher mole fractions, and some stations reported an enhancement of NO_2 in winter. An urban site in Southeast Asia showed higher mole fractions.

As there are few observational sites for NO, it is difficult to identify increasing or decreasing trends for NO mole fractions.

10.

SULPHUR DIOXIDE

(SO_2)

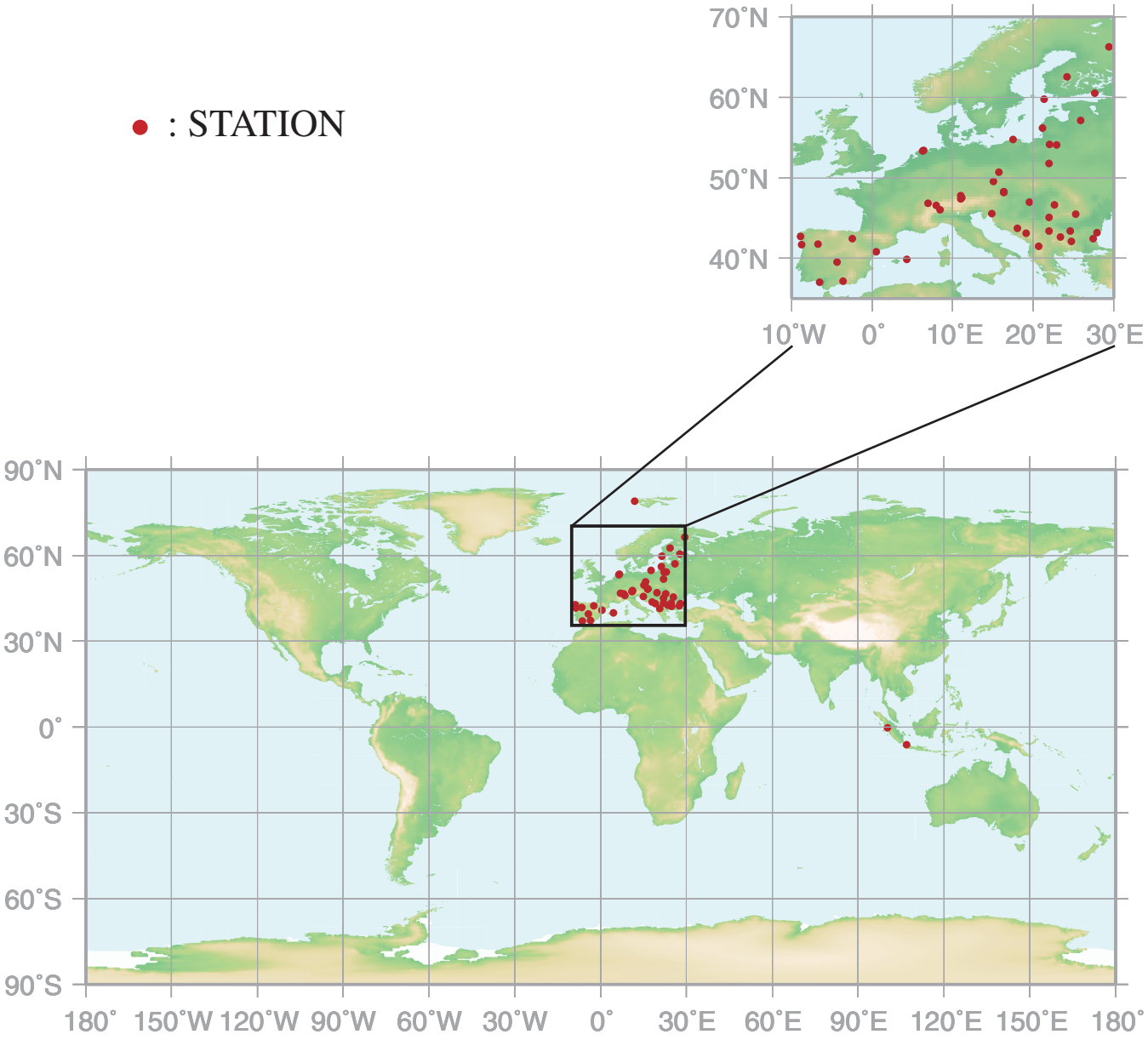

This map shows locations of the stations that have submitted data for monthly mean mole fraction.

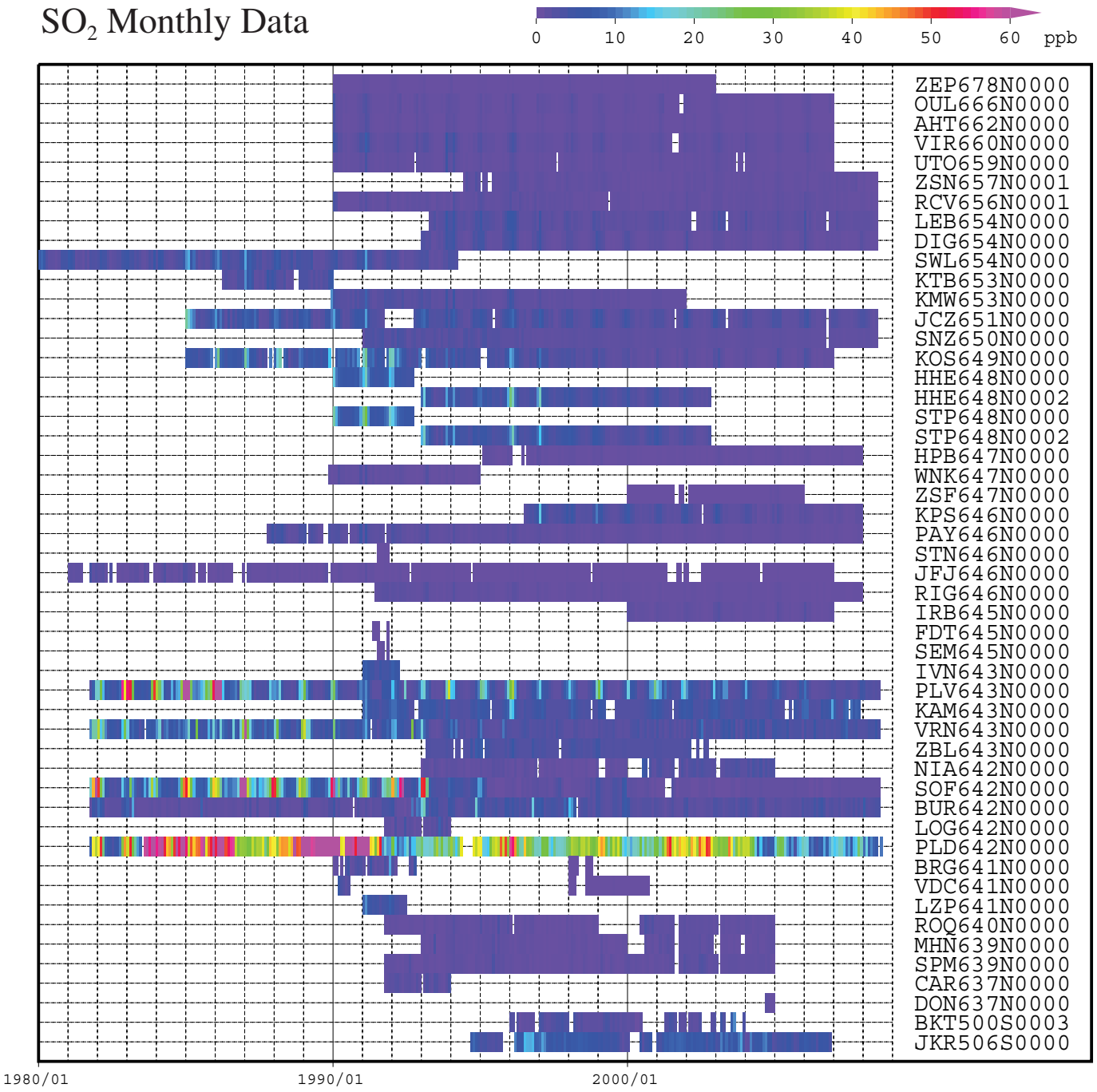

Plate 10.1 Monthly mean SO_2 mole fractions that have been reported to the WDCGG. The mole fractions are illustrated in different colors. The sites are listed in order from north to south.

10. Sulphur Dioxide (SO_2)

Basic information on SO_2 with regard to environmental issues

Sulphur dioxide (SO_2) is not a greenhouse gas, but is a precursor of atmospheric sulphuric acid (H_2SO_4) and sulphate aerosol. SO_2 is oxidised by hydroxyl radicals (OH) to form sulphuric acid, which then becomes aerosols through photochemical gas-to-particle conversion. While SO_2 reacts much more slowly with OH than does NO_2, SO_2 dissolves readily in suspended liquid droplets in the atmosphere. The global sulphur cycle affects atmospheric chemistry, including tropospheric ozone (Berglen *et al.*, 2004).

Sources of SO_2 include fossil fuel combustion by industry, biomass burning, volcanic release and the oxidation of dimethylsulphide (DMS) from the oceans (IPCC, 2001). Major SO_2 sinks are oxidation by OH and deposition onto wet surfaces. Anthropogenic SO_2 has caused acid rain and deposition throughout the industrial era. The mole fractions of SO_2 show large variations in both space and time because of its short lifetime and uneven anthropogenic source distribution.

Annual variation in the level of SO_2 in the atmosphere

The observational sites that have submitted data for SO_2 to the WDCGG are shown on the map at the beginning of this chapter. Most of these stations are located in Europe.

The monthly mean mole fractions of SO_2 that have been reported to the WDCGG are shown in Plate 10.1, with different mole fraction levels illustrated in different colours. Data for SO_2 are reported in various units, *i.e.*, ppb, $\mu g/m^3$, mg/m^3 and $\mu gS/m^3$. Units other than ppb are converted to ppb using the formulas:

$$X_p\,[\text{ppb}] = (R \times T / M / P_0) \times 10 \times X_g\,[\mu g/m^3]$$
$$X_p\,[\text{ppb}] = (R \times T / M / P_0) \times 10^4 \times X_g\,[mg/m^3]$$
$$X_p\,[\text{ppb}] = (R \times T / M_S / P_0) \times 10 \times X_g\,[\mu gS/m^3]$$

where R is the molar gas constant (8.31451 [J/K/mol]),
T is the absolute temperature as reported from the station,
M is the molecular weight of SO_2 (64.0648),
M_S is the atomic weight of S (32.066), and
P_0 is the standard pressure (1013.25 [hPa]).

Although some stations in southern Europe have reported higher mole fractions, it has been difficult to identify an increasing or decreasing trend for SO_2.

REFERENCES

References

Allen, D. J., P. Kasibhatla, A. M. Thompson, R. B. Rood, B. G. Doddridge, K. E. Pickering, R. D. Hudson, and S.-J. Lin, Transport-induced interannual variability of carbon monoxide determined using a chemistry and transport model, *J. Geophys. Res.,* **101**, 28655–28669, 1996.

Angert A., S. Biraud, C. Bonfils, W. Buermann, I. Fung, CO_2 seasonality indicates origins of post-Pinatubo sink, *Geophys. Res. Lett.*, **31**, L11103, doi:10.1029/2004GL019760, 2004.

Arellano Jr., A. F., P. S. Kasibhatla, L. Giglio, G. R. Werf, J. T. Randerson, Top-down esitmates of global CO sources using MOPITT measurements, *Geophys. Res. Lett*., **31**, L01104, doi:10.1029/2004GL018609, 2004.

Bekki, S., K. S. Law, and J. A. Pyle, Effects of ozone depletion on atmospheric CH_4 and CO concentrations, *Nature*, **371**, 595–597, 1994.

Bekki, S., and K. S. Law, Sensitivity of atmospheric CH_4 growth rate to global temperature change observed from 1980 to 1992, *Tellus*, **49B**, 409–416, 1997.

Bergamaschi, P., R. Hein, M. Heimann, and P. J. Crutzen, Inverse modeling of the global CO cycle, 1. Inversion of CO mixing ratios, *J. Geophys. Res.,* **105(D2)**, 1909–1928, 10.1029/1999JD900818, 2000.

Berglen, T. F., T. K. Berntsen, I. S. A. Isaksen, and J. K. Sundet, A global model of the coupled sulfur/oxidant chemistry in the troposphere: The sulfur cycle, *J. Geophys. Res*., **109**, D19310, doi:10.1029/2003JD003948, 2004.

Bousquet, P., P. Ciais, J. B. Miller, E. J. Dlugokencky, D. A. Hauglustaine, C. Prigent, G. R. Van der Werf, P. Peylin, E.-G. Brunke, C. Carouge, R. L. Langenfelds, J. Lathiere, F. Papa, M. Ramonet, M. Schmidt, L. P. Steele, S. C. Tyler and J. White, Contribution of anthropogenic and natural sources to atmospheric methane variability. *Nature*, **443**, 439-443, 2006.

Ciais, P., P. P. Tans, M. Trolier, J. W. C. White, and R. J. Francey, A large northern hemisphere terrestrial CO_2 sink indicated by the $^{13}C/^{12}C$ ratio of atmospheric CO_2, *Science*, **269**, 1098–1102, 1995.

Clerbaux, C, J. Hadji-Lazaro, D. Hauglustaine, G. Megie, B. Khattatov, and J-F. Lamarque, Assimilation of carbon monoxide meaured from satellite in a three-dimensional chemistry-transport model. *J. Geophys. Res.,* **106(D14)**, 15385–15394, 2001.

Cleveland, W. S., S. J. Devlin, Locally weighted regression: an approach to regression analysis by local fitting, *J. Amer. Statist. Assn.*, **83**, 596–610, 1988.Conway, T. J., P. P. Tans, L. S. Waterman, K. W. Thoning, D. R. Kitzis, K. A. Masarie, and N. Zhang, Evidence for interannual variability of the carbon cycle from the National Oceanic and Atmospheric Administration/Climate Monitoring and Diagnostics Laboratory global air sampling network, *J. Geophys. Res*., **99**, 22831–22855, 1994.

Conard, S. G., A. I. Sukhinin, B. J. Stocks, D. R. Cahoon, E. P. Davidenko, and G. A. Ivanova, Determining Effects of Area Burned and Fire Severity on Carbon Cycling and Emissions in Siberia. *Climatic Change*, 55, 197–211, 2002.

Daniel, J. S. and S. Solomon, On the climate forcing of carbon monoxide. *J. Geophys. Res*., **103(D11)**, 13249–13260, 1998.

Denman, K. L., G. Brasseur, A. Chidthaisong, P. Ciais, P. M. Cox, R. E. Dickinson, D. Hauglustaine, C. Heinze, E. Holland, D. Jacob, U. Lohmann, S. Ramachandran, P. L. da Silva Dias, S. C. Wofsy and X. Zhang, 2007: Couplings Between Changes in the Climate System and Biogeochemistry. In: Climate Change 2007: The Physical Science Basis. Contribution of Working Group I to the Fourth Assessment Report of the Intergovernmental Panel on Climate Change [Solomon, S., D. Qin, M. Manning, Z. Chen, M. Marquis, K. B. Averyt, M. Tignor and H. L. Miller (eds.)]. Cambridge University Press, Cambridge, United Kingdom and New York, NY, USA.

Dettinger, M. D. and M. Ghill, Seasonal and interannual variations of atmospheric CO_2 and climate, *Tellus*, **50B**, 1–24, 1998.

Dlugokencky, E. J., L. P. Steele, P. M. Lang, and K. A. Masarie, The grouth rate and distribution of atmospheric methane, *J. Geophys. Res*., **99**, 17021–17043, 1994.

Dlugokencky, E. J., E. G. Dutton, P. C. Novelli, P. P. Tans, K. A. Masarie, K. O. Lantz, and S. Mardronich, Changes in CH_4 and CO growth rates after the eruption of Mt. Pinatubo and their link with changes in tropical tropospheric UV flux, *Geophys. Res. Lett*., **23**, 2761–2764, 1996.

Dlugokencky, E. J., K. A. Masarie, P. M. Lang, and P. P. Tans, Continuing decline in the growth rate of the atmospheric methane burden, *Nature*, **393**, 447–450, 1998.

Dlugokencky, E. J., B. P. Walter, K. A. Masarie, P. M. Lang and E. S. Kasischke, Measurements of an anomalous global methane increase during 1998, *Geophys. Res. Lett.*, **28**, 499–502, 2001.

Duchon, C. E., Lanczos filtering in one and two dimensions, *J. Appl. Meteor.*, **18**, 1016-1022, 1979.

Duncan, B. N., R. V. Martin, A. C. Staudt, R. Yevich, and J. A. Logan, Interannual and seasonal variability of biomass burning emissions

constrained by satellite observations, *J. Geophys. Res*., **108 (D2)**, 4100, doi:10.1029/2002JD002378, 2003.

Etherridge, D. M., L. P. Steele, R. J. Francey, and R. L. Langenfelds, Atmospheric methane between 1000 A.D. and present: Evidence of anthropogenic emissions and climatic variability, *J. Geophys. Res.*, **103**, 15979–15993, 1998.

Fiore, A. M., L. W. Horowitz, E. J. Dlugokencky, and J. J. West , Impact of meteorology and emissions on methane trends, 1990–2004, *Geophys. Res. Lett*., **33**, L12809, doi:10.1029/2006GL026199, 2006.

Francey, R. J., P. P. Tans, C. E. Allison, I. G. Enting, J. W. C. White, and M. Trolier, Changes in oceanic and terrestrial carbon uptake since 1982, *Nature*, **373**, 326–330, 1995.

Gu, L., D. D. Baldocchi, S. C. Wofsy, J. W. Munger, J. J. Michalsky, S. P. Urbanski, and T. A. Bonden, Response of a deciduous forest to the Mount Pinatubo eruption enhanced photosysthesis, *Science*, **299**, 2035–2038, 2003.

Haan, D. and D. Raynaud, Ice core record of CO variations during the last two millennia: atmospheric implications and chemical interactions within the Greenland ice, *Tellus*, **50B**, 253–262, 1998.

Hansen, J., A.Lacis, R. Ruedy, and M. Sato, Potential Clim. Impact of Mount-Pinatubo Eruption, *Geophys. Res. Lett.,* **19(2)**, 215–218, 1992.

Holloway, T., H. Levy II, and P. Kasibhatla, Global distribution of carbon monoxide. *J. Geophys. Res.,* **105(D10)**, 12123–12148, 2000.

IPCC, Climate Change 2001: The Science Basis, Contribution of Working Group I to the Third Assessment Report of the Intergovernmental Panel on Climate Change, Cambridge University Press, Cambridge, United Kingdom and New York, NY, USA, 881pp, 2001.

IPCC, Climate Change 2007: The Physical Science Basis. Contribution of Working Group I to the Fourth Assessment Report of the Intergovernmental Panel on Climate Change [Solomon, S., D. Qin, M.Manning, Z.Chen, M.Marquis, K.B.Averyt, M.Tignor and H.L.Miller(eds.)]. Cambridge University Press, Cambridge, United Kingdom and New York, NY, USA, 2007.

IPCC/TEAP, IPCC/TEAP Special Report on Safeguarding the Ozone Layer and the Global Climate System: Issues Related to Hydrofluorocarbons and Perfluorocarbons, Summary for Policymakers and Technical Summary, WMO and UNEP, 88pp., 2005.

Kajii, Y., S. Kato, D. G. Streets, N. Y. Tsai, A. Shvidenko, S. Nilsson, I. McCallum, N. P. Minko, N. Abushenko, D. Altyntsev, and T. V. Khodzer, Boreal forest fires in Siberia in 1998: Estimation of area burned and emissions of pollutants by advanced very high resolution radiometer satellite data. *J. Geophys. Res*., **107(D24)**, 4745–4752, 2002.

Kasibhatla, P., A. Arellano, J. A. Logan, P. I. Palmer, and P. Novelli, Top-down estimate of a large source of atmospheric carbon monoxide associated with fuel combustion in Asia. *Geophys. Res. Lett.,* 29(19), 1900, doi:10.1029/2002GL015581, 2002.

Kasischke, E. S., K. Bergen, R. Fennimore, F. Sotelo, G. Stephens, A. Janetos, and H. H. Shugart, Satellite imagery gives a clear picture of Russia's boreal forest fires, *EOS Trans*. AGU, **80**, 141–147, 1999.

Kasischke, E. S., and L. P. Bruhwiler, Emission of carbon dioxide, carbon monoxide, and methane from boreal forest fires in 1998, *J. Geophys. Res*., **108(D1)**, 8146, doi:10.1029/2001JD000461, 2003.

Keeling, C. D., R. B. Bacastow, A. F. Carter, S. C. Piper, T. P. Whorf, M. Heimann, W. G. Mook, and H. Roeloffzen, A three-dimensional model of atmospheric CO_2 transport based on observed winds: 1. Analysis of observational data, in aspects of climate variability in the Pacific and the Western Americas, edited by D. H. Peterson, *Geophysical Monograph* **55**, 165–236, American Geophysical Union, Washington, D.C, 1989.

Keeling, C. D., T. P. Whorf, M. Wahlen, and J. van der Plicht, Interannual extremes in the rate of rise of atmospheric carbon dioxide since 1980, *Nature*, **375**, 666–670, 1995.

Keppler, F., John T. G. Hamilton, M. Braß, and T. Röckmann, Methane emissions from terrestrial plants under aerobic conditions, *Nature*, **439**, 187–191, 2006.

Lambert, G., P. Monfray, B. Ardouin, G. Bonsang,, A.Gaudry, V. Kazan and G. Polian, Year-to-year changes in atmospheric CO_2, *Tells*, **47B**, 35–55, 1995.

Lelieveld, J., P. J. Crutzen, and F. J. Dentener: Changing concentration, lifetime and climate forcing of atmospheric methane, *Tellus*, **50B**, 128–150, 1998.

Lowe, D. C., M. R. Manning, G. W. Brailsford, and A. M. Bromley, The 1991-1992 atmospheric methane anomaly: Southern hemisphere ^{13}C decrease and growth rate fluctuations, *Geophys. Res. Lett.*, **24**, 857–860, 1997.

Marenco, A, and F. Said: Meridional and vertical ozone distribution in the background troposphere from Scientific aircraft measurements during the STRATOZ III experiment. *Atmos. Env.,* **23**, 201–214, 1989.

Matsueda, H., H. Inoue, Y. Sawa, Y. Tsutsumi, and M. Ishii, Carbon monoxide in the upper troposphere over the western Pacific between 1993 and 1996, *J. Geophys. Res.*, **103**, 19093–19110, 1998.

Matsueda, H., S. Taguchi, H.Y. Inoue, and M. Ishii, A

large impact of tropical biomass burning on CO and CO_2 in the upper troposphere. *Science in China (Series C)*, **45**, 116–125, 2002.

Morimoto, S., T. Nakazawa, K. Higuchi, and S. Aoki, Latitudinal distribution of atmospheric CO_2 sources nad sinks inferred by $\delta^{13}C$ measurements from 1985 to 1991. *J. Geophys. Res*., **105(D19)**, 24,315–24,326, 2000.

Morimoto, S., S. Aoki, T. Nakazawa, and T. Yamanouchi, Temporal variations of the carbon isotopic ratio of atmospheric methane observed at Ny Alesund, Svalbard from 1996 to 2004, *Geophys. Res. Lett*., **33**, L01807, doi:10.1029/2005GL024648, 2006.

Nakazawa, T., K. Miyashita, S. Aoki, and M. Tanaka, Temporal and spatial variations of upper tropospheric and lower stratospheric carbon dioxide, *Tellus*, **43B**, 106–117, 1991.

Nakazawa, T., S. Morimoto, S. Aoki and M. Tanaka, Time and space variations of the carbon isotopic ratio of tropospheric carbon dioxide over Japan, *Tellus*, **45B**, 258–274, 1993.

Nakazawa, T., S. Morimoto, S. Aoki and M. Tanaka, Temporal and spatial variations of the carbon isotopic ratio of atmospheric carbon dioxide in the western Pacific region, *J. Geophys. Res.*, **102**, 1271–1285, 1997a.

Nakazawa, T., S. Murayama, M. Toi, M. Ishizawa, K. Otonashi, S. Aoki and S. Yamamoto, Temporal variations of CO_2 concentration and its carbon and oxygen isotopic ratios in a temperate forest in the central part of the main island of Japan, *Tellus*, **49B**, 364–381, 1997b.

Nemry, B., L. Francois, P. Warnant, F. Robinet, and J.C. Gerard, The seasonality of the CO_2 exchange between the atmosphere and the land biosphere: A study with a global mechanistic vegetation model, *J. Geophys. Res.*, **101**, 7111–7125, 1996.

Novelli, P. C., K. A. Masarie, and P. M. Lang, Distributions and recent changes of carbon monoxide in the lower troposphere, *J. Geophys. Res.*, **103**, 19015–19033, 1998.

Novelli, P. C., K. A. Masarie, P. M. Lang, B. D. Hall, R. C. Myers, and J. W. Elkins, Reanalysis of tropospheric CO trends: Effects of the 1997–1998 wildfires. *J. Geophys. Res.,* **108(D15)**, 4464, doi:10.1029/2002JD003031, 2003.

Oltmans et al., Long-term changes in tropospheric ozone, *Atmos. Env*., **40**, 3156–3173, 2006.

Onogi, J. K., Tsutsui, H. Koide, M. Sakamoto, S. Kobayashi, H. Hatsushika, T. Matsumoto, N. Yamazaki, H. Kamahori, K. Takahashi, S. Kadokura, K. Wada, K. Kato, R. Oyama, T. Ose, N. Mannoji, and R. Taira, The JRA-25 Reanalysis. *Journal of the Meteorological Society of Japan*, **85,** No.3, 369–432, 2007.

Pétron, G., C. Granier, B. Khattatov, J. Lamarque, V. Yudin, J. Muller, and J. Gille, Inverse modeling of carbon monoxide surface emissions using Climate Monitoring and Diagnostics Laboratory network observations, *J. Geophys. Res.,* **107(D24)**, 4761, doi:10.1029/2001JD001305, 2002.

Prinn, R. G., J. Huang, R. F. Weiss, D. M. Cunnold, P. J. Fraser, P. G. Simmonds, A. McCulloch, C. Harth, P. Salameh, S. O'Doherty, R. H. J. Wang, L. Porter and B. R. Miller, Evidence for substantial variations of atmospheric hydroxyl radicals in the past two decades, *Science*, **292**, 1882–1888, 2001.

Rayner, P. J., I. G. Enting, R. J. Francey and R. Langenfelds, Reconstructing the recent carbon cycle from atmospheric CO_2,$\delta^{13}C$ and O_2/N_2 observations, *Tellus*, **51B**, 213–232, 1999.

Ramonet, M. and P. Monfray, CO_2 baseline concept in 3-D atmospheric transport models, *Tellus*, **48B**, 502–520, 1996.

Rigby, M., R. G. Prinn, P. J. Fraser, P. G. Simmonds, R. L. Langenfelds, J. Huang, D. M. Cunnold, L. P. Steele, P. B. Krummel, R. F. Weiss, S. O'Doherty, P. K. Salameh, H. J. Wang, C. M. Harth, J. Mühle, and L. W. Porter, Renewed growth of atmospheric methane, *Geophys. Res. Lett.*, **35**, L22805, doi:10.1029/2008GL036037, 2008.

Shindell, D., G. Faluvegi, A. Lacis, J. Hansen, R. Ruedy, and E. Aguilar, Role of tropospheric ozone increases in 20th-century climate change, *J. Geophys. Res.,* **111**, D08302, doi:10.1029/2005JD006348, 2006.

Simmonds, P. G., A. J. Manning, R. G. Derwent, P. Ciais, M. Ramonet, V. Kazan, and D. Ryall, A burning question. Can recent growth rate anomalies in the greenhouse gases be attributed to large scale biomass burning events? *Atmos. Env*., **39**, 2513–2517, 2005.

Solomon, S., D. Qin, M. Manning, R.B. Alley, T. Berntsen, N.L. Bindoff, Z. Chen, A. Chidthaisong, J.M. Gregory, G.C. Hegerl, M. Heimann, B. Hewitson, B.J. Hoskins, F. Joos, J. Jouzel, V. Kattsov, U. Lohmann, T. Matsuno, M. Molina, N. Nicholls, J. Overpeck, G. Raga, V. Ramaswamy, J. Ren, M. Rusticucci, R. Somerville, T.F. Stocker, P. Whetton, R.A. Wood and D. Wratt, Technical Summary. In: Climate Change 2007: The Physical Science Basis. Contribution of Working Group I to the Fourth Assessment Report of the Intergovernmental Panel on Climate Change [Solomon, S., D. Qin, M. Manning, Z. Chen, M. Marquis, K.B. Averyt, M. Tignor and H.L. Miller (eds.)]. Cambridge University Press, Cambridge, United Kingdom and New York, NY, USA., 2007.

Staehelin, J., J. Thudium, R.Buehler, A. Voltz-Thomas, and W. Graber, Trends in surface ozone concentrations at Arosa (Switzerland), *Atmos. Env*., **28**, 75–87, 1994.

Stavrakou, T., and J.-F. Müller , Grid-based versus big

region approach for inverting CO emissions using Measurement of Pollution in the Troposphere (MOPITT) data, *J. Geophys. Res*., **111**, D15304, doi:10.1029/2005JD006896, 2006.

Stenchikov, G., A.Robock, V. Ramaswamy, M. D. Schwarzkopf, K. Hamilton, and S. Ramachandran, Arctic Oscillation response to the 1991 Mount Pinatubo eruption: Effects of volcanic aerosols and ozone depletion, *J. Geophys. Res.*, **107(D24)**, 4803, doi:10.1029/2002JD002090., 2002.

Taguchi, S., H. Matsueda, H. Y. Inoue, and Y. Sawa, Long-range transport of carbon monoxide from tropical ground to upper troposphere: a case study for South East Asia in October 1997. *Tellus*, **54B**, 22–40, 2002.

Tanaka, M., T. Nakazawa, S. Aoki, Seasonal and meridional variations of atmospheric carbon dioxide in the lower troposphere of the northern and southern hemispheres, *Tellus*, **39B**, 29–41, 1987.

Tsutsumi, Y, Y. Makino, and J. B. Jensen: Vertical and latitudinal distributions of tropospheric ozone over the western Pacific: Case studies from the PACE aircraft missions. *J. Geophys. Res.*, **108(D8)**, 4251, doi:10.1029/2001JD001374, 2003.

Thoning, K. W., P. P. Tans, and W. D. Komhyr, Atmospheric carbon dioxide at Mauna Loa observatory, 2. Analysis of the NOAA GMCC data, 1974-1985, *J. Geophys. Res.*, **94**, 8549–8565, 1989.

Van der Werf, G. R., J. T. Randerson, G. J. Collatz, L. Giglio, P. S. Kasibhatla, A. F. Arellano, Jr., S. C. Olsen, and E. S. Kasischke, Continental-scale partitioning of fire emissions during the 1997 to 2001 El Nino/La Nina period, *Science*, **303**, 73–76, 2004.

Wittenberg, U., M. Heimann, G. Esser, A.D. Mcguire, and W. Sauf, On the influence of biomass burning on the seasonal CO_2 signal as observed at monitoring stations, *Global Biogeochem. Cycles*, **12**, 531–544, 1998.

WMO, Scientific assessment of ozone depletion: 1998. WMO global ozone research and monitoring project—Report No. 44, World Meteorological Organization, Geneva, 1999a.

WMO, WMO statement on the status of the global climate in 1998, WMO-No.896, World Meteorological Organization, Geneva, 1999b.

WMO, World Data Centre for Greenhouse Gases (WDCGG) Data Summary, WDCGG No. 22, 84pp, 2000.

WMO, Global Amospheric Watch (GAW) Strategic Plan: 2008–2015, GAW Report No. 172, WMO TD No. 1384, 2007a.

WMO, World Data Centre for Greenhouse Gases Data Submission and Disseminatin Guide, GAW Report No. 174, WMO TD No. 1416, 2007b

WMO, Scientific Assessent of Ozone Depletion: 2006, Global Ozone Research and Monitoring Project—Report No. 50, 572pp, Geneva, Switzerland, 2007c.

WMO, Technical Report of Global Analysis Method for Major Greenhouse Gases by the World Data Center for Greenhouse Gases, GAW Report No. 184, WMO/TD - No. 1473, 2009

Wotawa, G., P. C. Novelli, M. Trainer, and C. Granier, Inter-annual variability of summertime CO concentrations in the Northern Hemisphere explained by boreal forest fires in North America and Russia. *Geophys. Res. Lett.*, **28**, 4575–4578, 2001.

Yurganov, L. N., et al., A quantitative assessment of the 1998 carbon monoxide emission anomaly in the Northern Hemisphere based on total column and surface concentration measurements. *J. Geophys. Res.*, **109**, D15305, doi:10.1029/2004JD004559, 2004.

APPENDICES

Calibration and Standard Scales

1. Calibration System in the GAW programme

Under the Global Atmosphere Watch (GAW) programme, the World Calibration Centres (WCCs) are responsible for maintaining calibration standards for certain compounds, establishing instrument calibrations and providing training to the stations. A Reference Standard is designated for each variable to be used for all GAW measurements of that variable at the Central Calibration Laboratories. Table 1 lists the organizations that serve as WCCs and CCLs for GAW [*WMO*, 2007].

Table 1. Overview of the GAW Central Calibration Laboratories (GAW-CCL, Reference Standard) and World Calibration Centres for greenhouse and other related gases. The World Calibration Centres have assumed global responsibilities, except where indicated (Am, Americas; E/A, Europe and Africa; A/O, Asia and the South-West Pacific)

Compounds	Central Calibration Laboratory (Host of Primary Standard)	World Calibration Centre
Carbon Dioxide (CO_2)	NOAA/GMD	NOAA/GMD
Methane (CH_4)	NOAA/GMD	EMPA (Am, E/A) JMA (A/O)
Nitrous Oxide (N_2O)	NOAA/GMD	IMK-IFU
Chlorofluorocarbons (CFCs)		
Surface Ozone (O_3)	NIST	EMPA
Carbon Monoxide (CO)	NOAA/GMD	EMPA
Volatile Organic Compounds (VOCs)		IMK-IFU
Sulphur Dioxide (SO_2)		
Nitrogen Oxides (NO_x)		

2. Carbon Dioxide (CO_2)

In 1995, the National Oceanic and Atmospheric Administration Earth System Research Laboratory, Global Monitoring Division (NOAA/GMD, formerly CMDL) in Boulder, Colorado, USA took over the role of the Central Calibration Laboratory (CCL) from the Scripps Institution of Oceanography (SIO) in San Diego, California, USA. Since then, NOAA/GMD has been designated by WMO as the CCL responsible for the maintenance of the GAW Primary Standard for CO_2. As the World Calibration Centre (WCC) for CO_2, NOAA/GMD maintains a high-precision manometric system for absolute calibration of CO_2 as the reference for GAW measurements throughout the world [*Zhao et al.*, 1997]. It is recommended that the standards of the GAW measurement laboratories be calibrated every two years at the CCL (WMO, 2003).

Under the WMO calibration system, there have been several calibration scales for CO_2 data, *e.g.*, SIO-based X74, X85, X87, X93 and X2002 scales and the NOAA/GMD-based WMO Mole Fraction Scale partially based on previous SIO scales. The NOAA/GMD and SIO are working to resolve the possible small differences between their scales. The CCL adopted the WMO X2005 scale, reflecting historical manometric calibrations of the CCL's set of cylinders and the possible small differences between SIO and NOAA/GMD calibrations.

To assess the differences in standard scales among measuring laboratories, NOAA/GMD organizes intercomparisons or Round Robin experiments endorsed by WMO every few years. Many laboratories participated in the experiments organized in 1991–1992, 1995–1997, 1999–2000, and 2002–2006. Table 2 shows the results of the experiments performed in 1996–1997, in which the mole fractions measured by various laboratories are compared with the mole fractions measured by NOAA/GMD [*Peterson et al.*, 1999]. In addition, many laboratories compare their standards bilaterally or multilaterally.

Table 3 lists laboratories and sites used in the present issue of the *Data Summary* with standard scales of reported data and history of participation in WMO intercomparison experiments.

Table 2. Round robin results for the mole fraction of carbon dioxide. Differences between the mole fractions measured by various laboratories and the mole fractions measured by NOAA (Laboratory minus NOAA, ppm).

Laboratory	Analysis Date	Mole fraction Difference (ppm)		
		Low 340–350 ppm	Medium 350–360 ppm	High 370–380 ppm
NIWA	Feb-96	0.02	0.1	0.2
CSIRO	May-96	–0.07	–0.02	–0.02
AES	Jun-97	–0.04	0	–0.02
CMA	Dec-95	–0.07	–0.01	–0.02
Tohoku Univ.	Jun-96	–0.01	0.04	0.02
AIST (NIRE)	Jul-96	–0.11	–0.04	–0.06
NIES	Aug-96	–0.02	0.09	0.12
MRI	Dec-96	0.04	0.07	0.14
JMA	Jan-97	0.07	0.31	0.3
SNU	Mar-97	0.24	0.13	0.29
CFR	Jan-96	0.1	0.08	0.16
IMS	Mar-96	0.04	0.06	0.07
ENEA	Apr-96	–0.29	–0.06	0.19
UBA	Jul-96	0	–0.02	0.11
HMS	Dec-96	–1.22	–1.04	–0.8

Table 3. Status of standard scales and calibration/intercomparison for CO_2 at laboratories.

Laboratory	WDCGG Filename Code	Calibration Scale	WMO Intercomparison
AEMET	IZO128N0000	WMO	91/92, 96/97, 99/00
Aichi	MKW234N0000	WMO	
AIST (NIRE)	TKY236N0000	NIRE	96/97, 99/00, 02/06
BoM & CSIRO	CGO540S0010,CGO540S0000	WMO	
CAMS	WLG236N0000	WMO	96/97, 99/00, 02/06
CESI	PRS645N0000	WMO	99/00, 02/06
CSIRO	ALT482N0003,CFA519S0003,CGO540S0003,CYA766S0001, ESP449N0003,MAA767S0003,MLO519N0003,MQA554S0003, SIS660N0003,SPO789S0003	WMO	91/92, 96/97, 99/00, 02/06
EC	ALT482N0005,CSJ451N0000,SBL443N0000	WMO	91/92, 96/97, 99/00, 02/06
ENEA	LMP635N0001	WMO	91/92, 96/97, 99/00, 02/06
FMI	PAL667N0000	WMO	02/06
GERC	GSN233N0103		
HMS	KPS646N0000,HUN646N0000	WMO	91/92, 96/97, 99/00, 02/06
IAFMS	CMN644N0000	WMO	91/92, 96/97, 02/06

IGP	HUA312S0000	WMO	
IMK-IFU	WNK647N0000,ZUG647N0014	WMO	99/00
INMH	FDT645N0102		
ICES	JBN762S0000	WMO	
IOEP	DIG654N0000		
ITM	ZEP678N0000	WMO	96/97, 99/00
JMA	MNM224N0000,RYO239N0000,YON224N0000	WMO	91/92, 96/97, 99/00, 02/06
KMA	AMY236N0000		02/06
KSNU	ISK242N0000		
LSCE	AMS137S0000,MHD653N0002	WMO	91/92, 96/97, 99/00, 02/06
METRI	KSN233N0000	WMO	96/97
MGO	BER255N0001,KOT276N0001,KYZ240N0001,STC652N0000, TER669N0001	WMO	
MMD	DMV504N0000	WMO	
MRI	TKB236N0102	MRI	91/92, 96/97, 99/00, 02/06
NIES	COI243N0000,HAT224N0000	NIES	96/97, 99/00, 02/06
NIPR&Tohoku Univ.	SYO769S0000		Tohoku Univ.:91/92, 96/97, 99/00, 02/06
NIWA	BAR541S0000	WMO	91/92, 96/97, 99/00, 02/06
NOAA/GMD	BRW471N0000,MLO519N0000,SMO514S0000,SPO789S0000, NOAA/GMD flask network*	WMO	91/92, 96/97, 99/00, 02/06
Osaka Univ.	STA234N0000		
RIVM	KMW653N0000	NIST	
Saitama	URW235N0000,KIS236N0000,DDR236N0000	WMO	
SAWS	CPT134S0000	WMO	99/00, 02/06
Shizuoka Univ.	HMM234N0000		
UBA	BRT648N0000,DEU649N0000,LGB652N0000,NGL653N0000 SNB647N0000,SSL647N0000,SSL647N0001,WES654N0000, ZGT654N0000,ZSF647N0010,ZUG647N0000	WMO	91/92, 96/97, 99/00, 02/06

* NOAA/GMD flask network:
ALT482N0001,AMS137S0101,ASC107S0001,ASK123N0101,AVI417N0001,AZR638N0001,BAL655N0001,BKT500S0001,BME432N0001, BMW432N0001,BRW471N0001,BSC644N0001,CBA455N0001,CGO540S0001,CHR501N0001,CMO445N0001,CRZ146S0001,EIC329S0001, GMI513N0001,GOZ636N0001,HBA775S0001,HUN646N0101,ICE663N0001,ITN435N0001,IZO128N0001,KCO204N0001,KEY425N0001, KUM519N0001,KZD244N0001,KZM243N0001,LEF445N0001,MBC476N0001,MHD653N0001,MID528N0001,MKN100S0001,MLO519N0001, NMB123S0001,NWR440N0101,OPW448N0001,PAL667N0001,POC90000001,POC905N0001,POC905S0001,POC910N0001,POC910S0001, POC915N0001,POC915S0001,POC920N0001,POC920S0001,POC925N0001,POC925S0001,POC930N0001,POC930S0001,POC935S0001, PSA764S0001,PTA438N0001,RPB413N0001,SCS903N0001,SCS906N0001,SCS909N0001,SCS912N0001,SCS915N0001,SCS918N0001, SCS921N0001,SEY104S0001,SGP436N0001,SHM452N0001,SMO514S0001,SPO789S0001,STC654N0001,STM666N0001,SUM672N0001, SYO769S0001,TAP236N0001,TDF354S0001,TRH441N0001,UTA439N0001,UUM244N0001,WIS631N0001,WLG236N0001,ZEP678N0001

3. Methane (CH_4)

The GAW programmes have established two WCCs for CH_4: the Swiss Federal Laboratory for Materials Testing and Research (EMPA), Dübendorf, Switzerland; and the Japan Meteorological Agency (JMA), Tokyo, Japan [*WMO*, 2007]. In addition, the Central Calibration Centre for methane has been established in NOAA/GMD [*Dlugokencky, et. al.*, 2005; *WMO*, 2007].

The NOAA04 scale has been designated as the Primary Standards of the GAW programme. This scale results in CH_4 mole fractions that are a factor of 1.0124 greater than the previous NOAA scale [*Dlugokencky et al.*, 2005].

Table 4 summarizes the methane standard scales

used by laboratories contributing to the WDCGG and lists tentative multiplying conversion factors applied for analysis in this issue of the *Data Summary*. The standard is the NOAA04 scale, and conversion factors were calculated from the results of intercomparisons of the mole fractions with other laboratories performed bilaterally or multilaterally before the establishment of the GAW Standards. The conversion factors are not used when a station employs the NOAA04 scale.

The former CMDL scale is lower than an absolute gravimetric scale [*Aoki et al.*, 1992] by ~1.5% [*Dlugokencky et al.*, 1994] and lower than the AES (MSC) scale by a factor of 1.0151 [Worthy et al., 1998]. The former CMDL scale can be converted to the Tohoku University standard by multiplying by 1.0121 [*Dlugokencky et al.*, 2005]. The conversion factors 1.0124 / 1.0151 = 0.9973 and 1.0124 / 1.0121 = 1.0003 have been adopted for comparisons with the NOAA04 scale.

Table 4. Status of the standard scales of CH_4 at laboratories with conversion factors.

Laboratory	WDCGG Filename Code	Calibration Scale	Conversion Factor
AEMET	IZO128N0000	NOAA/CMDL	1.0124
AGAGE	CGO540S0011,CGO540S0013,CMO445N0011, MHD653N0011,MHD653N0013,RPB413N0000, RPB413N0011,SMO514S0014,SMO514S0016, THD441N0000	Tohoku Univ.	1.0003
CESI	PRS645N0000	NOAA/CMDL	1.0124
CHMI	KOS649N0000	CHMI	0.9973
CSIRO	ALT482N0003,CFA519S0003,CGO540S0003, CYA766S0000,ESP449N0003,MAA767S0003, MLO519N0003,MQA554S0003,SIS660N0003, SPO789S0003	NOAA04	1
ENEA	LMP635N0000	NOAA/CMDL	1.0124
ENPA	JFJ646N0000	NOAA04	1
JMA	MNM224N0000,RYO239N0000,YON224N0000	NOAA04	1
KMA	AMY236N0000		
KSNU	ISK242N0000		
METRI	GSN233N0000		
MGO	TER669N0001	NOAA04	1
MRI	TKB236N0000	MRI	0.9973
NIES	COI243N0000,HAT224N0000	NIES	0.9973
NOAA/GMD	BRW471N0000,MLO519N0000, NOAA/GMD flask network*	NOAA04	1
	KPA432N0001,LEF445N0001,MCM777S0001 NZL543S0001,POC935S0001,SGI354S0001,SIO432N0001	NOAA/CMDL	1.0124
RIVM	KMW653N0000	NIST	0.9973
SAWS	CPT134S0000	NOAA04	1
UBA	DEU649N0000,NGL653N0000,SSL647N0000, ZGT654N0000,ZSF647N0010,ZUG647N0000	NOAA04	1

* NOAA/GMD flask network:
ALT482N0001,AMS137S0101,ASC107S0101,ASK123N0101,AVI417N0001,AZR638N0001,BAL655N0001,BKT500S0001,BME432N0001, BMW432N0001,BRW471N0001,BSC644N0001,CBA455N0001,CGO540S0001,CHR501N0001,CMO445N0001,CRZ146S0001,EIC329S0001, GMI513N0001,GOZ636N0001,HBA775S0001,HUN646N0101,ICE663N0001,ITN435N0001,IZO128N0001,KEY425N0001,KUM519N0001, KZD244N0001,KZM243N0001,MBC476N0001,MHD653N0001,MID528N0001,MLO519N0001,NWR440N0101,OPW448N0001,POC90000001, POC905N0001,POC905S0001,POC910N0001,POC910S0001,POC915N0001,POC915S0001,POC920N0001,POC920S0001,POC925N0001, POC925S0001,POC930N0001,POC930S0001,PSA764S0001,PTA438N0001,RPB413N0001,SCS903N0001,SCS906N0001,SCS909N0001, SCS912N0001,SCS915N0001,SCS918N0001,SCS921N0001,SEY104S0001,SGP436N0000,SHM452N0001,SMO514S0001,SPO789S0001, STM666N0001,SYO769S0001,TAP236N0001,UTA439N0001,UUM244N0001,WIS631N0001,WLG236N0001,ZEP678N0101

4. Nitrous Oxide (N_2O)

The Halocarbons and other Atmospheric Trace Species (HATS) Group of NOAA/GMD maintains a set of standards for N_2O [*Hall et al.*, 2001]. The NOAA-2006 N_2O scale [*Hall et al.*, 2007] has been designated as the Primary Standards of the GAW programme. This group analyses the standards of laboratories, including the Meteorological Service of Canada (MSC) and the Australian Commonwealth Scientific and Industrial Research Organisation (CSIRO). The Fraunhofer Institut für Atmosphärische Umweltforschung (IFU) in Garmisch-Partenkirchen, Germany, serves as the GAW WCC.

The SIO-98 scale is essentially equivalent to the NOAA-2006 scale, with an average difference of 0.01% over the range of 299–319 ppb, and the NOAA-2000 scale can be converted to the 2006 scale by using the factor 0.99402 [*Hall et al.*, 2007]. A constant ratio of 1.0017 between CSIRO and AGAGE data was used by Huang *et al.* (2008), and a factor of 1 / 1.0017 = 0.9983 has been used in this report to convert CSIRO data to the NOAA-2006 scale.

Table 5. Status of the standard scales of N_2O at laboratories.

Submitter	WDCGG Filename Code	Calibration Scale	Conversion Factor
AGAGE	ADR652N0010,CGO540S0011,CGO540S0012, CGO540S0013,CMO445N0010,CMO445N0011, MHD653N0011,MHD653N00013,RPB413N0000, RPB413N0010,RPB413N0011,SMO514S0014, SMO514S0015,SMO514S0016,THD441N0000	SIO 1998	1
CSIRO	ALT482N0003,CFA519S0003,CGO540S0003, CYA766S0000,EPC449N0003,MAA767S0003, MLO519N0003,MQA554S0003,SIS660N0003, SPO789S0003	CSIRO	0.9983
ENEA	LMP635N0001	CMDL 2000	0.999402
EMPA	JFJ646N0000	SIO 1998	1
GERC	GSN233N0103		
JMA	RYO239N0000	NOAA-2006	1
KMA	AMY236N0000		
METRI	GSN233N0000		
MRI	MMB243N0000	MRI	
Nagoya University	NGY235N0000		
NIES	HAT224N0000	NIES	
NILU	ZEP678N0000		
NOAA/GMD	ALT482N0001,BRW471N0001,BRW471N0011, CGO540S0001,KUM519N0001,MLO519N0001, MLO519N0011,NWR440N0001, NWR440N0011, SMO514S0001, SMO514S0011,SPO789S0001, SPO789S0011	CMDL 2000	0.999402
	BRW471N0010, MLO519N0010, NWR440N0010, SMO514S0010, SPO789S0010,SUM672N0000	NOAA-2006	1
SAWS	CPT134S0000	CMDL 2000	0.999402
UBA	SSL647N0000,ZSF647N0010	SIO 1998	1

5. Surface Ozone (O_3)

The National Institute of Standards and Technology (NIST) has developed and deployed Standard Reference Photometers (SRPs) in the USA and other countries. The GAW has designated the SRP #2 maintained at NIST as the Primary Standard for the GAW programme, making NIST the CCL for O_3. The Swiss Federal Laboratory for Materials Testing and Research (EMPA) maintains NIST SRP #15 as the reference and is GAW WCC for surface ozone [*Hoferetal.,* 1998]. The traceability and uncertainty of O_3 within the GAW network were reported by Klausen *et al.,* (2003). Regional Calibration Centres

have been established at the Solar and Ozone Observatory, Hradec Kralove, Czech Republic, and Observatorio Central Buenos Aires, Argentina [*WMO,* 2007]. The former maintains the SRP #17 directly purchased from NIST.

Table 6. Status of surface ozone standard scales at laboratories

Laboratory	WDCGG Filename Code	Calibration Scale	Audit EMPA-WCC
AEMET	IZO128N0000	WMO (NIST & EMPA)	96, 98, 00, 04
AQRB	ALG447N0000,BRA450N0000,CHA446N0000, EGB444N0000,EST451N0000,ELA449N0000, KEJ444N0000,SAT448N0000		
AWI	NMY770S0000		
BMG	BKT500S0000	WMO (NIST & EMPA)	99,01,04,07,08
BoM & CSIRO	CGO540S0000	WMO (NIST & EMPA)	02
CESI	PRS645N0000		
CHMI	KOS649N0000	WMO (NIST & EMPA)	
DEFRA	EDM655N0000		
DWD	HPB647N0000	WMO (NIST & EMPA)	97,06
EARS	IRB645N0000,KVV646N0000,KVK646N0000, ZRN646N0000	WMO (NIST & EMPA)	
EMPA	JFJ646N0000,MKN100S0000,PAY646N0000, RIG647N0000	WMO (NIST & EMPA)	Jungfraujoch: 99, 06
FMI	AHT662N0000,OUL666N0000,PAL667N0000, UTO659N0000,VIR660N0000		Pallas-Sammaltunturi: 97, 03, 07
HMS	KPS646N0000		
IM	ANG638N0000,BEJ638N0000,CAS639N0000, FUN132N0000,LIS638N0000,MVH638N0000, PEN640N0000		
INM	DON637N0000,MHN639N0000,NIA642N0000, ROQ640N0000,SPM639N0000	NPL (U. K.)	
INMH	FDT645N0102		
IOEP	DIG654N0000	WMO (NIST & EMPA)	
ISAC	CMN644N0000		
IVL	VDL664N0000	Stockholm Univ. (Sweden)	
JMA	MNM224N0000,RYO239N0000,SYO769S0002, YON224N0000	WMO (NIST & EMPA)	Ryori: 05
	TKB236N1003		
KSNU	ISK242N0000		
LEGMA	RCV656N0000	WMO (NIST & EMPA)	

MMD	TAR504N0000		
NILU	ZEP678N0000	WMO (NIST & EMPA)	97, 01, 05
NIWA	BAR541S0000	WMO (NIST & EMPA)	
NOAA/GMD	BMW432N0004,BRW471N0004,ICE663N0004, LAU545S0004, MCM777S0104,MLO519N40, NWR440N0002,NWR440N0204,RPB413N0004, SMO514S0004,SPO789S0004,SUM672N0004, THD441N0004	NOAA/GMD	Mauna Loa: 03 Barrow: 08
NUI	MHD653N0000	WMO (NIST & EMPA)	96, 98, 02, 05
ONM	ASK123N0000		03, 07
PolyU	HKG222N0000		
RIVM	KMW653N0000		
Roshydromet	DAK654N0000, SHP659N0000		
SAWS	CPT134S0000	WMO (NIST & EMPA)	97, 98, 02, 06
SMN	USI354S0000	WMO (NIST & EMPA)	98, 03
UBA	BRT648N0000,DEU649N0000,LGB652N0000, NGL653N0000,SNB647N0000,SSL647N0000, WES654N0000,ZGT654N0000,ZSF647N0010, ZUG647N0000	WMO (NIST & EMPA)	Zugspitze: 96, 97, 01 Sonnblick: 98 Zugspitze/Schneefern erhaus: 06
UM	GLH636N0000		

6. Carbon Monoxide (CO)

The Swiss Federal Laboratory for Materials Testing and Research (EMPA) serves as the WCC under GAW based on its secondary standards calibrated against the standard at NOAA/GMD designated as the Primary Standard for GAW.

Table 7. Status of carbon monoxide standard scales at laboratories

Laboratory	WDCGG Filename Code	Calibration Scale	Audit EMPA-WCC
AGAGE	CGR540S0011,MCH653N0011	SIO 1998	
CHMI	KOS649N0000	CHMI	
CSIRO	ALT482N0003,CFA519S0003,CGO540S0003, CYA766S0000, ESP449N0003,MAA767S0003, MLO519N0003,MQA554S0003,SIS660N0003, SPO789S0003	WMO (NOAA/GMD & EMPA)	Cape Grim: 02
DWD	HPB647N0000	WMO (NOAA/GMD & EMPA)	06
EARS	KVV646N0000		
EMPA	JFJ646N0000,MKN100S0000,PAY646N0000, RIG646N0000	WMO (NOAA/GMD & EMPA)	Jungfraujoch: 99,06
JMA	RYO239N0000, MNM224N0000, YON224N0000	JMA	Ryori:05
NOAA/GMD	NOAA/GMD flask network*	WMO (NOAA/GMD & EMPA)	Mauna Loa: 03 Barrow: 08

PolyU	HKG222N0000		
RIVM	KMW653N0000,KTB653N0000	National	
SAWS	CPT134S0000	WMO (NOAA/GMD & EMPA)	98, 02, 06
SMN	USI354S0000	WMO (NOAA/GMD & EMPA)	98, 03
UBA	NGL653N0000,SNB647N0000,SSL647N0000, ZUG647N0000	WMO (NOAA/GMD & EMPA)	Zugspitze: 01 Sonnblick: 98
UM	GLH636N0000		

NOAA/GMD flask network:

ALT482N0001,ASC107S0001,ASK123N0101,AZR638N0001,BAL655N0001,BME432N0001,BMW432N0001,BRW471N0001,BSC644N0001, CBA455N0001,CGO540S0001,CHR501N0001,CMO445N0001,CRZ146S0001,EIC329S0001,GMI513N0001,GOZ636N0001,HBA775S0001, HUN646N0101,ICE663N0001,ITN435N0001,IZO128N0001,KEY425N0001,KUM519N0001,KZD244N0001,KZM243N0001,LEF445N0001, MBC476N0001,MHD653N0001,MID528N0001,MLO519N0001,NWR440N0001,PAL667N0001,POC90000001,POC905N0001,POC905S0001, POC910N0001,POC910S0001,POC915N0001,POC915S0001,POC920N0001,POC920S0001,POC925N0001,POC925S0001,POC930N0001, POC930S0001,POC935N0001,POC935S0001,PSA764S0001,PTA438N0001,RPB413N0001,SCS903N0001,SCS906N0001,SCS909N0001, SCS912N0001,SCS915N0001,SCS918N0001,SCS921N0001,SEY104S0001, SGP436N0000,SHM452N0001,SMO514S0001,SPO789S0001, STM666N0001,SYO769S0001,TAP236N0001,TDF354S0001, THD441N0000,UTA439N0001,UUM244N0001,WIS631N0001,WLG236N0001, ZEP678N0101

References

Aoki, S., T. Nakazawa, S. Murayama and S. Kawaguchi, Measurements of atmospheric methane at the Japanese Antarctic station, Syowa, *Tellus, Ser. B,* **44**, 273–281, 1992.

CMDL, Climate Monitoring and Diagnostics Laboratory Summary Report No.26 2000-2001, 2002.

Cunnold, D. M., L. P. Steele, P. J. Fraser, P. G. Simmonds, R. G. Prinn, R. F. Weiss, L. W. Porter, S. O'Doherty, R. L. Langenfelds, P. B. Krummel, H. J. Wang, L. Emmons, X. X. Tie, and E. J. Dlugokencky, In situ measurements of atmospheric methane at GAGE/AGAGE sites during 1985–2000 and resulting source inferences, *J. Geophys, Res,* **107(D14)**, 10.1029/2001JD001226, 2002.

Dlugokencky, E. J., L. P. Steele, P. M. Lang, and K. A. Masarie, The growth rate and distribution of atmospheric methane, *J. Geophys. Res.,* **99**, 17021-17043, 1994.

Dlugokencky, E. J., R. C. Myers, P. M. Lang, K. A. Masarie, A. M. Crotwell, K. W. Thoning, B. D. Hall, J. W. Elkins, and L. P. Steele, Conversion of NOAA atmospheirc dry air CH4 mole fractions to a gravimetrically prepared standard scale, *J. Geophys. Res. ,***110**, D18306, doi: 10.1029/2005JD006035, 2005.

Hall, B. D. (ed.), J. W. Elkins, J. H. Butler, S. A. Montzka, T. M. Thompson, L. Del Negro, G. S. Dutton, D. F. Hurst, D. B. King, E. S. Kline, L. Lock, D. Mactaggart, D. Mondeel, F. L. Moore, J. D. Nance, E. A. Ray, and P. A. Romashkin, Halocarbons and Other Atmospheric Gases, Section 5 in Climate Monitoring and Diagnostics Laboratory, Summary Report N. 25, 1998–1999, R. S. Schnell, D. B. King, R. M. Rosson (eds.), NOAA-CMDL, Boulder, CO., USA, 2001.

Hall, B. D., G. S. Dutton, and J. W. Elkins, The NOAA nitrous oxide standard scale for atmospheric observations, *J. Geophys. Res.*, 112, D09305, doi:10.1029/2006JD007954, 2007.

Hofer, P., B. Buchmann and A. Herzog, Traceability, Uncertainty and Assessment Criteria of Surface Ozone Measurements, *EMPA-WCC Report 98/5*, 20 pp, 1998.

Huang, J., A. Golombek, R. Prinn, R. Weiss, P. Fraser, P. Simmonds, E J. Dlugokencky, B. Hall, J. Elkins, P. Steele, R. Langenfelds, P. Krummel, G. Dutton, and L. Porter, Estimation of regional emissions of nitrous oxide from 1997 to 2005 using multinetowrk measurements, a chemical transport model, and an inverse method, *J. Geophys. Res.*, **113**, D17313, doi:10.1029/2007JD009381, 2008.

Klausen, J., C. Zellweger, B. Buchmann, and P. Hofer, Uncertainty and bias of surface ozone measurements at selected Global Atmosphere Watch sites, *J. Geophys. Res.,* **108(D19)**, 4622, doi:10.1029/2003JD003710, 2003.

Peterson, J., P. Tans, and D. Kitzis, "CO_2 Round-Robin Reference Gas Intercomparison" in Report of the Ninth WMO Meeting of Experts on Carbon Dioxide Concentration and Related Tracer Measurement Techniques, Aspendale, Vic. Australia, 1 - 4 September 1997, edited by R. Francey, WMO/GAW Report No. 132, 1999.

WMO, Report of the Eleventh WMO/IAEA Meeting of Experts on Carbon Dioxide Concentration and Related Tracer Measurement Techniques, Global Atmosphere Watch Report Series No.148, 2003.

WMO, WMO Global Atmosphere Watch (GAW) Strategic Plan: 2008–2015, WMO/GAW Report No. 172, 104pp, 2007.

Worthy, D. E. J., I. Levin, N. B. A. Trivett, A. J. Kuhlmann, J. F. Hopper and M. K. Ernst, Seven years of continuous methane observations at a remote boreal site in Ontario, Canada, *J. Geophys. Res.,* **103**, 15995–16007, 1998.

Zhao, C. L., P. P. Tans, and K. W. Thoning, A high precision manometric system for absolute calibrations of CO_2 in dry air, *J. Geophys. Res.,* **102**, 5885–5894, 1997.

LIST OF OBSERVATION STATIONS

Station	Country/Territory	Index Number	Location Latitude (° ')	Location Longitude (° ')	Altitude (m)	Parameter
REGION I (Africa)						
Amsterdam Island	France	AMS137S00	37 47 S	77 31 E	65	CO_2
Amsterdam Island	France	AMS137S00	37 47 S	77 31 E	65	CH_4, CO_2
Ascension Island	United Kingdom of Great Britain and Northern Ireland	ASC107S00	7 55 S	14 25 W	54	$^{13}CO_2$, $C^{18}O_2$, CH_4, CO, CO_2, H_2
Assekrem	Algeria	ASK123N00	23 16 N	5 37 E	2710	$^{13}CO_2$, $C^{18}O_2$, CH_4, CO, CO_2, H_2
Assekrem	Algeria	ASK123N00	23 16 N	5 37 E	2710	O_3
Cape Point	South Africa	CPT134S00	34 21 S	18 28 E	230	CH_4, CO, CO_2, N_2O, O_3
Cape Verde Observatory	Cape Verde	GVA116N00	16 50 N	24 52 W	10	CO, O_3
Crozet	France	CRZ146S00	46 27 S	51 51 E	120	$^{13}CO_2$, $C^{18}O_2$, CH_4, CO, CO_2, H_2
Funchal	Portugal	FUN132N00	32 38 N	16 52 W	58	O_3
Gobabeb	Namibia	NMB123S00	23 34 S	15 1 E	461	$^{13}CO_2$, $C^{18}O_2$, CH_4, CO_2
Izaña (Tenerife)	Spain	IZO128N00	28 18 N	16 30 W	2367	CH_4, CO_2, O_3
Izaña (Tenerife)	Spain	IZO128N00	28 18 N	16 30 W	2367	$^{13}CO_2$, $C^{18}O_2$, CH_4, CO, CO_2, H_2
Mahe Island	Seychelles	SEY104S00	4 40 S	55 10 E	7	$^{13}CO_2$, $C^{18}O_2$, CH_4, CO, CO_2, H_2
Mt. Kenya	Kenya	MKN100S00	0 3 S	37 17 E	3678	CO, O_3
Mt. Kenya	Kenya	MKN100S00	0 3 S	37 17 E	3678	$^{13}CO_2$, $C^{18}O_2$, CH_4, CO_2
REGION II (Asia)						
Anmyeon-do	Republic of Korea	AMY236N00	36 31 N	126 19 E	47	CFCs, CH_4, CO_2, N_2O
Bering Island	Russian Federation	BER255N00	55 12 N	165 58 E	13	CO_2
Cape Ochi-ishi	Japan	COI243N00	43 8 N	145 30 E	45	CH_4, CO_2
Gosan	Republic of Korea	GSN233N00	33 16 N	126 10 E	72	CFCs, CH_4, CO_2, N_2O
Gosan	Republic of Korea	GSN233N01	33 8 N	126 7 E	72	CFCs, CH_4, CO_2, N_2O
Hamamatsu	Japan	HMM234N00	34 43 N	137 43 E	35	CO_2
Hateruma	Japan	HAT224N00	24 3 N	123 47 E	10	CH_4, CO_2, N_2O
Hok Tsui	Hong Kong, China	HKG222N00	22 13 N	114 15 E	60	CO, O_3
Issyk-Kul	Kyrgyzstan	ISK242N00	42 37 N	76 58 E	1640	CH_4, CO_2, O_3
Kaashidhoo	Maldives	KCO204N00	4 58 N	73 28 E	1	$^{13}CO_2$, CH_4, CO_2
Kisai	Japan	KIS236N00	36 4 N	139 33 E	13	CO_2
Kotelny Island	Russian Federation	KOT276N00	76 0 N	137 52 E	5	CO_2
Kyzylcha	Uzbekistan	KYZ240N00	40 52 N	66 9 E	340	CO_2
Lulin	China	LLN223N00	23 28 N	120 52 E	2867	CH_4, CO_2
Memanbetsu	Japan	MMB243N00	43 55 N	144 11 E	32.9	N_2O
Mikawa-Ichinomiya	Japan	MKW234N00	34 51 N	137 25 E	50	CO_2
Minamitorishima	Japan	MNM224N00	24 16 N	153 58 E	8	CH_4, CO, CO_2, O_3
Mt. Dodaira	Japan	DDR236N00	36 0 N	139 10 E	840	CO_2
Mt. Waliguan	China	WLG236N00	36 16 N	100 54 E	3810	$^{13}CO_2$, $C^{18}O_2$, CH_4, CO, CO_2, H_2
Mt. Waliguan	China	WLG236N00	36 16 N	100 54 E	3810	CO_2
Nagoya	Japan	NGY235N00	35 8 N	136 58 E	35	N_2O
Plateau Assy	Kazakhstan	KZM243N00	43 15 N	77 52 E	2519	$^{13}CO_2$, $C^{18}O_2$, CH_4, CO, CO_2, H_2
Ryori	Japan	RYO239N00	39 1 N	141 49 E	260	CCl_4, CFCs, CH_3CCl_3, CH_4, CO, CO_2, N_2O, O_3
Sary Taukum	Kazakhstan	KZD244N00	44 27 N	75 34 E	412	$^{13}CO_2$, $C^{18}O_2$, CH_4, CO, CO_2, H_2
Ship between Ishigaki Island and Hateruma Island	Japan	SIH224N00	24 7 N	123 49 E	5	CO_2
South China Sea (03N)	N/A	SCS903N00	3 0 N	105 0 E	15	$^{13}CO_2$, $C^{18}O_2$, CH_4, CO, CO_2, H_2
South China Sea (06N)	N/A	SCS906N00	6 0 N	107 0 E	15	$^{13}CO_2$, $C^{18}O_2$, CH_4, CO, CO_2, H_2
South China Sea (09N)	N/A	SCS909N00	9 0 N	109 0 E	15	$^{13}CO_2$, $C^{18}O_2$, CH_4, CO, CO_2, H_2
South China Sea (12N)	N/A	SCS912N00	12 0 N	111 0 E	15	$^{13}CO_2$, $C^{18}O_2$, CH_4, CO, CO_2, H_2

LIST OF OBSERVATION STATIONS (continued)

Station	Country/Territory	Index Number	Location Latitude (° ')	Location Longitude (° ')	Altitude (m)	Parameter
South China Sea (15N)	N/A	SCS915N00	15 0 N	113 0 E	15	$^{13}CO_2$, $C^{18}O_2$, CH_4, CO, CO_2, H_2
South China Sea (18N)	N/A	SCS918N00	18 0 N	113 0 E	15	$^{13}CO_2$, $C^{18}O_2$, CH_4, CO, CO_2, H_2
South China Sea (21N)	N/A	SCS921N00	21 0 N	114 0 E	15	$^{13}CO_2$, $C^{18}O_2$, CH_4, CO, CO_2, H_2
Suita	Japan	STA234N00	34 49 N	135 31 E	63	CO_2
Tae-ahn Peninsula	Republic of Korea	TAP236N00	36 43 N	126 7 E	20	$^{13}CO_2$, $C^{18}O_2$, CH_4, CO, CO_2, H_2
Takayama	Japan	TKY236N00	36 8 N	137 25 E	1420	CO_2
Tsukuba	Japan	TKB236N00	36 2 N	140 7 E	26	CH_4, CO_2
Tsukuba	Japan	TKB236N10	36 2 N	140 7 E	25	O_3
Ulaan Uul	Mongolia	UUM244N00	44 27 N	111 4 E	914	$^{13}CO_2$, $C^{18}O_2$, CH_4, CO, CO_2, H_2
Urawa	Japan	URW235N00	35 52 N	139 35 E	10	CO_2
Yonagunijima	Japan	YON224N00	24 28 N	123 1 E	30	CH_4, CO, CO_2, O_3
REGION III (South America)						
Arembepe	Brazil	ABP312S00	12 46 S	38 10 W	0	CH_4
Arembepe	Brazil	ABP312S00	12 46 S	38 10 W	0	O_3
Bird Island	United Kingdom of Great Britain and Northern Ireland	SGI354S00	54 0 S	38 2 W	30	CH_4, CO_2
Easter Island	Chile	EIC327S00	27 7 S	109 27 W	50	$^{13}CO_2$, $C^{18}O_2$, CH_4, CO, CO_2, H_2
Huancayo	Peru	HUA312S00	12 4 S	75 31 W	3313	CO_2
Tierra del Fuego	Argentina	TDF354S00	54 52 S	68 28 W	20	$^{13}CO_2$, $C^{18}O_2$, $CBrClF_2$, CFCs, CH_3Br, CH_3CCl_3, CH_4, CO, CO_2, H_2, HCFCs, HFCs
Ushuaia	Argentina	USI354S00	54 51 S	68 19 W	18	CO, O_3
REGION IV (North and Central America)						
Alert	Canada	ALT482N00	82 27 N	62 31 W	210	CH_4, CO, CO_2, H_2, N_2O
Alert	Canada	ALT482N00	82 27 N	62 31 W	210	$^{13}CO_2$, $C^{18}O_2$, C_2Cl_4, $CBrClF_2$, $CBrF_3$, CCl_4, CFCs, CH_2Cl_2, CH_3Br, CH_3CCl_3, CH_4, CO, CO_2, H_2, HCFCs, HFCs, N_2O, SF_6
Alert	Canada	ALT482N00	82 27 N	62 31 W	210	CH_4, CO, CO_2, N_2O, SF_6
Algoma	Canada	ALG447N00	47 1 N	84 22 W	411	O_3
Barrow	United States of America	BRW471N00	71 19 N	156 35 W	11	$^{13}CH_4$, $^{13}CO_2$, $C^{18}O_2$, C_2Cl_4, $CBrClF_2$, $CBrF_3$, CCl_4, CFCs, CH_2Cl_2, CH_3Br, CH_3CCl_3, CH_3Cl, CH_4, CO, CO_2, H_2, HCFCs, HFCs, N_2O, O_3, SF_6
Bratt's Lake	Canada	BRA450N00	50 12 N	104 12 W	588	O_3
Candle Lake	Canada	CDL453N00	53 52 N	104 39 W	489	CH_4, CO, CO_2
Cape Meares	United States of America	CMO445N00	45 28 N	123 58 W	30	$^{13}CO_2$, $C^{18}O_2$, CH_4, CO, CO_2, H_2
Cape Meares	United States of America	CMO445N00	45 28 N	123 58 W	30	CCl_4, CFCs, CH_3CCl_3, CH_4, N_2O
Cape St. James	Canada	CSJ451N00	51 55 N	131 1 W	89	CO_2
Chalk River	Canada	CHA446N00	46 4 N	77 24 W	184	O_3
Chapais	Canada	CPS449N00	49 49 N	74 58 W	381	O_3
Cold Bay	United States of America	CBA455N00	55 12 N	162 43 W	25	$^{13}CO_2$, $C^{18}O_2$, CH_4, CO, CO_2, H_2
Egbert	Canada	EGB444N00	44 13 N	79 46 W	253	O_3
Estevan Point	Canada	ESP449N00	49 22 N	126 32 W	39	CH_4, CO_2, N_2O, SF_6
Estevan Point	Canada	ESP449N00	49 22 N	126 32 W	39	CH_4, CO, CO_2, H_2, N_2O

LIST OF OBSERVATION STATIONS (continued)

Station	Country/Territory	Index Number	Location Latitude (° ')	Location Longitude (° ')	Altitude (m)	Parameter
Esther	Canada	EST451N00	51 40 N	110 12 W	707	O_3
Experimental Lakes Area	Canada	ELA449N00	49 40 N	93 43 W	369	O_3
Frasedale	Canada	FSD449N00	49 52 N	81 34 W	210	CH_4, CO, CO_2
Grifton	United States of America	ITN435N00	35 21 N	77 22 W	505	$^{13}CO_2$, $C^{18}O_2$, CCl_4, CFCs, CH_4, CO, CO_2, H_2, N_2O, SF_6
Harvard Forest	United States of America	HFM442N00	42 53 N	72 17 W	340	$CBrClF_2$, CCl_4, CFCs, CH_3Br, CH_3CCl_3, HCFCs, HFCs, N_2O, SF_6
Kejimkujik	Canada	KEJ444N00	44 25 N	65 12 W	127	O_3
Key Biscayne	United States of America	KEY425N00	25 40 N	80 12 W	3	$^{13}CO_2$, $C^{18}O_2$, CH_4, CO, CO_2, H_2
Kitt Peak	United States of America	KPA431N00	31 58 N	111 35 W	2083	CH_4
La Jolla	United States of America	SIO432N00	32 49 N	117 16 W	14	CH_4
La Palma	Cuba	PLM422N00	22 45 N	83 31 W	47	NO_2
Longwoods	Canada	LON442N00	42 52 N	81 28 W	239	O_3
Moody	United States of America	WKT431N00	31 19 N	97 19 W	708	CH_4
Mould Bay	Canada	MBC476N00	76 15 N	119 19 W	58	$^{13}CO_2$, $C^{18}O_2$, CH_4, CO, CO_2, H_2
Niwot Ridge (C-1)	United States of America	NWR440N00	40 2 N	105 32 W	3021	C_2Cl_4, $CBrClF_2$, $CBrF_3$, CCl_4, CFCs, CH_2Cl_2, CH_3Br, CH_3CCl_3, CH_3Cl, HCFCs, HFCs, N_2O, O_3, SF_6
Niwot Ridge (Saddle)	United States of America	NWR440N02	40 3 N	105 35 W	3528	O_3
Niwot Ridge (T-van)	United States of America	NWR440N01	40 3 N	105 35 W	3523	$^{13}CH_4$, $^{13}CO_2$, $C^{18}O_2$, CH_4, CO, CO_2, H_2
Olympic Peninsula	United States of America	OPW448N00	48 15 N	124 25 W	488	CH_4, CO_2, H_2
Pacific Ocean (15N)	N/A	POC915N00	15 0 N	145 0 W	10	$^{13}CO_2$, $C^{18}O_2$, CH_4, CO, CO_2, H_2
Pacific Ocean (20N)	N/A	POC920N00	20 0 N	141 0 W	10	$^{13}CO_2$, $C^{18}O_2$, CH_4, CO, CO_2, H_2
Pacific Ocean (25N)	N/A	POC925N00	25 0 N	139 0 W	10	$^{13}CO_2$, $C^{18}O_2$, CH_4, CO, CO_2, H_2
Pacific Ocean (30N)	N/A	POC930N00	30 0 N	135 0 W	10	$^{13}CO_2$, $C^{18}O_2$, CH_4, CO, CO_2, H_2
Pacific Ocean (35N)	N/A	POC935N00	35 0 N	137 0 W	10	$^{13}CO_2$, $C^{18}O_2$, CO, H_2
Pacific Ocean (40N)	N/A	POC940N00	40 0 N	136 0 W	10	$^{13}CO_2$, H_2
Pacific Ocean (45N)	N/A	POC945N00	45 0 N	131 0 W	10	$^{13}CO_2$, H_2
Park Falls	United States of America	LEF445N00	45 55 N	90 16 W	868	$^{13}CO_2$, $C^{18}O_2$, $CBrClF_2$, CFCs, CH_3Br, CH_3CCl_3, CH_4, CO, CO_2, H_2, HCFCs, HFCs, N_2O, SF_6
Point Arena	United States of America	PTA438N00	38 57 N	123 43 W	17	$^{13}CO_2$, $C^{18}O_2$, CH_4, CO, CO_2
Ragged Point	Barbados	RPB413N00	13 10 N	59 25 W	45	$^{13}CO_2$, $C^{18}O_2$, CH_4, CO, CO_2, H_2, O_3
Ragged Point	Barbados	RPB413N00	13 10 N	59 25 W	45	$CBrClF_2$, $CBrF_3$, CCl_4, CFCs, CH_2Cl_2, CH_3Br, CH_3CCl_3, CH_3Cl, CH_4, $CHCl_3$, HCFCs, HFCs, N_2O, SF_6
Sable Island	Canada	WSA443N00	43 55 N	60 1 W	5	CH_4, CO, CO_2, N_2O, SF_6
Saturna	Canada	SAT448N00	48 46 N	123 7 W	178	O_3
Shemya Island	United States of America	SHM452N00	52 43 N	174 4 E	40	$^{13}CO_2$, $C^{18}O_2$, CH_4, CO, CO_2, H_2

LIST OF OBSERVATION STATIONS (continued)

Station	Country/Territory	Index Number	Location Latitude (° ')	Location Longitude (° ')	Altitude (m)	Parameter
Southern Great Plains	United States of America	SGP436N00	36 46 N	97 30 W	314	$^{13}CO_2$, $C^{18}O_2$, CH_4, CO, CO_2
St. Croix	United States of America	AVI417N00	17 45 N	64 45 W	3	CH_4, CO_2
St. David's Head	United Kingdom of Great Britain and Northern Ireland	BME432N00	32 22 N	64 39 W	30	$^{13}CO_2$, $C^{18}O_2$, CH_4, CO, CO_2, H_2
Sutton	Canada	SUT445N00	45 4 N	72 40 W	243	O_3
Trinidad Head	United States of America	THD441N00	41 2 N	124 9 W	120	$CBrClF_2$, $CBrF_3$, CCl_4, CFCs, CH_2Cl_2, CH_3Br, CH_3CCl_3, CH_3Cl, CH_4, $CHCl_3$, HCFCs, HFCs, N_2O, SF_6
Trinidad Head	United States of America	THD441N00	41 2 N	124 9 W	120	$^{13}CO_2$, $C^{18}O_2$, $CBrClF_2$, CCl_4, CFCs, CH_3Br, CH_3CCl_3, CH_4, CO, CO_2, HCFCs, HFCs, N_2O, O_3, SF_6
Tudor Hill	United Kingdom of Great Britain and Northern Ireland	BMW432N00	32 16 N	64 52 W	30	$^{13}CO_2$, $C^{18}O_2$, CH_4, CO, CO_2, H_2, O_3
Wendover	United States of America	UTA439N00	39 52 N	113 43 W	1320	$^{13}CO_2$, $C^{18}O_2$, CH_4, CO, CO_2, H_2
REGION V (South-West Pacific)						
Baring Head	New Zealand	BAR541S00	41 25 S	174 52 E	85	CH_4, CO_2
Baring Head	New Zealand	BAR541S00	41 25 S	174 52 E	85	$^{13}CH_4$, $^{14}CO_2$, CH_4, CO, CO_2, N_2O, O_3, VOCs
Bukit Koto Tabang	Indonesia	BKT500S00	0 12 S	100 19 E	864.5	O_3
Bukit Koto Tabang	Indonesia	BKT500S00	0 12 S	100 19 E	864.5	NO_2, SO_2
Bukit Koto Tabang	Indonesia	BKT500S00	0 12 S	100 19 E	864.5	$^{13}CO_2$, $C^{18}O_2$, CH_4, CO_2
Cape Ferguson	Australia	CFA519S00	19 16 S	147 3 E	2	CH_4, CO, CO_2, H_2, N_2O
Cape Grim	Australia	CGO540S00	40 40 S	144 40 E	94	CO_2, O_3
Cape Grim	Australia	CGO540S00	40 40 S	144 40 E	94	CH_4, CO, CO_2, H_2, N_2O
Cape Grim	Australia	CGO540S00	40 40 S	144 40 E	94	$^{13}CH_4$, $^{13}CO_2$, $C^{18}O_2$, C_2Cl_4, $CBrClF_2$, $CBrF_3$, CCl_4, CFCs, CH_2Cl_2, CH_3Br, CH_3CCl_3, CH_4, CO, CO_2, H_2, HCFCs, HFCs, N_2O, SF_6
Cape Grim	Australia	CGO540S00	40 40 S	144 40 E	94	$CBrClF_2$, $CBrF_3$, CCl_4, CFCs, CH_2Cl_2, CH_3Br, CH_3CCl_3, CH_3Cl, CH_4, $CHCl_3$, CO, H_2, HCFCs, HFCs, N_2O, SF_6
Cape Kumukahi	United States of America	KUM519N00	19 31 N	154 49 W	3	$^{13}CO_2$, $C^{18}O_2$, C_2Cl_4, $CBrClF_2$, $CBrF_3$, CCl_4, CFCs, CH_2Cl_2, CH_3Br, CH_3CCl_3, CH_4, CO, CO_2, H_2, HCFCs, HFCs, N_2O, SF_6
Christmas Island	Kiribati	CHR501N00	1 42 N	157 10 W	3	$^{13}CO_2$, $C^{18}O_2$, CH_4, CO, CO_2, H_2
Danum Valley GAW Baseline Station	Malaysia	DMV504N00	4 58 N	117 49 E	426	CO_2
Guam	United States of America	GMI513N00	13 25 N	144 46 E	2	$^{13}CO_2$, $C^{18}O_2$, CH_4, CO, CO_2, H_2
Jakarta	Indonesia	JKR506S00	6 10 S	106 49 E	7	NO_2, SO_2
Kaitorete Spit	New Zealand	NZL543S00	43 49 S	172 37 E	3	CH_4
Lauder	New Zealand	LAU545S00	45 1 S	169 40 E	370	O_3

LIST OF OBSERVATION STATIONS (continued)

Station	Country/Territory	Index Number	Location Latitude (° ')	Location Longitude (° ')	Altitude (m)	Parameter
Macquarie Island	Australia	MQA554S00	54 28 S	158 58 E	12	CH_4, CO, CO_2, H_2, N_2O
Mauna Loa	United States of America	MLO519N00	19 32 N	155 34 W	3397	$^{13}CH_4$, $^{13}CO_2$, $C^{18}O_2$, C_2Cl_4, $CBrClF_2$, $CBrF_3$, CCl_4, CFCs, CH_2Cl_2, CH_3Br, CH_3CCl_3, CH_3Cl, CH_4, CO, CO_2, H_2, HCFCs, HFCs, N_2O, O_3, SF_6
Mauna Loa	United States of America	MLO519N00	19 32 N	155 34 W	3397	CH_4, CO, CO_2, H_2, N_2O
Pacific Ocean (00N)	N/A	POC900N00	0 0 N	155 0 W	10	$^{13}CO_2$, $C^{18}O_2$, CH_4, CO, CO_2, H_2
Pacific Ocean (05N)	N/A	POC905N00	5 0 N	151 0 W	10	$^{13}CO_2$, $C^{18}O_2$, CH_4, CO, CO_2, H_2
Pacific Ocean (05S)	N/A	POC905S00	5 0 S	159 0 W	10	$^{13}CO_2$, $C^{18}O_2$, CH_4, CO, CO_2, H_2
Pacific Ocean (10N)	N/A	POC910N00	10 0 N	149 0 W	10	$^{13}CO_2$, $C^{18}O_2$, CH_4, CO, CO_2, H_2
Pacific Ocean (10S)	N/A	POC910S00	10 0 S	161 0 W	10	$^{13}CO_2$, $C^{18}O_2$, CH_4, CO, CO_2, H_2
Pacific Ocean (15S)	N/A	POC915S00	15 0 S	171 0 W	10	$^{13}CO_2$, $C^{18}O_2$, CH_4, CO, CO_2, H_2
Pacific Ocean (20S)	N/A	POC920S00	20 0 S	174 0 W	10	$^{13}CO_2$, $C^{18}O_2$, CH_4, CO, CO_2, H_2
Pacific Ocean (25S)	N/A	POC925S00	25 0 S	171 0 W	10	$^{13}CO_2$, $C^{18}O_2$, CH_4, CO, CO_2, H_2
Pacific Ocean (30S)	N/A	POC930S00	30 0 S	176 0 W	10	$^{13}CO_2$, $C^{18}O_2$, CH_4, CO, CO_2, H_2
Pacific Ocean (35S)	N/A	POC935S00	35 0 S	180 0 E	10	$^{13}CO_2$, $C^{18}O_2$, CH_4, CO, CO_2, H_2
Sand Island	United States of America	MID528N00	28 11 N	177 22 W	7.7	$^{13}CO_2$, $C^{18}O_2$, CH_4, CO, CO_2, H_2
Tanah Rata	Malaysia	TAR504N00	4 28 N	101 22 E	1545	O_3
Tutuila (Cape Matatula)	United States of America	SMO514S00	14 14 S	170 34 W	42	$^{13}CH_4$, $^{13}CO_2$, $C^{18}O_2$, C_2Cl_4, $CBrClF_2$, $CBrF_3$, CCl_4, CFCs, CH_2Cl_2, CH_3Br, CH_3CCl_3, CH_3Cl, CH_4, CO, CO_2, H_2, HCFCs, HFCs, N_2O, O_3, SF_6
Tutuila (Cape Matatula)	United States of America	SMO514S00	14 14 S	170 34 W	42	$CBrClF_2$, $CBrF_3$, CCl_4, CFCs, CH_2Cl_2, CH_3Br, CH_3CCl_3, CH_3Cl, CH_4, $CHCl_3$, HCFCs, HFCs, N_2O, SF_6
REGION VI (Europe)						
Adrigole	Ireland	ADR651N00	51 40 N	9 43 W	50	CCl_4, CFCs, CH_3CCl_3, N_2O
Angra do Heroismo	Portugal	ANG638N00	38 40 N	27 13 W	74	O_3
Baltic Sea	Poland	BAL655N00	55 21 N	17 13 E	28	$^{13}CO_2$, $C^{18}O_2$, CH_4, CO, CO_2, H_2
Beja	Portugal	BEJ638N00	38 1 N	7 52 W	246	O_3
Black Sea	Romania	BSC644N00	44 10 N	28 40 E	3	$^{13}CO_2$, $C^{18}O_2$, CH_4, CO, CO_2, H_2
Braganca	Portugal	BRG641N00	41 47 N	6 43 W	690	SO_2
Brotjacklriegel	Germany	BRT648N00	48 49 N	13 13 E	1016	VOCs
Brotjacklriegel	Germany	BRT648N00	48 49 N	13 13 E	1016	CO_2, O_3
Burgas	Bulgaria	BUR642N00	42 28 N	27 28 E	16	NO_2, SO_2
Campisabalos	Spain	CAM641N00	41 16 N	3 8 W	1360	VOCs
Castelo Branco	Portugal	CAS639N00	39 49 N	7 28 W	386	O_3
Danki	Russian Federation	DAK654N00	54 53 N	37 47 E	140	O_3
Deuselbach	Germany	DEU649N00	49 46 N	7 2 E	480	CH_4, CO_2, O_3
Donon	France	DNN648N00	48 30 N	7 7 E	775	VOCs
Doñana	Spain	DON637N00	37 2 N	6 32 W	5	NO_2, O_3, SO_2
Dwejra Point	Malta	GOZ636N00	36 2 N	14 10 E	30	$^{13}CO_2$, $C^{18}O_2$, CH_4, CO, CO_2, H_2
Eskdalemuir	United Kingdom of Great Britain and Northern Ireland	EDM655N00	55 19 N	3 12 W	242	O_3
Fundata	Romania	FDT645N00	45 28 N	25 18 E	1383.5	CO_2, NO_2, O_3
Fundata	Romania	FDT645N00	45 28 N	25 18 E	1383.5	NO_2, SO_2

LIST OF OBSERVATION STATIONS (continued)

Station	Country/Territory	Index Number	Location Latitude (° ')	Location Longitude (° ')	Altitude (m)	Parameter
Giordan Lighthouse	Malta	GLH636N00	36 4 N	14 13 E	167	CO, O_3
Hegyhatsal	Hungary	HUN646N00	46 57 N	16 38 E	248	CO_2
Hegyhatsal	Hungary	HUN646N00	46 57 N	16 38 E	248	$^{13}CO_2$, $C^{18}O_2$, CH_4, CO, CO_2, H_2
Heimaey	Iceland	ICE663N00	63 23 N	20 16 W	100	$^{13}CO_2$, $C^{18}O_2$, CH_4, CO, CO_2, H_2, O_3
Hohe Warte	Austria	HHE648N00	48 15 N	16 22 E	202	NO, NO_2, SO_2
Hohe Warte	Austria	HHE648N00	48 15 N	16 22 E	202	NO, NO_2, SO_2
Hohenpeissenberg	Germany	HPB647N00	47 47 N	11 1 E	985	^{222}Rn, CO, H_2O_2, NO, NO_2, NOx, NOy, O_3, PAN, ROOH, SO_2, VOCs
Hohenpeissenberg	Germany	HPB647N00	47 47 N	11 1 E	985	CH_4, CO_2
Iskrba	Slovenia	IRB645N00	45 34 N	14 52 E	520	O_3, SO_2
Ivan Sedlo	Bosnia and Herzegovina	IVN643N00	43 46 N	18 1 E	970	NO_2, SO_2
Jarczew	Poland	JCZ651N00	51 49 N	21 58 E	180	NO_2, SO_2
Jungfraujoch	Switzerland	JFJ646N00	46 32 N	7 59 E	3580	CH_4, CO, N_2O, NO, NO_2, NOx, O_3, SF_6, SO_2
K-puszta	Hungary	KPS646N00	46 58 N	19 33 E	125	CO_2, NO_2, O_3, SO_2
Kamenicki Vis	Serbia	KAM643N00	43 23 N	21 56 E	813	NO_2, SO_2
Kloosterburen	Netherlands (the)	KTB653N00	53 23 N	6 25 E	0	CO, NO, NO_2, NOx, SO_2
Kollumerwaard	Netherlands (the)	KMW653N00	53 19 N	6 16 E	0	CH_4, CO, CO_2, NO, NO_2, NOx, O_3, SO_2
Kosetice	Czech Republic	KOS649N00	49 34 N	15 4 E	534	CH_4, CO, NO, NO_2, O_3, SO_2
Kosetice	Czech Republic	KOS649N00	49 34 N	15 4 E	534	VOCs
Kovk	Slovenia	KVK646N00	46 7 N	15 5 E	600	O_3
Krvavec	Slovenia	KVV646N00	46 17 N	14 31 E	1720	CO, O_3
La Cartuja	Spain	CAR637N00	37 12 N	3 36 W	720	NO_2, SO_2
La Tardiere	France	LAT646N00	46 38 N	0 45 W	133	VOCs
Lampedusa	Italy	LMP635N00	35 31 N	12 37 E	45	CH_4, CO_2
Lampedusa	Italy	LMP635N00	35 31 N	12 37 E	45	CFCs, CH_4, CO_2, HCFCs, HFCs, N_2O, SF_6
Lazaropole	The former Yugoslav Republic of Macedonia	LZP641N00	41 31 N	20 41 E	1320	NO_2, SO_2
Leba	Poland	LEB654N00	54 45 N	17 31 E	2	NO_2, SO_2
Lisboa / Gago Coutinho	Portugal	LIS638N00	38 46 N	9 7 W	105	O_3
Logroño	Spain	LOG642N00	42 27 N	2 30 W	370	NO_2, SO_2
Mace Head	Ireland	MHD653N00	53 19 N	9 54 W	25	$^{13}CO_2$, $C^{18}O_2$, $CBrClF_2$, $CBrF_3$, CCl_4, CFCs, CH_3Br, CH_3CCl_3, CH_4, CO, CO_2, H_2, HCFCs, HFCs, N_2O, SF_6
Mace Head	Ireland	MHD653N00	53 19 N	9 54 W	25	$CBrClF_2$, $CBrF_3$, CCl_4, CFCs, CH_2Cl_2, CH_3Br, CH_3CCl_3, CH_3Cl, CH_4, $CHCl_3$, CO, H_2, HCFCs, HFCs, N_2O, SF_6
Mace Head	Ireland	MHD653N00	53 19 N	9 54 W	25	CO_2
Mace Head	Ireland	MHD653N00	53 19 N	9 54 W	25	O_3
Mahón	Spain	MHN639N00	39 52 N	4 19 E	78	NO_2, O_3, SO_2
Monte Cimone	Italy	CMN644N00	44 10 N	10 41 E	2165	O_3
Monte Cimone	Italy	CMN644N00	44 10 N	10 41 E	2165	CO_2
Monte Velho	Portugal	MVH638N00	38 4 N	8 48 W	43	O_3
Neuglobsow	Germany	NGL653N00	53 10 N	13 1 E	65	CH_4, CO, CO_2, O_3
Noia	Spain	NIA642N00	42 43 N	8 55 W	685	NO_2, O_3, SO_2
Ocean Station "C"	United States of America	STC654N00	54 0 N	35 0 W	6	CO_2
Ocean Station "M"	Norway	STM666N00	66 0 N	2 0 E	5	$^{13}CO_2$, $C^{18}O_2$, CH_4, CO, CO_2, H_2

LIST OF OBSERVATION STATIONS (continued)

Station	Country/Territory	Index Number	Location Latitude (° ')	Location Longitude (° ')	Altitude (m)	Parameter
Ocean Station Charlie	Russian Federation	STC652N00	52 45 N	35 30 W	5	CO_2
Ochsenkopf	Germany	OXK650N00	50 1 N	11 48 E	1185	CH_4
Oulanka	Finland	OUL666N00	66 19 N	29 23 E	310	NO_2, O_3, SO_2
Pallas-Sammaltunturi	Finland	PAL667N00	67 58 N	24 7 E	560	CO_2, O_3
Pallas-Sammaltunturi	Finland	PAL667N00	67 58 N	24 7 E	560	VOCs
Pallas-Sammaltunturi	Finland	PAL667N00	67 58 N	24 7 E	560	$^{13}CO_2$, $C^{18}O_2$, $CBrF_3$, CH_4, CO, CO_2
Payerne	Switzerland	PAY646N00	46 49 N	6 57 E	490	CO, NO, NO_2, NOx, O_3, SO_2
Penhas Douradas	Portugal	PEN640N00	40 25 N	7 32 W	1380	O_3
Peyrusse Vieille	France	PVI643N00	43 37 N	0 10 E	200	VOCs
Plateau Rosa	Italy	PRS645N00	45 55 N	7 42 E	3480	CH_4, CO_2, O_3
Pleven	Bulgaria	PLV643N00	43 25 N	24 36 E	64	NO_2, SO_2
Plovdiv	Bulgaria	PLD642N00	42 7 N	24 45 E	179	NO_2, SO_2
Puszcza Borecka/Diabla Gora	Poland	DIG654N00	54 8 N	22 4 E	157	CO_2, NO_2, O_3, SO_2
Rigi	Switzerland	RIG646N00	46 4 N	8 26 E	1031	CO, NO, NO_2, NOx, O_3, SO_2, VOCs
Roquetes	Spain	ROQ640N00	40 49 N	0 28 E	50	NO_2, O_3, SO_2
Rucava	Latvia	RCV656N00	56 10 N	21 10 E	18	NO_2, O_3, SO_2
San Pablo de los Montes	Spain	SPM639N00	39 32 N	4 20 W	917	NO_2, O_3, SO_2
Schauinsland	Germany	SSL647N00	47 55 N	7 55 E	1205	CH_4, CO, CO_2, N_2O, NO, NO_2, O_3, SF_6
Schmuecke	Germany	SCH650N00	50 38 N	10 46 E	937	VOCs
Sede Boker	Israel	WIS631N00	31 7 N	34 52 E	400	$^{13}CO_2$, $C^{18}O_2$, CH_4, CO, CO_2, H_2
Semenic	Romania	SEM645N00	45 7 N	21 58 E	1432	NO_2, SO_2
Shepelevo	Russian Federation	SHP659N00	59 58 N	29 7 E	4	O_3
Shetland	United Kingdom of Great Britain and Northern Ireland	SIS660N00	60 4 N	1 15 W	30	CH_4, CO, CO_2, H_2, N_2O
Site J	Denmark	GRL666N00	66 30 N	46 12 W	2030	CH_4
Sniezka	Poland	SNZ650N00	50 43 N	15 43 E	1603	NO_2, SO_2
Sofia	Bulgaria	SOF642N00	42 38 N	23 22 E	586	NO_2, SO_2
Sonnblick	Austria	SNB647N00	47 2 N	12 56 E	3106	CO, CO_2, NO, NOy, O_3
Starina	Slovakia	STA649N00	49 2 N	22 16 E	345	VOCs
Stephansplatz	Austria	STP648N00	48 13 N	16 22 E	171	NO, NO_2, SO_2
Stephansplatz	Austria	STP648N00	48 13 N	16 22 E	171	NO, NO_2, SO_2
Stîna de Vale	Romania	STN646N00	46 40 N	22 37 E	1116	NO_2, SO_2
Summit	Denmark	SUM672N00	72 34 N	38 28 W	3238	$^{13}CO_2$, $C^{18}O_2$, $CBrClF_2$, CCl_4, CFCs, CH_3Br, CH_3CCl_3, CH_4, CO_2, HCFCs, HFCs, N_2O, O_3, SF_6
Suwalki	Poland	SWL654N00	54 7 N	22 56 E	184	NO_2, SO_2
Terceira Island	Portugal	AZR638N00	38 46 N	27 22 W	40	$^{13}CO_2$, $C^{18}O_2$, CH_4, CO, CO_2, H_2
Teriberka	Russian Federation	TER669N00	69 12 N	35 6 E	40	CH_4, CO_2
Utö	Finland	UTO659N00	59 46 N	21 22 E	7	VOCs
Utö	Finland	UTO659N00	59 46 N	21 22 E	7	NO_2, O_3, SO_2
Varna	Bulgaria	VRN643N00	43 12 N	27 55 E	41	NO_2, SO_2
Viana do Castelo	Portugal	VDC641N00	41 42 N	8 48 W	16	SO_2
Vindeln	Sweden	VDL664N00	64 15 N	19 46 E	271	O_3
Virolahti	Finland	VIR660N00	60 31 N	27 40 E	4	NO_2, O_3, SO_2
Waldhof	Germany	LGB652N00	52 47 N	10 46 E	74	VOCs
Waldhof	Germany	LGB652N00	52 47 N	10 46 E	74	CO_2, O_3
Wank Peak	Germany	WNK647N00	47 31 N	11 9 E	1780	CO_2, NOx, SO_2
Westerland	Germany	WES654N00	54 55 N	8 19 E	12	CO_2, O_3

LIST OF OBSERVATION STATIONS (continued)

Station	Country/Territory	Index Number	Location Latitude (° ')	Location Longitude (° ')	Altitude (m)	Parameter
Zabljak	Montenegro	ZBL643N00	43 8 N	19 7 E	1450	NO_2, SO_2
Zavodnje	Slovenia	ZRN646N00	46 25 N	15 0 E	770	O_3
Zeppelinfjellet (Ny-Alesund)	Norway	ZEP678N00	78 54 N	11 52 E	475	CCl_4, CFCs, CH_3CCl_3, N_2O, O_3, SO_2
Zeppelinfjellet (Ny-Alesund)	Norway	ZEP678N00	78 54 N	11 52 E	475	$^{13}CO_2$, $C^{18}O_2$, CH_4, CO, CO_2, H_2
Zeppelinfjellet (Ny-Alesund)	Norway	ZEP678N00	78 54 N	11 52 E	475	CO_2
Zingst	Germany	ZGT654N00	54 25 N	12 43 E	1	CH_4, CO_2, O_3
Zingst	Germany	ZGT654N00	54 25 N	12 43 E	1	VOCs
Zoseni	Latvia	ZSN657N00	57 7 N	25 55 E	183	NO_2, SO_2
Zugspitze	Germany	ZUG647N00	47 25 N	10 58 E	2960	CH_4, CO, CO_2, NO, NOx, NOy, O_3
Zugspitze	Germany	ZUG647N00	47 25 N	10 58 E	2960	CO_2
Zugspitze / Schneefernerhaus	Germany	ZSF647N00	47 25 N	10 58 E	2656	SO_2
Zugspitze / Schneefernerhaus	Germany	ZSF647N00	47 25 N	10 58 E	2656	CH_4, CO, CO_2, N_2O, NO, NO_2, NOy, O_3, SF_6
Ähtäri	Finland	AHT662N00	62 34 N	24 11 E	180	NO_2, O_3, SO_2
ANTARCTICA						
Arrival Heights	New Zealand	ARH777S00	77 47 S	166 40 E	184	$^{13}CH_4$, $^{14}CO_2$, CH_4, CO, N_2O, VOCs
Casey Station	Australia	CYA766S00	66 16 S	110 31 E	60	CH_4, CO, CO_2, H_2, N_2O
Halley Bay	United Kingdom of Great Britain and Northern Ireland	HBA775S00	75 34 S	26 30 W	33	$^{13}CO_2$, $C^{18}O_2$, CH_4, CO, CO_2, H_2
Jubany	Argentina	JBN762S00	62 13 S	58 40 W	15	CO_2
Mawson	Australia	MAA767S00	67 37 S	62 52 E	32	CH_4, CO, CO_2, H_2, N_2O
McMurdo Station	United States of America	MCM777S00	77 49 S	166 34 E	11	CH_4, O_3
Mizuho	Japan	MZH770S00	70 42 S	44 17 E	2230	CH_4
Neumayer	Germany	NMY770S00	70 39 S	8 15 W	42	O_3
Palmer Station	United States of America	PSA764S00	64 55 S	64 0 W	10	$^{13}CO_2$, $C^{18}O_2$, $CBrClF_2$, CCl_4, CFCs, CH_3Br, CH_3CCl_3, CH_4, CO, CO_2, H_2, HCFCs, HFCs, N_2O, SF_6
South Pole	United States of America	SPO789S00	89 58 S	24 48 W	2810	CH_4, CO, CO_2, H_2, N_2O
South Pole	United States of America	SPO789S00	89 58 S	24 48 W	2810	$^{13}CH_4$, $^{13}CO_2$, $C^{18}O_2$, C_2Cl_4, $CBrClF_2$, $CBrF_3$, CCl_4, CFCs, CH_2Cl_2, CH_3Br, CH_3CCl_3, CH_3Cl, CH_4, CO, CO_2, H_2, HCFCs, HFCs, N_2O, O_3, SF_6
Syowa Station	Japan	SYO769S00	69 0 S	39 34 E	21	CO_2
Syowa Station	Japan	SYO769S00	69 0 S	39 34 E	21	$^{13}CO_2$, $C^{18}O_2$, CH_4, CO, CO_2, H_2
Syowa Station	Japan	SYO769S00	69 0 S	39 34 E	21	O_3
MOBILE STATION						
Aircraft (over Bass Strait and Cape Grim)	Australia	AIA999900				CH_4, CO, CO_2, H_2, N_2O

LIST OF OBSERVATION STATIONS (continued)

Station	Country/Territory	Index Number	Location Latitude (° ')	Location Longitude (° ')	Altitude (m)	Parameter
Akademik Korolev, R/V	United States of America	AKD999900				CH_4
Alligator liberty, M/V	Japan	ALG999900				CO_2
Atlantic Ocean	United States of America	AOC9XXX00			10	CH_4, CO_2
BACPAC 99	United States of America	BAC999900				CCl_4, CFCs, CH_3Br, CH_3CCl_3, CH_3Cl, HCFCs
BLAST1	United States of America	BLA999900				CCl_4, CFCs, CH_3Br, CH_3CCl_3, CH_3Cl, HCFCs
BLAST2	United States of America	BLA999901				CCl_4, CFCs, CH_3Br, CH_3CCl_3, CH_3Cl, HCFCs
BLAST3	United States of America	BLA999902				CCl_4, CFCs, CH_3Br, CH_3CCl_3, CH_3Cl, HCFCs
CLIVAR 01	United States of America	CLI999900				CCl_4, CFCs, CH_3Br, CH_3CCl_3, CH_3Cl, HCFCs
Comprehensive Observation Network for TRace gases by AIrLiner (CONTRAIL)	Japan	EOM999900				CH_4, CO_2
Discoverer 1983 & 1984, R/V	United States of America	DIS999900				CH_4
Discoverer 1985, R/V	United States of America	DSC999900				CH_4
Gas Change Experiment	United States of America	GAS999900				CCl_4, CFCs, CH_3Br, CH_3CCl_3, CH_3Cl, HCFCs
HATS Ocean Projects	United States of America	HOP999900				HFCs
INSTAC-I (International Strato/Tropospheric Air Chemistry Project)	Japan	INS999900				$^{13}CO_2$, CH_4, CO_2
John Biscoe, R/V	United States of America	JBS999900				CH_4
Keifu Maru, R/V	Japan	KEF999900				CO_2
Kofu Maru, R/V	Japan	KOF999900				CO_2
Korolev, R/V	United States of America	KOR999900				CH_4
Long Lines Expedition, R/V	United States of America	LLE999900				CH_4
MRI Research, 1978-1986, R/V	Japan	MRI999900				CH_4
MRI Research, Hakuho Maru, R/V	Japan	HKH999900				CO_2
MRI Research, Kaiyo Maru, R/V	Japan	KIY999900				CO_2
MRI Research, Mirai, R/V	Japan	MMR999900				CO_2
MRI Research, Natushima, R/V	Japan	NTU999900				CO_2
MRI Research, Ryofu Maru, R/V	Japan	RFM999900				CO_2
MRI Research, Wellington Maru, R/V	Japan	WLT999900				CO_2
Mexico Naval H-02, R/V	United States of America	MXN999900				CH_4

LIST OF OBSERVATION STATIONS (continued)

Station	Country/Territory	Index Number	Location Latitude (° ')	Location Longitude (° ')	Altitude (m)	Parameter
NOPACCS - Hakurei Maru -	Japan	HAK999900				TIC
Oceanographer, R/V	United States of America	OCE999900				CH_4
PHASE I-04	United States of America	PHA999900				CCl_4, CFCs, CH_3Br, CH_3CCl_3, CH_3Cl, HCFCs
Pacific Ocean	United States of America	POC9XXX00			10	$^{13}CO_2$, $C^{18}O_2$, CH_4, CO, CO_2, H_2
Polar Star, R/V	United States of America	PLS999900				CH_4
Ryofu Maru, R/V	Japan	RYF999900				CFCs, CH_4, CO_2, N_2O, TIC
South China Sea	United States of America	SCS9XXX00			15	$^{13}CO_2$, $C^{18}O_2$, CH_4, CO, CO_2, H_2
Soyo Maru, R/V	Japan	SOY999900				CO_2
Surveyor, R/V	United States of America	SUR999900				CH_4
The Observation of Atmospheric Methane Over Japan	Japan	OAM999900				CH_4
The Observation of Atmospheric Sulfur Hexafluoride Over Japan	Japan	OAS999900				SF_6
WEST COSMIC - Hakurei Maru No.2 -	Japan	HAK999901				TIC
Western Pacific	United States of America	WPC9XXX00			10	CH_4, CO_2

LIST OF CONTRIBUTORS

Station Country/Territory	Name	Address
REGION I (Africa)		
Izaña (Tenerife) (Spain)	Angel J. Gomez-Pelaez Carlos Marrero	Izana Atmospheric Research Center, Meteorological State Agency of Spain (AEMET) C/ La Marina, 20, Planta 6. Apartado 880. 38071 Santa Cruz de Tenerife
Cape Point (South Africa)	Ernst-Gnther Brunke	South African Weather Service (Climate Division) SAWS, c/o CSIR (Environmentek), P.O. Box 320,Stellenbosch 7599
Mt. Kenya (Kenya)	Josiah Kariuki Murageh Jörg Klausen (Dr.) Stephan Henne	KMD, Kenyan Meteorological Department Kenya Meteorological Department Dagoretti Corner P.O. Box 30259 00100 Nairobi
Cape Verde Observatory (Cape Verde)	Katie Read	Department of Chemistry, University of York Department of Chemistry, University of York, Heslington, York, Y010 5DD
Funchal (Portugal)	Maria Amelia V.Lopes Clotilde P.N.Goncalves	Instituto de Meteorologia Rua C-Aeroporto de Lisboa1749-077 Lisboa Portugal
Amsterdam Island (France)	Michel Ramonet	LSCE (Laboratoire des Sciences du Climat et de l'Environnement) UMR CEA-CNRS LSCE - CEA Saclay - Orme des Merisiers - Bat.709 91191 Gif-sur-Yvette, France
Assekrem (Algeria)	Mimouni Mohamed	Office National de la Meteorologie POBox 31 Tamanrasset 11000, Algeria
REGION II (Asia)		
Nagoya (Japan)	A. Matsunami	Research Center for Advanced Energy Conversion, Nagoya University Furo-cho, Chikusaku, Nagoya 464-8603
Cape Ochi-ishi Hateruma (Japan)	Hitoshi MUKAI	Center for Global Environmental Research, National Institute for Environmental Studies 16-2, Onogawa, Tsukuba-shi, Ibaraki 305-8506, Japan
Gosan (Republic of Korea)	Jaebum Lee Okjung Ju Sang-Kyun Kim	Researcher of Global Environment Research Center Environmental Research Complex, Gyeongseo-dong, Seo-gu, Incheon, 404-708
Hok Tsui (Hong Kong, China)	Ka Se Lam	Department of Civil and Structural Engineering,Hong Kong Polytechnic University Hung Hom, Kowloon, Hong Kong

LIST OF CONTRIBUTORS (continued)

Station Country/Territory	Name	Address
Minamitorishima Ryori Yonagunijima (Japan)	Kazuhiro TSUBOI	Atmospheric Environment Division, Global Environment and Marine Department,Japan Meteorological Agency (JMA) 1-3-4 Otemachi, Chiyoda-ku, Tokyo 100-8122, Japan
Mikawa-Ichinomiya (Japan)	Koji Ohno	Aichi Air Environment Division 1-2 Sannomaru-3chome, Naka-ku, Nagoya, Aichi 460-8501, Japan
Memanbetsu (Japan)	Michio Hirota	Geochemical Research Department, Meteorological Research Institute 1-1, Nagamine, Tsukuba, Ibaraki 305-0052
Tsukuba (Japan)	Michio Hirota Yousuke Sawa	Geochemical Research Department, Meteorological Research Institute 1-1, Nagamine, Tsukuba, Ibaraki 305-0052
Hamamatsu (Japan)	Mitsuo TODA	Shizuoka University 3-5-1 Jyohoku, Hamamatsu 432-8561, Japan
Bering Island Kotelny Island (Russian Federation) Kyzylcha (Uzbekistan)	Nina Paramonova	Main Geophysical Observatory (MGO) Karbyshev Street 7, St. Petersburg, 194021, Russian Federation
Takayama (Japan)	Shohei Murayama	Research Institute for Environmental Management Technology, National Institute of Advanced Industrial Science and Technology (AIST) AIST Tsukuba West, 16-1 Onogawa, Tsukuba, Ibaraki 305-8569, Japan
Gosan (Republic of Korea)	So-young Bang	Applied Meteorology Research Laboratory,Meteorological Research Institute (METRI),Korea Meteorological Administration (KMA) 460-18, Shindaebang-dong, Dongjak-gu, Seoul 156-720, Rep. of Korea
Ship between Ishigaki Island and Hateruma Island (Japan)	Takakiyo Nakazawa Shuji Aoki	Center for Atmospheric and Oceanic Studies, Graduate School of Science, Tohoku University Aoba, Sendai 980-8578, Japan
Mt. Waliguan (China)	Tang Jie	Chinese Academy of Meteorological Sciences 46 Zhongguancun Nandajie, Haidian, Beijing 100081, P.R. of China

LIST OF CONTRIBUTORS (continued)

Station Country/Territory	Name	Address
Suita (Japan)	Tomohiro Oda	Division of Sustainable Energy and Environmental Engineering, Graduate School of Engineering, Osaka Universiy, Japan Green Engieering Lab Division of Sustainable Energy and Environmental Engineering 2-1 Yamadaoka, Suita, Osaka 565-0871 Japan
Tsukuba (Japan)	Tosiro Kimura	Lower Aerological Observations Division, Aerological Observatory, Japan Meteorological Agency (JMA) Lower Aerological Observations Division, Aerological Observatory1-2 Nagamine, Tsukuba, Ibaraki, 305-0052, Japan
Issyk-Kul (Kyrgyzstan)	V. Sinyakov	Laboratory of Geophysics, Institute of Fundamental sciences at the Kyrgyz National University Manas Street 101, Bishkek, 720033, Kyrgyz Republic
Mt. Dodaira Kisai Urawa (Japan)	Yosuke MUTO	Center for Environmental Science in Saitama 914 Kamitanadare, Kisai-machi, Kita-Saitama-gun, Saitama 347-0115, Japan
Anmyeon-do (Republic of Korea)	Youngmoon YOUN	Climate Change Science Program Division Korea Meteorological Administration
REGION III (South America)		
Arembepe (Brazil)	Joelmo Oliveira	
Huancayo (Peru)	Mutsumi Ishitsuka	Observatorio de Huancayo, Instituto Geofisico del Peru Apartado 46, Huancayo, Peru
Ushuaia (Argentina)	Sergio Luppo	Servicio Meteorológico Nacional - Gobierno de Tierra del Fuego Estación VAG Ushuaia Subsecretaria de Ciencia y Tecnología, Ministerio de Educación, Cultura, Ciencia y Tecnología Gobierno de Tierra del Fuego 9410 Ushuaia, Tierra del Fuego, Argentina
REGION IV (North and Central America)		

LIST OF CONTRIBUTORS (continued)

Station Country/Territory	Name	Address
Alert Candle Lake Cape St. James Estevan Point Frasedale Sable Island (Canada)	Doug Worthy	Environment Canada (EC) 4905 Dufferin Street, Toronto, Ontario, Canada, M3H 5T4
Algoma Bratt's Lake Chalk River Chapais Egbert Experimental Lakes Area Esther Kejimkujik Longwoods Saturna Sutton (Canada)	Mike Shaw	Environment CanadaMeteorological Service of CanadaAir Quality Research Branch 4905 Dufferin StreetToronto, Ontario CANADA M3H 5T4
La Palma (Cuba)	Osvaldo Cuesta Santos	Institute of Meteorology, Atmospheric Environment Research Center Aptdo. 17032, Postal Code 11700, Havana 17, Cuba
REGION V (South-West Pacific)		
Baring Head (New Zealand)	Antony Gomez Sylvia Nichol Gordon Brailsford	National Institute of Water & Atmospheric Research Ltd. 301 Evans Bay Parade, Greta PointPrivate Bag 14-901, Kilbirnie, Wellington
Cape Grim (Australia)	Bruce Forgan Ian Galbally	Commonwealth Bureau of Meteorology 700 Collins St, Docklands GPO Box 1289K, Melbourne, Victoria 3001
Danum Valley GAW Baseline Station Tanah Rata (Malaysia)	Lim Sze Fook	Environmental Studies DivisionMalaysian Meteorological Department Jalan Sultan46667 Petaling Jaya, Selangor, Malaysia
Bukit Koto Tabang Jakarta (Indonesia)	Nurhayati	Bureau of Meteorology and Geophysics Jalan Angkasa 1 No.2 Jakarta 10720, Indonesia
Bukit Koto Tabang (Indonesia)	Nurhayati Ilahi, Asep Firman (Mr.) Jörg Klausen (Dr.)	Bureau of Meteorology and Geophysics Jalan Angkasa 1 No.2 Jakarta 10720, Indonesia
REGION VI (Europe)		

LIST OF CONTRIBUTORS (continued)

Station Country/Territory	Name	Address
Puszcza Borecka/Diabla Gora (Poland)	Anna Degorska	Institute of Environmental Protection Kolektorska 4 01-692 Warsaw
Hohe Warte Stephansplatz (Austria)	August Kaiser	Department for Environmental MeteorologyCentral Institute for Meteorology and Geodynamics Postfach 342, Hohe Warte 38, A-1191 Wien
Jungfraujoch (Switzerland)	Brigitte Buchmann	Empa, Swiss Federal Laboratories for Materials Testing and Research, Air Pollution / Environmental Technology Uberlandstrasse 129 CH-8600 Dubendorf
Payerne Rigi (Switzerland)	Brigitte Buchmann Thomas Seitz	Empa, Swiss Federal Laboratories for Materials Testing and Research, Air Pollution / Environmental Technology Uberlandstrasse 129 CH-8600 Dubendorf
Fundata Semenic Stîna de Vale (Romania)	Daniela ZISU	National Research and Development Institute for Environmental Protection Splaiul Independentei nr. 294, sector 6, 77703 Bucuresti
Kamenicki Vis (Serbia)	Dragan Djordjevic	Republic Hydrometeorological Service, Environmental Control Department Kneza Viseslava 66, 11030 Belgrade, Serbia
Burgas Plovdiv Pleven Sofia Varna (Bulgaria)	Ekaterina Batchvarova	National Institute of Meteorology and Hydrology 66 Tzarigradsko chaussee, 1784 Sofia
Jarczew Leba Sniezka Suwalki (Poland)	Eugeniusz Brejnak	Institute of Meteorology and Water Management;Laboratory for Research and Monitoring of Air Pollution 61 Podlesna Street, 01-673 Warszawa
Fundata (Romania)	Florin Nicodim	National Meteorological Administration Sos. Bucuresti-Ploiesti nr. 97, 71552 Bucharest
Lampedusa (Italy)	Florinda Artuso Salvatore Piacentino Alcide di Sarra	Italian National Agency for New Technology, Energy and the Environment (ENEA) ENEA CLIM-OSS, Via Anguillarese 301, 00060 S.Maria di Galeria, Rome, Italy.ENEA-Station for Climate Observations, Capo Grecale, 92010 Lampedusa (AG), Italy
Plateau Rosa (Italy)	Francesco Apadula Daniela Heltai Andrea Lanza	CESI RICERCA Environment and Sustainable Development Department via Rubattino 54, 20134 Milano

LIST OF CONTRIBUTORS (continued)

Station Country/Territory	Name	Address
Site J (Denmark)	Gen Hashida Shinji Morimoto Shuji Aoki	National Institute of Polar Research Kaga 1-9-10, Itabashi-ku, Tokyo 173-8515
Mace Head (Ireland)	Gerard Spain	National University of Ireland, Galway (NUI) Mace Head Research StationCarna, Co. Galway
Hohe Warte Stephansplatz (Austria)	Guenther Schermann	Municipal Department 22 - Environmental ProtectionAir quality subdepartment, City of Vienna Ebendorferstrasse 4, A-1082 Vienna, Austria
Vindeln (Sweden)	Hakan Blomgren	IVL Swedish Environmental Research Institute P.O.Box 5302S-400 14 Goteborg, Sweden
Kollumerwaard Kloosterburen (Netherlands (the))	Hans Berkhout	RIVM-Laboratory for Environmental Monitoring PO Box 1 3720 BA Bilthoven the Netherlands
Wank Peak Zugspitze (Germany)	Hans-Eckhart Scheel	Fraunhofer-Institute for Atmospheric Environmental Research, since 1.1.2002:Forschungszentrum Karlsruhe, IMK-IFU D-82467 Garmisch-Partenkirchen, Germany
Rucava Zoseni (Latvia)	Iraida Lyulko	Observation Network Department, Latvian Environment, Geology and Meteorology Agency, Ministry of Environmental 165 Maskavas str. LV-1019, Riga, Latvia
Danki Shepelevo (Russian Federation)	Irina Brouskina	
La Cartuja Doñana Logroño Mahón Noia Roquetes San Pablo de los Montes (Spain)	J.M. Saenz	Servicio de Desarrollos Medioambientales, Instituto Nacional de Meteorologia,Ministerio de Medio Ambiente Leonardo Prieto Castro, 8, 28071 Madrid, Spain
Zeppelinfjellet (Ny-Alesund) (Norway)	Johan Strom	Department of Applied Environmental Science (ITM), Stockholm University SE-106 91 Stockholm, Sweden
Pallas-Sammaltunturi (Finland)	Juha Hatakka Timo Salmi	Finnish Meteorological Institute P.O.Box 503,FI-00101 Helsinki, Finland

LIST OF CONTRIBUTORS (continued)

Station Country/Territory	Name	Address
Brotjacklriegel Deuselbach Waldhof Neuglobsow Schauinsland Westerland Zingst Zugspitze / Schneefernerhaus Zugspitze (Germany)	Karin Uhse	Umweltbundesamt (UBA, Federal Environmental Agency) Air Monitoring Network Paul-Ehrlich-Strasse 29 D-63225 Langen, Germany
Hegyhatsal K-puszta (Hungary)	Laszlo Haszpra	Hungarian Meteorological Service P.O. Box 39, H-1675 Budapest, Hungary
Braganca Viana do Castelo (Portugal)	Maria Amelia V.Lopes	Instituto de Meteorologia Rua C-Aeroporto de Lisboa1749-077 Lisboa Portugal
Angra do Heroismo Beja Castelo Branco Lisboa / Gago Coutinho Monte Velho Penhas Douradas (Portugal)	Maria Amelia V.Lopes Clotilde P.N.Goncalves	Instituto de Meteorologia Rua C-Aeroporto de Lisboa1749-077 Lisboa Portugal
Iskrba Kovk Krvavec Zavodnje (Slovenia)	Marijana Murovec	Environmental Agency of Republic of Slovenia Environment Office Sektor za kakovcost zraka / Air Quality Division Vojkova 1b, 1001 Ljubljana, p.p. 2608
Sonnblick (Austria)	Marina Fröhlich Wolfgang Spangl Elisabeth Friedbacher	Federal Environment Agency Austria Spittelauer Lände 5, A-1090 Wien, Austria
Ivan Sedlo (Bosnia and Herzegovina)	Martin Tais	Meteoroloski zavod Bosne i Hercegovine Bardakcije 12, 71000 Sarajevo, Bosnia and Herzegovina
Mace Head (Ireland)	Michel Ramonet	LSCE (Laboratoire des Sciences du Climat et de l'Environnement) UMR CEA-CNRS LSCE - CEA Saclay - Orme des Merisiers - Bat.709 91191 Gif-sur-Yvette, France
Kosetice (Czech Republic)	Milan Vana	Czech Hydrometeorological Institute, Kosetice Observatory Na Sabatce 17, 143 06 Praha 4 - Komorany, Czech Republic

LIST OF CONTRIBUTORS (continued)

Station Country/Territory	Name	Address
Ocean Station Charlie Teriberka (Russian Federation)	Nina Paramonova	Main Geophysical Observatory (MGO) Karbyshev Street 7, St. Petersburg, 194021, Russian Federation
Zeppelinfjellet (Ny-Alesund) (Norway)	Ove Hermansen	Norwegian Institute for Air Research (NILU) P. O. Box 100 Instituttveien 18, N-2027 Kjeller, Norway
Monte Cimone (Italy)	Paolo Bonasoni	National Research Council, Institute of Atmospheric Sciences and Climate (CNR-ISAC) Via Gobetti 10140129 Bologna, Italy
Eskdalemuir (United Kingdom of Great Britain and Northern Ireland)	Peter Kuria	Air and Environment Quality Division, DEFRA 4/F15, Ashdown House123 Victoria StreetLondon, SW1E 3DE, United Kingdom
Giordan Lighthouse (Malta)	Raymond Ellul	Atmospheric Research Unit / Physics Department /University of Malta Msida MSD 06, Malta
Monte Cimone (Italy)	Riccardo Santaguida	Italian Air Force Meteorological Service C.A.M.M. Mt. CIMONE,Via delle Ville 40, 41029-Sestola (MO), Italy
Hohenpeissenberg Zugspitze / Schneefernerhaus (Germany)	Stefan Gilge Christian Plass-Duelmer	Deutscher Wetterdienst (DWD, German Meteorological Service)Meteorologisches Observatorium Hohenpeissenberg Albin-Schwaiger-Weg 10D-82383 Hohenpeissenberg, Germany
Lazaropole (The Former Yugoslav Republic of Macedonia)	Suzana Alcinova Monevska	Hydrometeorological Service Skupi bb, 1000 Skopie,The former Yugoslav Republic of Macedonia

LIST OF CONTRIBUTORS (continued)

Station Country/Territory	Name	Address
Kosetice (Czech Republic)	Sverre Solberg	Norwegian Institute for Air Research P.O.Box 100NO-2027 Kjeller
Pallas-Sammaltunturi Utö (Finland)		
Donon La Tardiere Peyrusse Vieille (France)		
Brotjacklriegel Waldhof Schmuecke Zingst (Germany)		
Starina (Slovakia)		
Campisabalos (Spain)		
Ähtäri Oulanka Utö Virolahti (Finland)	Timo Salmi	Finnish Meteorological Institute Erik Palmenin aukio 1, P.O.Box 503, FIN-00101 Helsinki, Finland
ANTARCTICA		
Arrival Heights (New Zealand)	Antony Gomez Sylvia Nichol Gordon Brailsford	National Institute of Water & Atmospheric Research Ltd. 301 Evans Bay Parade, Greta PointPrivate Bag 14-901, Kilbirnie, Wellington
Jubany (Italy)	Luigi Ciattaglia	ICES (Int.l Center for Earth Sciences) c/o CNR-Istituto di Acustica- Area della Ricerca di Roma Tor Vergata,via Fosso del Cavaliere, 10000133 Rome, Italy
Neumayer (Germany)	Rolf Weller	Alfred Wegener Institute Am Handelshafen 12,27570 Bremerhaven, Germany
Mizuho (Japan)	Takakiyo Nakazawa	Center for Atmospheric and Oceanic Studies, Graduate School of Science, Tohoku University Aoba, Sendai 980-8578, Japan
Syowa Station (Japan)	Takakiyo Nakazawa Gen Hashida Shinji Morimoto	Center for Atmospheric and Oceanic Studies, Graduate School of Science, Tohoku University Aoba, Sendai 980-8578, Japan

LIST OF CONTRIBUTORS (continued)

Station Country/Territory	Name	Address
Syowa Station (Japan)	Yasuo Shudou	Office of Antarctic Observations,Japan Meteorological Agency (JMA) 1-3-4 Otemachi, Chiyoda-ku, Tokyo 100-8122, Japan
MOBILE STATION		
NOPACCS - Hakurei Maru - WEST COSMIC - Hakurei Maru No.2 - (Japan)	General Environmental Texhnos	The General Environmental Technos Co., Ltd. (Old:Kansai Environmental Engineering Center, Co., Ltd.) 1-3-5, Azuchi machi, Chuo-ku, Osaka 541-0052
INSTAC-I (International Strato/Tropospheric Air Chemistry Project) (Japan)	Hidekazu Matsueda	Geochemical Research Department, Meteorological Research Institute Nagamine 1-1, Tsukuba, Ibaraki 305-0052, Japan
Comprehensive Observation Network for TRace gases by AIrLiner (CONTRAIL) (Japan)	Hidekazu Matsueda Toshinobu Machida	Geochemical Research Department, Meteorological Research Institute Nagamine 1-1, Tsukuba, Ibaraki 305-0052, Japan
MRI Research, Mirai, R/V (Japan)	Hisayuki Yoshikawa-Inoue	Laboratory of Marine and Atmospheric GeochemistryGraduate School of Environmental Earth ScienceHokkaido University N10W5, Kita-ku, Sapporo 060-0810, Japan
MRI Research, Hakuho Maru, R/V MRI Research, Kaiyo Maru, R/V MRI Research, 1978-1986, R/V MRI Research, Natushima, R/V MRI Research, Ryofu Maru, R/V MRI Research, Wellington Maru, R/V (Japan)	Masao Ishii	Geochemical Research Department, Meteorological Research Institute Nagamine 1-1, Tsukuba, Ibaraki 305-0052, Japan
The Observation of Atmospheric Methane Over Japan The Observation of Atmospheric Sulfur Hexafluoride Over Japan (Japan)	Michio Hirota	Geochemical Research Department, Meteorological Research Institute 1-1, Nagamine, Tsukuba, Ibaraki 305-0052

LIST OF CONTRIBUTORS (continued)

Station Country/Territory	Name	Address
Alligator liberty, M/V Keifu Maru, R/V Kofu Maru, R/V Ryofu Maru, R/V (Japan)	Takashi Miyao	Pollutants Chemical Analysis Center, Marine Division, Climate and Marine Department, Japan Meteorological Agency (JMA) 1-3-4 Otemachi, Chiyoda-ku, Tokyo 100-8122, Japan
Soyo Maru, R/V (Japan)	Tsuneo Ono	Hokkaido National Fisheries Research Institute 116 Katsurakoi, Kushiro 085-0802, Japan

LIST OF CONTRIBUTORS (continued)

Station Country/Territory	Name	Address
NOAA/CMDL Flask Network		
Assekrem (Algeria)	Bruce Vaughn** James White** ($^{13}CH_4$, $^{13}CO_2$ and $C^{18}O_2$)	(*)NOAA/ESRL Global Monitoring Division 325 Broadway R/GMD1 Boulder, CO 80305-3328, U.S.A
Tierra del Fuego (Argentina)	Edward J. Dlugokencky* (CH_4)	(**)Institute of Arctic and Alpine Research (INSTAAR) Campus box 450, University of Colorado, Boulder, CO 80309-0450, U.S.A.
Cape Grim (Australia)	Paul C. Novelli* (CO and H_2)	
Ragged Point (Barbados)	Thomas J. Conway* (CO_2)	
Arembepe (Brazil)		
Alert Mould Bay (Canada)		
Easter Island (Chile)		
Lulin Mt. Waliguan (China)		
Summit (Denmark)		
Pallas-Sammaltunturi (Finland)		
Amsterdam Island Crozet (France)		
Hohenpeissenberg Ochsenkopf (Germany)		
Hegyhatsal (Hungary)		
Heimaey (Iceland)		
Bukit Koto Tabang (Indonesia)		
Mace Head (Ireland)		

LIST OF CONTRIBUTORS (continued)

Station Country/Territory	Name	Address
Sede Boker (Israel)		
Lampedusa (Italy)		
Syowa Station (Japan)		
Sary Taukum Plateau Assy (Kazakhstan)		
Mt. Kenya (Kenya)		
Christmas Island (Kiribati)		
Kaashidhoo (Maldives)		
Dwejra Point (Malta)		
Ulaan Uul (Mongolia)		
Gobabeb (Namibia)		
Baring Head Lauder Kaitorete Spit (New Zealand)		
Ocean Station "M" Zeppelinfjellet (Ny-Alesund) (Norway)		
Baltic Sea (Poland)		
Terceira Island (Portugal)		
Tae-ahn Peninsula (Republic of Korea)		
Black Sea (Romania)		

LIST OF CONTRIBUTORS (continued)

Station Country/Territory	Name	Address
Mahe Island (Seychelles)		
Izaña (Tenerife) (Spain)		
Ascension Island St. David's Head Tudor Hill Halley Bay Bird Island (United Kingdom of Great Britain and Northern Ireland)		
Akademik Korolev, R/V Atlantic Ocean St. Croix Barrow Cold Bay Cape Meares Discoverer 1983 & 1984, R/V Drake Passage Discoverer 1985, R/V Guam Grifton John Biscoe, R/V Key Biscayne Korolev, R/V Kitt Peak Cape Kumukahi Park Falls Long Lines Expedition, R/V McMurdo Station Sand Island Mauna Loa Mexico Naval H-02, R/V Niwot Ridge (T-van) Niwot Ridge (Saddle) Oceanographer, R/V Olympic Peninsula Pacific-Atlantic Ocean Polar Star, R/V Pacific Ocean Palmer Station Point Arena South China Sea Southern Great Plains Shemya Island La Jolla		

LIST OF CONTRIBUTORS (continued)

Station Country/Territory	Name	Address
Tutuila (Cape Matatula) South Pole Ocean Station "C" Surveyor, R/V Trinidad Head Wendover Moody Western Pacific (United States of America)		

NOAA/CMDL/HATS Network

Tierra del Fuego (Argentina) Cape Grim (Australia) Alert (Canada) Summit (Denmark) Mace Head (Ireland) BACPAC 99 BLAST1 BLAST2 BLAST3 Barrow CLIVAR 01 Gas Change Experiment Harvard Forest HATS Ocean Projects Grifton Cape Kumukahi Park Falls Mauna Loa Niwot Ridge (C-1) PHASE I-04 Palmer Station Tutuila (Cape Matatula) South Pole Trinidad Head (United States of America)	Geoffrey S. Dutton James W. Elkins Stephen A. Montzka	Halocarbons and Other Atmosphere Trace Species Group (HATS)/NOAA/ESRL Global Monitoring Division 325 Broadway R/GMD1 Boulder, CO 80305-3328, U.S.A

NOAA/CMDL Surface Ozone Network

LIST OF CONTRIBUTORS (continued)

Station Country/Territory	Name	Address
Ragged Point (Barbados)	Sam Oltmans	NOAA/ESRL Global Monitoring Division 325 Broadway R/GMD1 Boulder, CO 80305-3328, U.S.A
Summit (Denmark)		
Heimaey (Iceland)		
Lauder (New Zealand)		
Tudor Hill (United Kingdom of Great Britain and Northern Ireland)		
Barrow McMurdo Station Mauna Loa Niwot Ridge (C-1) Niwot Ridge (Saddle) Tutuila (Cape Matatula) South Pole Trinidad Head (United States of America)		

LIST OF CONTRIBUTORS (continued)

Station Country/Territory	Name	Address
CSIRO Flask Network		
Aircraft (over Bass Strait and Cape Grim) Cape Ferguson Cape Grim Casey Station Mawson Macquarie Island (Australia)	Ray Langenfelds Paul Krummel Paul Steele	Commonwealth Scientific and Industrial Research Organisation (CSIRO) CSIRO Marine and Atmospheric Research Private Bag 1 Aspendale, Vic, Australia 3195
Alert Estevan Point (Canada)		
Shetland (United Kingdom of Great Britain and Northern Ireland)		
Mauna Loa South Pole (United States of America)		
ALE/GAGE/AGAGE Network		
Cape Grim (Australia)	Ray Wang Derek Cunnold	School of Earth and Atmospheric Sciences, Georgia Institute of Technology 311 Ferst Drive School of Earth and Atmospheric Sciences Georgia Institute of Technology Atlanta, GA 30332-0340
Ragged Point (Barbados)		
Adrigole Mace Head (Ireland)		
Cape Meares Tutuila (Cape Matatula) Trinidad Head (United States of America)		

GLOSSARY

AGENCIES AND PROGRAMMES:

AEMET	Agencia Estatal de Meteorologia (Spain)
AES	Atmospheric Environment Service (Canada, presently MSC)
AGAGE	Advanced Global Atmospheric Gases Experiment
Aichi	Aichi Prefecture (Japan)
AIST	National Institute of Advanced Industrial Science and Technology (Japan)
AQRB	Air Quality Research Branch, Meteorological Service of Canada (Canada)
ALE	Atmospheric Lifetime Experiment
AWI	Alfred Wegener Institute (Germany)
BMG	Bureau of Meteorology and Geophysics (Indonesia)
BoM	Commonwealth Bureau of Meteorology (Australia)
CAMS	Chinese Academy of Meteorological Sciences (China)
CESI	Italian Electrical Experimental Center (Italy)
CFR	Centre des Faibles Radioactivites (France)
CHMI	Czech Hydrometeorological Institute (Czech Republic)
CMA	China Meteorological Administration (China)
CMDL	Climate Monitoring and Diagnostics Laboratory (NOAA, USA, presently ESRL/GMD)
CNRS	Centre National de la Recherche Scientifique (France)
CSIRO	Commonwealth Scientific and Industrial Research Organisation (Australia)
DEFRA	Department for Environment, Food and Rural Affairs (United Kingdom)
DNA-IAA	Direccion Nacional del Antartico-Instituto Antartico Argentino (Argentina)
DWD	Deutscher Wetterdienst (German Meteorological Service, Germany)
EARS	Environmental Agency of the Republic of Slovenia
EC	Environment Canada (Canada)
EMPA	Swiss Federal Laboratories for Material Testing and Research (Switzerland)
ENEA	Italian National Agency for New Technology, Energy and the Environment (Italy)
FMI	Finnish Meteorological Institute
GAGE	Global Atmospheric Gases Experiment
GAW	Global Atmosphere Watch (WMO)
GERC	Global Environment Research Center of NIER (Republic of Korea)
HATS	Halocarbons and other Atmospheric Trace Species
HMS	Hungarian Meteorological Service (Hungary)
IAFMS	Italian Air Force Meteorological Service (Italy)
ICES	International Center for Earth Sciences c/o CNR. (Italy)
IGP	Instituto Geofísico del Perú (Peru)
IM	Instituto de Meteorologia (Portugal)
IMK-IFU	Institut für Meteorologie und Klimatologie, Atmosphärische Umweltforschung, Forschungszentrum Karlsruhe (Germany)
INM	Instituto Nacional de Meteorología (Spain)
INMET	Instituto Nacional de Meteorologia (Brazil)
INMH	National Meteorological Administration (Romania)
IOEP	Institute of Environmental Protection (Poland)
ISAC	Istituto di Scienze dell'Atmosfera e del Clima, Consiglio Nazionale delle Ricerche (Italy)
ITM	Department of Applied Environmental Science, Stockholm University, (Sweden)

IVL	Swedish Environmental Research Institute, Göteborg (Sweden)
JMA	Japan Meteorological Agency (Japan)
JMA/AO	Aerological Observatory, Japan Meteorological Agency, Tsukuba, Japan
KMA	Korea Meteorological Administration (Republic of Korea)
KMD	Kenya Meteorological Department (Kenya)
KSNU	Kyrgyz State National University (Kyrgyzstan)
LEGMA	Latvian Environment, Geology and Meteorology Agency (Latvia)
LSCE	Laboratoire des Sciences du Climat et de l'Environnement (France)
METRI	Meteorological Research Institute (KMA, Republic of Korea)
MGO	Main Geophysical Observatory (Russian Federation)
MMD	Malaysian Meteorological Department
MISU	Department of Meteorology, Stockholm University (Sweden)
MRI	Meteorological Research Institute (Japan/JMA)
MSC	Meteorological Service of Canada (Canada, formerly AES)
NCEP	National Centers for Environmental Prediction (USA/NOAA)
NIES	National Institute for Environmental Studies (Japan)
NILU	Norwegian Institute for Air Research (Norway)
NIMH	Institutul National de Meteorologie, Hidrologie si Gospodarirea Apelor (Romania)
NIPR	National Institute of Polar Research (Japan)
NIRE	National Institute for Resources and Environment (Japan)
NIST	National Institute of Standards and Technology (USA)
NIWA	National Institute of Water & Atmospheric Research (New Zealand)
NOAA/GMD	Earth System Research Laboratory, Global Monitoring Division (NOAA, USA, formerly CMDL)
NUI	National University of Ireland, Galway (Ireland)
ONM	Office National de la Météorologie (Algeria)
Osaka Univ.	Osaka University (Japan)
PolyU	Hong Kong Polytechnik University, Hong Kong (China)
RIVM	National Institute for Health and Environment (Netherlands)
Roshydromet	Russian Hydrometeorological Service
Saitama	Saitama Prefecture (Japan)
SAWS	South African Weather Service (South Africa)
Shizuoka	Shizuoka University (Japan)
SIO	Scripps Institution of Oceanography, University of California at San Diego (USA)
SMN	Servicio Meteorológico Nacional (Argentina)
SNU	Seoul National University (Republic of Korea)
Tohoku Univ.	Tohoku University (Japan)
UBA	Umweltbundesamt (Germany)
UBA Austria	Umweltbundesamt (Federal Environmental Agency), Austria
UHEI-IUP	Institut für Umweltphysik, Universität Heidelberg (Germany)
UM	University of Malta
WDCGG	World Data Centre for Greenhouse Gases, operated by JMA, Japan (WMO)
WMO	World Meteorological Organization
ZAMG	Central Institute of Meteorology and Geodynamics (Austria)

ATMOSPHERIC SPECIES:

CCl_4	tetrachloromethane (carbon tetrachloride)
CFC-11	chlorofluorocarbon-11 (trichlorofluoromethane, CCl_3F)
CFC-12	chlorofluorocarbon-12 (dichlorodifluoromethane, CCl_2F_2)
CFC-113	chlorofluorocarbon-113 (1,1,2-trichlorotrifluoroethane, CCl_2FCClF_2)
CFCs	chlorofluorocarbons
CH_2Cl_2	dichloromethane (methylene chloride)
CH_3Cl	chloromethane (methyl chloride)
CH_3Br	bromomethane (methyl bromide)
Halon-1211	chlorodifluorobromomethane ($CBrClF_2$)
Halon-1301	bromotrifluoromethane ($CBrF_3$)
HCFC-141b	hydrochlorofluorocarbon-141b (1,1-dichloro-1-fluoroethane, CH_3CCl_2F)
HCFC-142b	hydrochlorofluorocarbon-142b (1,1-difluoro-1-chloroethane, CH_3CClF_2)
HCFC-22	hydrochlorofluorocarbon-22 (chlorodifluoromethane, $CHClF_2$)
HCFCs	hydrochlorofluorocarbons
HFC-134a	hydrofluorocarbon-134a (1,1,1,2- tetrafluoroethane, CH_2FCF_3)
HFC-152a	hydrofluorocarbon -152a (1,1- difluoroethane, CHF_2CH_3)
HFCs	hydrofluorocarbons
CH_4	methane
CH_3CCl_3	trichloroethane (methyl chloroform)
CO	carbon monoxide
CO_2	carbon dioxide
N_2O	nitrous oxide
NO	nitrogen monoxide
NO_2	nitrogen dioxide
NO_X	nitrogen oxides
O_3	ozone
SF_6	sulphur hexafluoride
SO_2	sulphur dioxide

UNITS:

ppb	parts per billion
ppm	parts per million
ppt	parts per trillion

Others:

ENSO	El Niño-Southern Oscillation
M/V	merchant vessel
R/V	research vessel
SOI	Southern Oscillation Index
SST	Sea Surface Temperature

LIST OF WMO WDCGG PUBLICATIONS

DATA REPORTING MANUAL:

WDCGG No. 1	January	1991

WMO WDCGG DATA REPORT:

			(period of data accepted)				
WDCGG No. 2 Part A	October	1992	October	1990	~	August	1992
WDCGG No. 2 Part B	October	1992	October	1990	~	August	1992
WDCGG No. 3	October	1993	September	1992	~	March	1993
WDCGG No. 5	March	1994	April	1993	~	September	1993
WDCGG No. 6	September	1994	September	1993	~	March	1994
WDCGG No. 7	March	1995	April	1994	~	December	1994
WDCGG No. 9	September	1995	January	1995	~	June	1995
WDCGG No.10	March	1996	July	1995	~	December	1995
WDCGG No.11	September	1996	January	1996	~	June	1996
WDCGG No.12	March	1997	July	1996	~	November	1996
WDCGG No.14	September	1997	December	1996	~	June	1997
WDCGG No.16	March	1998	July	1997	~	December	1997
WDCGG No.17	September	1998	January	1998	~	June	1998
WDCGG No.18	March	1999	July	1998	~	December	1998
WDCGG No.20	September	1999	January	1999	~	June	1999
WDCGG No.21	March	2000	July	1999	~	December	1999
WDCGG No.23	September	2000	January	2000	~	June	2000
WDCGG No.25	March	2001	July	2000	~	December	2000

WMO WDCGG DATA CATALOGUE:

WDCGG No. 4	December	1993
WDCGG No.13	March	1997
WDCGG No.19	March	1999
WDCGG No.24	March	2001

WMO WDCGG DATA SUMMARY:

WDCGG No. 8	October	1995
WDCGG No.15	March	1998
WDCGG No.22	March	2000
WDCGG No.26	March	2002
WDCGG No.27	March	2003
WDCGG No.28	March	2004
WDCGG No.29	March	2005
WDCGG No.30	March	2006
WDCGG No.31	March	2007
WDCGG No.32	March	2008
WDCGG No.33	March	2009

WMO WDCGG CD-ROM:

			(period of data accepted)				
CD-ROM No. 1	March	1995	October	1990	~	December	1994
CD-ROM No. 2	March	1996	October	1990	~	June	1995
CD-ROM No. 3	March	1997	October	1990	~	June	1996
CD-ROM No. 4	March	1998	October	1990	~	December	1997
CD-ROM No. 5	March	1999	October	1990	~	December	1998
CD-ROM No. 6	March	2000	October	1990	~	December	1999
CD-ROM No. 7	March	2001	October	1990	~	December	2000
CD-ROM No. 8	March	2002	October	1990	~	January	2002
CD-ROM No. 9	March	2003	October	1990	~	December	2002
CD-ROM No.10	March	2004	October	1990	~	December	2003
CD-ROM No.11	March	2005	October	1990	~	December	2004

CD-ROM No.12	March	2006	October	1990	~	December	2005
CD-ROM No.13	March	2007	October	1990	~	November	2006
CD-ROM No.14	March	2008	October	1990	~	November	2007

WMO WDCGG DVD: (period of data accepted)

DVD No. 1	March	2009	October	1990	~	November	2008